



Turun yliopisto
University of Turku

MOLECULAR IMAGING OF TISSUE REPAIR AFTER MYOCARDIAL INFARCTION

Preclinical evaluation of novel ^{68}Ga -labeled PET tracers

Max Kiugel



Turun yliopisto
University of Turku

MOLECULAR IMAGING OF TISSUE REPAIR AFTER MYOCARDIAL INFARCTION

Preclinical evaluation of novel ^{68}Ga -labeled PET tracers

Max Kiugel

University of Turku

Faculty of Medicine

Department of Clinical Physiology and Nuclear Medicine

Drug Research Doctoral Programme

Turku PET Centre

Supervised by

Professor Anne Roivainen, PhD
Turku PET Centre and Turku Center for
Disease Modeling
University of Turku
Turku, Finland

Associate Professor Antti Saraste, MD, PhD
Turku PET Centre, Heart Center and
Institute of Clinical Medicine
University of Turku and
Turku University Hospital
Turku, Finland

Reviewed by

Professor Risto Kerkelä, MD, PhD
Institute of Biomedicine
Department of Pharmacology and Toxicology
Biocenter Oulu, University of Oulu,
Oulu, Finland

Professor Olivier Gheysens, MD, PhD
Nuclear Medicine and Molecular Imaging
Department of Imaging and Pathology
KU Leuven, University Hospitals Leuven
Leuven, Belgium

Opponent

Professor John Prior, MD, PhD
Nuclear Medicine, CHUV
University of Lausanne
Lausanne, Switzerland

The originality of this thesis has been checked in accordance with the University of Turku quality assurance system using the Turnitin OriginalityCheck service.

ISBN 978-951-29-7266-1 (PRINT)

ISBN 978-951-29-7267-8 (PDF)

ISSN 0355-9483 (Print)

ISSN 2343-3213 (Online)

Painosalama Oy - Turku, Finland 2018

To my dearest Grandmother

ABSTRACT

Max Kiugel

MOLECULAR IMAGING OF TISSUE REPAIR AFTER MYOCARDIAL INFARCTION

Preclinical evaluation of novel ⁶⁸Ga-labeled PET tracers

University of Turku, Faculty of Medicine, Department of Clinical Physiology and Nuclear Medicine, Drug Research Doctoral Programme, Turku PET Centre, Turku, Finland

Congestive heart failure (HF) develops soon after acute myocardial infarction (AMI) in almost 25% of initial survivors. Modern cardiac imaging methods are useful for HF diagnostics and, possibly, the detection of underlying molecular mechanisms involved in myocardial repair. CD44, a cell-surface glycoprotein, is involved in various cellular functions, including cell proliferation, adhesion, migration and lymphocyte activation. Integrins are transmembrane proteins involved in various signaling pathways related to inflammation, angiogenesis and fibrosis. Expression of proteolytic matrix metalloproteinases 2 and 9 (MMP-2/9) also associates with extracellular matrix remodeling.

The purpose of this thesis was to evaluate novel Gallium-68 labeled imaging agents targeting $\alpha_v\beta_3$ integrin, MMP-2/9, or CD44, for positron emission tomography (PET) imaging of post-MI repair in a surgical rat model. The MMP-2/9 targeting tracer watarvias also evaluated for imaging of atherosclerotic lesions in a hypercholesterolemic mouse model. *In vivo* PET imaging, *ex vivo* biodistribution, *ex vivo* autoradiography, and immunohistochemistry were utilized to assess tracer stability, uptake in various tissues, as well as uptake correlation with various cellular level processes. Of the studied tracers, $\alpha_v\beta_3$ integrin targeting tracer showed the most optimal characteristics for imaging of myocardial healing processes. Tracer uptake in the damaged myocardium was clearly visible *in vivo*, and blood clearance as well as tracer stability were sufficient. The CD44 targeting tracer showed initial potential warranting further development, as the tracer uptake was associated with myocardial inflammation. MMP-2/9 targeted imaging showed significant limitations due to tracer instability and slow clearance.

In conclusion, imaging of $\alpha_v\beta_3$ integrin expression is a potential tool for the purpose of evaluating myocardial repair after MI.

Keywords: coronary artery disease, atherosclerosis, myocardial ischemia, myocardial infarction, heart failure, positron emission tomography (PET)

TIIVISTELMÄ

Max Kiugel

SYDÄNKUDOKSEN INFARKTINJÄLKEISEN PARANEMISEN MOLEKYYYLIKUVANTAMINEN

Uusien ⁶⁸Ga-leimattujen merkkiaineiden prekliininen arviointi

Turun yliopisto, Lääketieteellinen tiedekunta, Kliininen fysiologia ja isotooppilääketiede, Lääketutkimuksen tohtoriohjelma, Valtakunnallinen PET-keskus, Turku, Suomi

Sydämen vajaatoiminta kehittyy pian akuutin sydäninfarktin jälkeen lähes 25 prosentille eloonjääneistä. Nykyaikaiset sydämen kuvantamismenetelmät ovat hyödyllisiä diagnostiikassa ja mahdollisesti sydänlihaksen muovautumiseen liittyvien molekyylimekanismien havaitsemisessa. Solupinnan glykoproteiini CD44 osallistuu erilaisiin soluvälitteisiin toimintoihin, kuten proliferaatioon, adheesioon, migraatioon ja lymfosyyttien aktivaatioon. Integriinit ovat transmembraaniproteiineja, jotka osallistuvat erilaisiin signalointireitteihin liittyen tulehdukseen, angiogeneesiin ja fibroosiin. Proteolyyttisten matriksin metalloproteiinaasi 2:n ja 9:n (MMP-2/9) ilmentyminen liittyy niin ikään solunulkoisen matriksin uudelleenmuovautumiseen.

Tämän väitöskirjan tarkoituksena on arvioida uusia Gallium-68-leimattuja koettimia positroniemissiotomografiaa (PET) varten. Tutkitut koettimet kohdistuvat joko $\alpha_v\beta_3$ -integriiniin, MMP-2/9:ään tai CD44:ään. Tutkimus toteutettiin infarktinjälkeisen sydämen vajaatoiminnan kirurgisessa rottamallissa. MMP-2/9-koetinta arvioitiin myös ateroskleroottisten muutosten kuvantamiseen hyperkolesterolemisessä hiirimallissa. $\alpha_v\beta_3$ -integriiniin kohdentuvan merkkiaineen kertymä näkyi selkeästi *in vivo*, ja veren puhdistuma sekä merkkiaineen stabiilisuus olivat riittävät. CD44 kuvantamiskohteena osoitti alkuvaiheen potentiaalia, joka mahdollistaa jatkokehityksen, sillä merkkiaineen kertymä assosioitui infarktinjälkeiseen tulehdusreaktioon. MMP-2/9-kohdennetulle kuvantamiselle puolestaan ilmeni merkittäviä rajoituksia merkkiaineiden epävakauden ja hitaan veripuhdistuman vuoksi

Yhteenvetona voidaan todeta, että $\alpha_v\beta_3$ -integriinifragmentin kuvantaminen on potentiaalinen työkalu sydänlihaksen paranemisprosessien arvioimiseksi akuutin sydäninfarktin jälkeen.

Avainsanat: sepelvaltimotauti, ateroskleroosi, sydänlihasiskemia, sydäninfarkti, sydämen vajaatoiminta, positroniemissiotomografia (PET)

TABLE OF CONTENTS

ABSTRACT.....	4
TIIVISTELMÄ	5
ABBREVIATIONS	8
LIST OF ORIGINAL PUBLICATIONS.....	11
1 INTRODUCTION	12
2 REVIEW OF LITERATURE	14
2.1 Ischemic heart disease	14
2.1.1 Atherosclerosis and coronary artery disease.....	14
2.1.2 Inflammation and plaque vulnerability	15
2.1.3 Gelatinase (MMP-2 and MMP-9) activity in atherosclerosis.....	15
2.1.4 Myocardial ischemia.....	17
2.1.5 Acute myocardial infarction	17
2.1.6 Cardiac repair.....	19
2.1.7 Adverse remodeling and heart failure.....	23
2.1.8 Role of CD44, integrins and gelatinases.....	28
2.1.9 Overview of HF therapy	31
2.2 Advances in noninvasive assessment of cardiac function.....	32
2.2.1 Blood biomarkers.....	32
2.2.2 Cardiac ultrasound	33
2.2.3 Cardiac magnetic resonance	33
2.2.4 Computed tomography.....	34
2.2.5 Molecular imaging of cardiac tissue.....	34
3 AIMS OF THE STUDY	41
4 MATERIALS AND METHODS.....	42
4.1 Animal Models	42
4.1.1 Atherosclerosis model (IV).....	42
4.1.2 Surgical myocardial infarction model (I-III)	42
4.2 ⁶⁸ Ga-labeled tracers	43
4.3 <i>In vivo</i> tracer stability measurements	44
4.4 <i>In vivo</i> PET/CT.....	45
4.5 <i>Ex vivo</i> studies.....	47
4.5.1 Zymography (IV).....	47
4.6 Autoradiography.....	48
4.7 Histology and immunohistochemistry	49
4.8 Statistical analysis	51

5	RESULTS.....	52
5.1	Gelatinase (MMP-2/9) imaging in atherosclerosis (IV).....	52
5.1.1	Plaque size, inflammation, and gelatinase (MMP-2/9) activity.....	52
5.1.2	Tracer biodistribution, autoradiography, immunohistochemistry and in vivo PET/CT.....	52
5.2	Imaging of myocardial healing after MI.....	53
5.2.1	Histology and immunohistochemistry (I-III).....	53
5.2.2	In vivo stability of the tracers (I, III).....	53
5.2.3	PET/CT imaging (I, III).....	54
5.2.4	Ex vivo studies (I-IV).....	54
5.2.5	Autoradiography (I-IV).....	55
6	DISCUSSION.....	58
6.1	Animal models.....	58
6.1.1	LDLR ^{-/-} ApoB ^{100/100} atherosclerotic mice.....	58
6.1.2	Rat model of myocardial infarction.....	58
6.2	The evaluated PET tracers.....	59
6.2.1	⁶⁸ Ga-DOTA-E-[c(RGDfK)] ₂	59
6.2.2	⁶⁸ Ga-NOTA-HA-hexasaccharide-T ₆	60
6.2.3	⁶⁸ Ga-DOTA conjugated gelatinase (MMP-2/9) ligand.....	61
6.3	Future aspects.....	62
7	SUMMARY AND CONCLUSIONS.....	64
	ACKNOWLEDGMENTS.....	65
	REFERENCES.....	69
	ORIGINAL PUBLICATIONS.....	83

ABBREVIATIONS

AAR	Area at risk
ACE	Angiotensin converting enzyme
AMI	Acute myocardial infarction
Ang	Angiotensin
ANP	A-type natriuretic peptide
α SMA	Alpha smooth muscle actin
AT1R	Angiotensin 1 receptor
ARB	Angiotensin II type I receptor blocker
ARNI	Angiotensin receptor neprilysin inhibitors
ATP	Adenosine triphosphate
BPM	Beats per minute
BNP	B-type natriuretic peptide
CAD	Coronary artery disease
CFR	Coronary flow reserve
CMR	Cardiac magnetic resonance
COX	Cyclooxygenase
CRP	C-reactive protein
CT	Computed tomography
CTA	Computed tomographic angiography
CTGF	Connective tissue growth factor
CXCL	Chemokine ligand
DAMP	Danger-associated molecular pattern
DC	Dendritic cells
ECG	Electrocardiography
ECM	Extracellular matrix
EF	Ejection fraction
EMT	Epithelial to mesenchymal transition
FMCH	Fluoromethylcholine
FFR	Fractional flow reserve

Abbreviations

GDF	Growth differentiation factor
GLP	Glucagon-like peptide
HA	Hyaluronic acid, i.e., hyaluronan
HF	Heart failure
HFpEF	Heart failure with preserved ejection fraction
HFrfEF	Heart failure with reduced ejection fraction
HMGB1	High mobility group box 1 protein
HPLC	High-performance liquid chromatography
HSP	Heat shock protein
hsTnT	High sensitivity troponin
IFN	Interferon
IHD	Ischemic heart disease
IL	Interleukin
IMH	Intramyocardial hemorrhage
IPC	Ischemic preconditioning
I/R	Ischemia/reperfusion
LCA	Left coronary artery
LGE	Late gadolinium enhancement
LDL	Low density lipoprotein
LOX	Lipoxygenase
LVAD	Left ventricular assist device
LVEF	Left ventricle ejection fraction
LXA	Lipoxin
NEP	Neutral endopeptidase
NET	Norepinephrine transporter
MBF	Myocardial blood flow
MCS	Mechanic circulatory support
MI	Myocardial infarction
MIBG	Metaiodobenzylguanidine
MMP	Matrix metalloproteinase
MPTP	Mitochondrial permeability transition pore

Abbreviations

MRA	Mineralocorticoid-receptor antagonist
MRTF-A	Myocardin-related transcription factor
MVO	Microvascular obstruction
PCI	Percutaneous coronary intervention
PDGF	Platelet-derived growth factor
PET	Positron emission tomography
PRR	Pattern recognition receptors
PTX	Pentraxin
RAAS	Renin-angiotensin-aldosterone system
RAS	Renin-angiotensin system
RGD	Arginine-glycine-aspartate
RPC	Remote ischemic preconditioning
ROS	Reactive oxygen species
RR	Riva-Rocci, i.e., blood pressure
RT3DE	Real-time three-dimensional echocardiography
RV	Right ventricle
RvE	Resolvin E
SNS	Sympathetic nervous system
SPECT	Single-photon emission computed tomography
SR	Sarcoplasmic reticulum
STEMI	ST -segment elevation myocardial infarction
SUV	Standardized uptake value
TAC	Time-activity curves
Tcf21	Transcription factor 21
TFA	Trifluoroacetic acid
TGF- β	Transforming growth factor β
TLR	Toll-like receptors
TNF	Tumor necrosis factor
TRCP	Transient receptor potential channels
%ID	Percentage of injected dose

LIST OF ORIGINAL PUBLICATIONS

This thesis is based on following original publications:

- I. Max Kiugel, Ingrid Dijkgraaf, Ville Kytö, Semi Helin, Heidi Liljenbäck, Tiina Saanijoki, Cheng-Bin Yim, Vesa Oikonen, Pekka Saukko, Juhani Knuuti, Anne Roivainen, Antti Saraste. Dimeric [⁶⁸Ga]DOTA-RGD Peptide Targeting $\alpha_v\beta_3$ Integrin Reveals Extracellular Matrix Alterations after Myocardial Infarction. *Molecular Imaging and Biology* 2014 Dec;16(6):793-801
- II. Satish Jadhav, Meeri Käkälä, Jussi Mäkilä, Max Kiugel, Heidi Liljenbäck, Jenni Virta, Päivi Poijärvi-Virta, Tiina Laitala-Leinonen, Ville Kytö, Sirpa Jalkanen, Antti Saraste, Anne Roivainen, Harri Lönnberg, Pasi Virta. Synthesis and In Vivo PET Imaging of Hyaluronan Conjugates of Oligonucleotides. *Bioconjugate Chemistry*. 2016 Feb 17;27(2):391-403
- III. Max Kiugel, Ville Kytö, Tiina Saanijoki, Heidi Liljenbäck, Olli Metsälä, Mia Stähle, Johanna Tuomela, Xiang-Guo Li, Pekka Saukko, Juhani Knuuti, Anne Roivainen, Antti Saraste. Evaluation of ⁶⁸Ga-labeled peptide tracer for detection of gelatinase expression after myocardial infarction in rat. *Journal of Nuclear Cardiology*. 2016 Dec 2. [Epub ahead of print]
- IV. Max Kiugel, Sanna Hellberg, Meeri Käkälä, Heidi Liljenbäck, Tiina Saanijoki, Johanna Tuomela, Juhani Knuuti, Antti Saraste, Anne Roivainen. Evaluation of ⁶⁸Gallium-labeled peptide for the detection of metalloproteinase 2/9 expression in mouse atherosclerotic plaques. *Manuscript submitted for publication*

The original publications have been reprinted with the permission of copyright holders.

In the text, the publications are referred to by the Roman numerals I–IV.

1 INTRODUCTION

Ischemic heart disease (IHD) remains the leading cause of death worldwide regardless of the steady decline since the 1980s (Moran et al. 2014). While death toll caused by myocardial infarctions (MI) and related ischemic conditions has declined in Western countries, it has significantly increased in Eastern Europe and Asia, where, moreover, it is increasingly manifesting in relatively young individuals.

Coronary artery disease (CAD) caused by atherosclerosis of coronary arteries, is a slowly progressing disease characterized by inflammatory processes and cholesterol accumulation, which leads to narrowing of the coronary arteries. The process begins already in early childhood through intracellular lipid accumulation within artery walls. Over decades, the lesions progress into atheromas and subsequent formation of a fibrotic cap of smooth muscle cells and collagen.

Vulnerable atherosclerotic plaques, characterized by inflammatory activity and a thin fibrous cap, are particularly precarious due to their high risk of rupture. Acute myocardial infarction (AMI), a sudden and significant loss of viable cardiomyocytes, is typically a result of sudden coronary artery thrombosis caused by this kind of ruptured atherosclerotic plaque, rather than extensive narrowing of the coronary lumen (Libby 2012, Buja et al. 2016). Coronary occlusion causes sudden, severe and prolonged ischemia leading to loss of viable tissue.

Cardiac regenerative capacity cannot cover such sudden massive loss of cardiomyocytes, which are terminally differentiated cells with a very limited regenerative potential. Thus, the formation of collagenous scar is necessary to replace these perished cells. Cardiac repair after MI is a complex process that can be roughly divided in three overlapping phases, i.e., the inflammatory, proliferative, and maturation phases (Chen et al. 2017). The entire process usually takes at least 5–6 weeks (Thygesen et al. 2012).

IHD is also the most common cause of heart failure (HF). Treatment of AMI has improved and mortality has significantly declined over the past decades (Velagaleti et al. 2008). Consequently, this has led to an increased burden of progressive HF, that is, heart dysfunction resulting in insufficient blood supply for the metabolic needs of an organism. HF is a persistent problem developing soon after myocardial infarction in almost 25% of surviving patients, with numbers increasing over time (Hellermann et al. 2005, Velagaleti et al. 2008). Worldwide, 2–7% of patients die during their first admission with congestive HF. The subsequent mortality rate is 17–45% within one year of admission and >50% within five years (Dick et al. 2016).

The pathogenesis of adverse cardiac remodeling leading to HF is a combination of geometric, cellular and molecular alterations involving both infarcted and remote, non-infarcted myocardium (Chen et al. 2016). These changes occur due to either insufficient compensatory mechanisms or their inability to compensate for the loss of myocardial tissue, leading to changes, such as excess hypertrophy of surviving cardiomyocytes and excess reactive fibrosis.

Cardiac imaging is a useful tool for HF diagnosis, both for the demonstration of dysfunction and the underlying structural disease, as well as its etiology and molecular mechanisms. Positron emission tomography (PET) has become increasingly available, and nuclear cardiology has also benefited significantly from modern hybrid devices that combine PET imaging with computed tomography (CT) or magnetic resonance imaging (MRI).

Advancements in imaging technologies have led to evolution beyond isolated visualization of myocardial perfusion, toward the characterization of detailed molecular processes (Saraste et al. 2017), which may present an opportunity to predict the development of HF in very early stages, thus allowing for tailored therapies with a significant effect on the outcome. Molecular HF imaging strategies aim to detect the underlying processes, such as adverse inflammation, angiogenesis, extracellular matrix remodeling, reactive fibrosis and autonomic nerve damage. Thus, specific probes that are able to detect these specific molecular mechanisms are of great interest and demand.

2 REVIEW OF LITERATURE

2.1 Ischemic heart disease

Ischemia (ισχαιμία) is a Greek word referring to restriction of blood supply to the tissue. The restricted blood supply results in oxygen deficiency in tissues, causing anaerobic metabolism, tissue damage and necrosis. Different tissues have significantly variable ischemia endurance, from a couple of minutes (nervous tissue) to several hours (bone), as well as varying recovery capacity. Ischemic heart disease (IHD) is a broad term referring to conditions characterized by reduced blood supply to myocardial tissue, including both causes and consequences. IHD begins with atherosclerotic plaque formation in coronary arteries, which gradually leads to the narrowing of coronary lumen and subsequent blood flow insufficiency, causing angina pectoris (myocardial ischemia induced chest pain). Coronary thrombosis (occlusion or blockage of blood flow within a vessel caused by clotted blood) can lead to prolonged ischemia, resulting in myocardial infarction (MI), that is, a sudden, significant, and irrecoverable loss of viable cardiomyocytes. The surviving viable myocardium is later prone to cardiac remodeling, which compensates for the loss of functional tissue, and often progresses to heart failure.

2.1.1 *Atherosclerosis and coronary artery disease*

Atherosclerosis is a disease of the intima layer of arteries affecting mostly large and middle-sized vessels, especially the branching regions with non-laminar blood flow, which are most susceptible to endothelial dysfunction (Gimborne et al. 2016). The most prominent features of atherosclerosis are macrophage mediated inflammation and low-density lipoprotein (LDL) cholesterol influx into intima. The main risk factors contributing to atherosclerosis include age, male gender, dyslipidemia, hypertension, smoking, diabetes, and genetic background. Both innate and adaptive immunity contribute to atherosclerosis and most of the processes are either contributing to LDL influx or are a result of excess LDL within the lesions. Thus, inflammation is an important factor both in early atherosclerosis and its clinical complications (Gisterå et al. 2017, Hansson et al. 2015). The process begins by the appearance of fatty streaks (i.e., intracellular lipid accumulation). Over years or decades, the lesions progress into atheromas characterized by extracellular lipid cores and fibrotic cap formation by smooth muscle cells and collagen.

Coronary artery disease (CAD) is caused by atherosclerotic lesions within the coronary arteries. Atherosclerosis in coronary arteries remains asymptomatic for decades. At a later stage, the significant blood flow reduction results in myocardial ischemia. The slow narrowing of coronary arteries and reversible ischemia allow for limited adaptation of myocardial tissue (ischemic preconditioning) and growth of collateral blood vessels. In addition to the slow artery narrowing and decrease in blood flow, a plaque can rupture, thus causing acute occlusion of a coronary artery. Myocardial infarctions are typically a result of this kind of rupturing of atherosclerotic plaque.

2.1.2 Inflammation and plaque vulnerability

The degree of coronary stenosis as such is a poor predictor of plaque vulnerability. Rather, the possibility of clinical complications is determined by plaque morphology and immunologic activity. Vulnerable plaques often have a large, lipid-rich nucleus and a thin ligament cap prone to rupture or erosion, thereby exposing the lipid core and causing thrombosis. On cellular level, this means increased cholesterol influx, activation of inflammatory cells (i.e., monocytes, macrophages, foam cells, lymphocytes, dendritic cells, mast cells and neutrophils), smooth muscle cell apoptosis, necrotic core expansion, microcalcifications, and neovascularization (Hansson et al. 2015).

2.1.3 Gelatinase (MMP-2 and MMP-9) activity in atherosclerosis

Matrix metalloproteinases (MMPs) are a major pathophysiologic factor in atherosclerosis. MMPs are a group of zinc-containing endopeptidases, which degrade extracellular matrix (ECM) components, such as collagen, elastin, gelatin and casein (Bäck et al. 2010). The MMP family is today thought to contain approximately 23 genetically related human proteins (Newby 2012). Gelatinases A and B (MMP-2 and MMP-9) have been shown to be robustly expressed in atherosclerotic plaques as compared to the healthy regions of the vessel wall (Bäck et al. 2010, Kieffer et al. 2001), and may contribute to plaque vulnerability (Bäck et al. 2010).

Catalytic MMP activity is regulated at four points: gene expression, compartmentalization, zymogen activation and enzyme activation (Bench et al. 2011, Newby 2008). Gelatinases are secreted by several vascular cell types, such as endothelial cells, fibroblasts and myofibroblasts, monocyte-derived macrophages and local-tissue macrophages (Hopps et al. 2012, Bourbolia et al.

2010). Gelatinases MMP-2 (Newby 2012, Welgus et al. 1990) and MMP-9 (Newby 2012) are especially expressed in macrophages after differentiation. In contrast to MMP-2, which is constantly expressed on cell surface, MMP-9 is stored in secretory granules of the abovementioned cells and its expression is triggered by exogenous stimuli, such as cytokines, growth factors and altered cell-matrix contacts (Hopps 2012). Human MMP-9 has several functional genetic polymorphisms, and numerous studies have been conducted on the role of these polymorphisms in enzymatic activity and correlation with adverse cardiac events (Abillera et al. 2006).

MMP-9 associates strongly with overall plaque instability (Chen 2005) and, more specifically, interplaque hemorrhage in advanced atherosclerotic plaques (de Nooijer et al. 2006). MMP production can cause plaque rupture through the destruction of ECM (Newby 2005) or by promoting death of macrophages (Newby 2012, Johnson et al. 2006) and smooth muscle cells (Newby 2006). However, controlled ECM remodeling is essential for the migration and proliferation of smooth muscle cells, which is important for fibrous cap thickening and plaque stability. These opposing actions prevent using of broad-spectrum target molecules or inhibitors for therapy (Johnson et al. 2006, Prescott et al. 1999) and imaging. Selective molecules, however, have been designed (Newby 2012). Gelatinase actions in atherosclerotic plaque pathobiology are visualized in Figure 1.

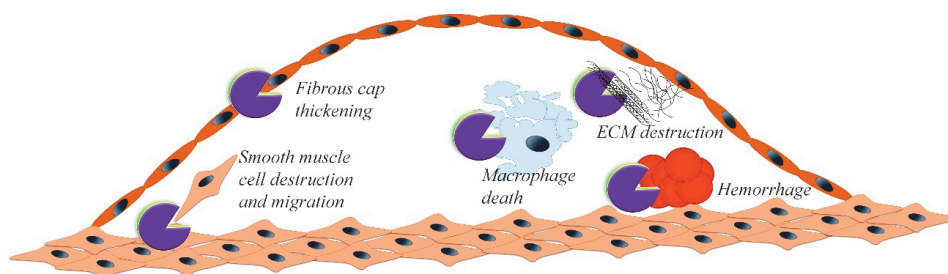


Figure 1. Actions of gelatinases (MMP-2 and MMP-9) in atherosclerotic plaque pathobiology.

In clinical trials, MMP-9 activity has been found to be associated with carotid plaque vulnerability. Instability was visualized with ultrasound as a markedly irregular or ulcerated surface, or a hypodense or heterogeneous structure (Tan et al. 2014). Plaque vulnerability was also detected retrospectively, in the form of a thin fibrous cap and/or recent intraplaque hemorrhage on histology (Silvello et al. 2014), as well as indicated by a previous stroke or peripheral vascular disease (Silvello et al. 2014). MMP-9 does not only affect the thinning of the fibrotic cap around the lipid core, but it also contributes strongly to the overall atherosclerotic process (Nenseter et al. 2013). A higher quantity of circulating MMP-9 in CAD patients seems to predict cardiovascular mortality (Nenseter et al. 2013, Servello et al. 2014). Elevated circulating levels of MMP-2/9 are also strongly associated with

the development of an acute MI, rather than stable angina as the initial clinical presentation of CAD (Hlatky 2007). In addition, genetic polymorphisms of MMP-9 contribute to the overall risk of cardiovascular events (Niu et al. 2012). The proteolytic activity of MMPs can be suppressed by tissue inhibitors of matrix metalloproteinases (TIMPs) (de Vries et al. 2012, Nagase et al. 2006). Downregulation of MMP-2 and MMP-9 has been shown to contribute to elevated collagen amounts in apoE^{-/-} mice plaques, resulting in the stabilization of the lesions (Lu et al. 2011).

2.1.4 Myocardial ischemia

Under normal conditions, fatty acid oxidation provides 60–90% of energy required for myocyte contraction. The rest is generated by pyruvate oxidation (derived from glycolysis and lactate oxidation), as well as the direct oxidation of lactate, ketone bodies and amino acids. Cardiac metabolic network is highly flexible, using abundantly available substrates, and nonischemic heart is a net consumer of lactate even under conditions of near-maximal cardiac power (Stanley et al. 2005, Kolwicz et al. 2013). Myocardial ischemia is a result of insufficient supply of blood and oxygen, most commonly caused by the narrowing of coronary arteries. Under ischemic conditions, myocyte metabolism shifts towards anaerobic glycolysis (i.e., transformation of glucose to lactate with a limited supply of oxygen), which results in insufficient muscle cell contractility, lactate accumulation, acidosis and cell swelling (Buja et al. 2016). The activation of various enzymes, such as phospholipases and proteases, and accumulation of toxic metabolites result in cell membrane damage. The process involves loss of function in membrane channels and ion pumps, progressing from mild alterations to severe ionic disturbances including uncontrolled Ca²⁺ influx. Ischemic cardiomyocyte injury is a hybrid form of cell injury comprising apoptotic, autophagic, necrotic and necroptotic components (Kalogeris et al. 2012) dominated by oncosis (i.e., cell death with swelling) (Buja et al. 2016, Weerasinghe et al. 2012). Both the degree to which blood flow is reduced and the duration of the ischemic period influence the extent of cell dysfunction, injury, and/or death (Kalogeris et al. 2016). Ischemia is considered reversible if it remains at a level that does not lead to cardiomyocyte death, thus enabling the myocardial tissue to recover.

2.1.5 Acute myocardial infarction

Acute myocardial infarction (MI) is defined as myocardial necrosis in a clinical setting, consistent with acute myocardial ischemia (Thygesen et al. 2012).

Diagnostic criteria for acute MI include rise and/or fall of circulating cardiac biomarker [preferably cardiac troponin (cTn)] values, in tandem with either symptoms of ischemia, pathological changes in ECG, or imaging evidence of an intracoronary thrombus, new loss of viable myocardium or new regional wall motion abnormality (Thygesen et al. 2012). Acute MI is typically a result of sudden coronary artery thrombosis caused by ruptured atherosclerotic plaque, rather than extensive narrowing of the coronary lumen (Libby 2012, Buja et al. 2016). This causes prolonged ischemia. Irreversible injury appears in approximately 20 minutes in papillary muscle and endocardium, moves progressively into mid-myocardium (60–90 min.) and forms full transmural infarction within 3 to 4 hours (Reimer et al. 1977 and 1979). Complete necrosis of myocardial cells at risk requires 2–4 hours or longer, depending on the presence of collateral circulation, persistency of coronary arterial occlusion, sensitivity of the myocytes to ischemia, and individual demand for oxygen and nutrients, as well as possible pre-conditioning (i.e., interruptions of sufficient oxygenation prior to MI) (Thygesen et al. 2007 and 2012). Cardiac regenerative capacity cannot cover massive sudden loss of cardiomyocytes. This results in the formation of a fibrotic collagenous scar over time. Diagnostic criteria for prior myocardial infarction are either pathological Q waves with or without symptoms or imaging evidence of a region of loss of viable myocardium that is thinned and fails to contract, both in the absence of a non-ischemic cause (Thygesen et al. 2012).

Ischemia/reperfusion injury (I/R)

Reperfusion restores the delivery of oxygen and substrates required for aerobic ATP synthesis and normalizes intracellular pH by washing out the accumulated H⁺ (Buja et al. 2016). However, reperfusion itself also induces myocardial injury, causing four types of cardiac dysfunction (Yellon and Hausenloy 2007): (1) myocardial stunning (i.e, prolonged wall motion abnormality) (Bolli and Marbán 1999), (2) the no-reflow phenomenon (i.e., lack of reperfusion in the ischemic area after the removal or bypass of physical obstruction) (Ito 2006), (3) reperfusion arrhythmias (Manning and Harse 1984) and (4) a lethal reperfusion injury accelerating the development of necrosis (Jennings et al. 1960). The mechanisms of lethal reperfusion injury are in many ways paradoxal (Yellon and Hausenloy 2007), including oxidative stress and formation of reactive oxygen species (ROS), excess intracellular and mitochondrial Ca²⁺, excessively fast restoration of pH, and rapid influx of leukocytes recruited by signal molecules during acute ischemia. More specifically, fast restoration of pH enables fast formation of mitochondrial permeability transition pores (MPTPs) in ATP-depleted tissue, leading to irreversible mitochondrial damage and cell necrosis (Cohen and Downey 2011).

2.1.6 Cardiac repair

Cardiomyocytes are terminally differentiated cells with a very limited regenerative potential. Thus, the formation of collagenous scar is necessary to replace the perished cells in case of MI. Cardiac repair is a complex process that can be roughly divided in three overlapping phases: (1) The inflammatory phase (0–4 days in murine models) is characterized by acute inflammation and immune cell recruitment, tissue digestion and phagocytosis. The initial response is followed by (2) the proliferative phase (4–14 days), in which the neurohormonal activation, mechanical stress and myofibroblast activation lead to inflammatory response resolution, wound healing and neovascularization (Prabhu et al. 2016). Finally, during (3) the maturation phase (>14 days) (Chen et al. 2017), extracellular matrix is crosslinked to form a collagen-rich scar, microvessels are coated with pericytes, and excess myofibroblasts undergo apoptosis. The entire process leading to a healed infarction in humans usually takes at least 5–6 weeks (Thygesen et al. 2012).

Inflammatory phase

Ischemic cardiomyocyte necrosis and ECM degradation release various endogenous ligands (Arslan et al. 2011, Chen et al. 2017), such as IL-1 α (Lugrin et al. 2015), high mobility group box 1 protein (HMGB1) (Herzog et al. 2014), S100 group proteins (Rohde et al. 2014), fibronectin (Arslan et al. 2011b, Trial et al. 1999), heat shock proteins 60 and 70 (HSP60/70) (Li et al. 2011, Prabhu et al. 2016), hyaluronan (hyaluronic acid, HA) (Huebener et al. 2008), uric acid (Mann 2015) and extracellular RNA (Chen et al. 2014). These danger-associated molecular patterns (DAMPs) (Arslan et al. 2011b) bind to pattern recognition receptors (PRRs), most notably Toll-like receptors (TLRs), and activate proinflammatory cascades in various cell types, such as remaining cardiomyocytes, endothelial cells, fibroblasts, mast cells, cardiac macrophages and infiltrating leukocytes. This local inflammatory reaction induces systemic immune response (Dutta et al. 2015) by releasing various cytokines and chemokines, which are a hallmark of the inflammatory phase in cardiac repair.

Chemokines, especially chemokine (C-X-C motif) ligand 8 / interleukin 8 (CXCL8/IL-8) (Kukielka et al. 1995), attract circulating neutrophils, which are subsequently captured by selectin action to roll along endothelium. The adhesive interaction is further strengthened by adhesion molecules (Detmers et al. 1990), and integrin activation (Herter and Zarbock 2013) within the neutrophils. This interaction propels the neutrophils to crawl towards endothelial junctions and transmigrate between pericytes (Prabhu et al. 2016). The transmigrated neutrophils amplify the immune response by producing cytokines, ROS, and a wide range of

proteolytic enzymes, such as serine proteases and MMPs. This inflicts direct injury to endothelial cells (Arslan et al. 2011a) and viable cardiomyocytes (Entman et al. 1992), while also contributing to the removal of cellular and matrix debris (Kain et al. 2014).

Mast cells are potent primary inflammatory mediators triggering cytokine cascades. Rapid mast cell degranulation during myocardial ischemia is also an important source of tumor necrosis factor α (TNF- α), histamine and tryptase (Somasundaram et al. 2005).

Monocytes are recruited to the site of injury in two major waves (proinflammatory and anti-inflammatory) with the subsets of the earlier phase potent proinflammatory and phagocytic macrophages (M1), and the later phase reparative macrophages (M2), which play a crucial role in either orchestrating (M1) or regulating (M2) the overall inflammatory response (Nahrendorf et al. 2007). These two major macrophage subpopulations with their different functions represent extremes of a continuum in the assortment of activation states. These cells are characterized by their expression of cell surface markers, secreted cytokines and chemokines, as well as transcription and epigenetic pathways (Zhou et al. 2014).

Lymphocyte subpopulations also have distinct roles in orchestrating the inflammatory response and regulation of cardiac repair, such as recruitment of proinflammatory monocytes (Zouggari et al. 2013), cytotoxic actions (Varda-Bloom et al. 2000), microvascular occlusion and reperfusion injury (Boag et al. 2015), as well as in contributing to inflammatory resolution (Chen et al. 2017). Pro- and anti-inflammatory monocyte and macrophage subtypes have been proposed to be the balancing forces in the complex and tightly regulated process of post-infarct inflammatory response (Rischpler et al. 2016).

Proliferative phase

Adequate resolution of the inflammatory repair phase is an active process that depends on multiple pathways and the proper cellular function of regulatory T cells, apoptotic neutrophils and transition towards inhibitory monocyte-macrophage subpopulations driven by dendritic cells (Anzai 2012). Molecular anti-inflammatory modulators include inhibitory cytokines, such as transforming growth factor β and interleukin 10 (TGF- β & IL-10), pentraxin-3 (Frangogiannis 2012) and lipid modulators, such as lipoxins, resolvins, protectins and maresins (Kain et al. 2014). The process results in the negative regulation of toll-like receptor (TLR) and cytokine signaling, termination of chemokine signaling and suppression of leukocyte adhesion cascades.

The proliferative phase of cardiac repair is characterized by dynamic alteration in the extracellular matrix regulating cellular functions (Prabhu et al. 2016) and causing cardiac fibroblast proliferation and differentiation into myofibroblasts (Turner et al. 2013). Myofibroblasts possess a more contractile and synthetic phenotype than regular fibroblasts, enabling them to effectively repair and remodel the cardiac interstitium after the local necrosis caused by MI (Turner et al. 2013). Myofibroblasts are not present in healthy myocardium, but they are the most prevalent cell type in the infarct scar, and, due to their specialized characteristics, the main effectors of fibrogenesis (Turner et al. 2013, Peterson et al. 1999). Myofibroblasts secrete high levels of MMPs and other extracellular ECM degrading enzymes that facilitate fibroblast migration, and contribute to the deposition of collagen and other ECM proteins, leading to scar formation (Travers et al. 2016). The cellular origins and actions of myofibroblasts are visualized in Figure 2.

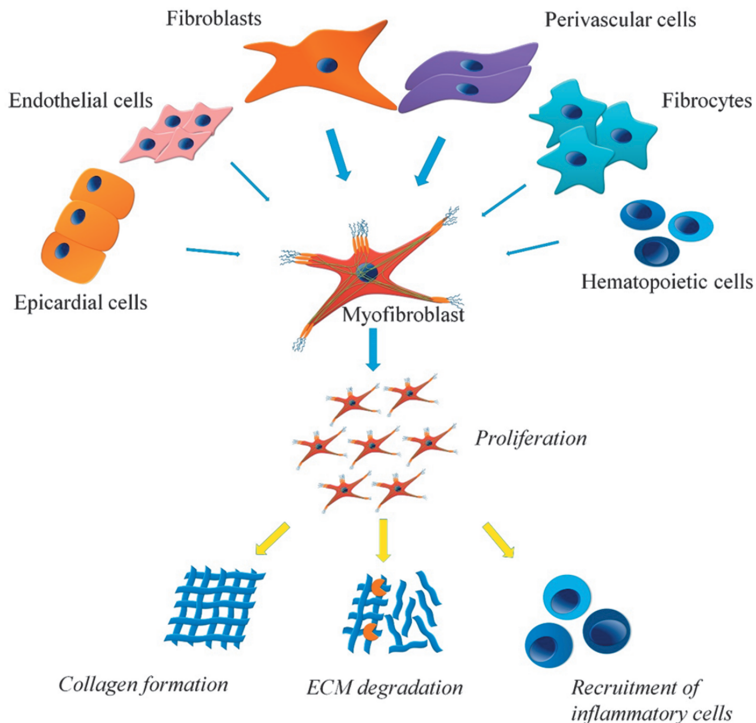


Figure 2. Cellular origins and action of myofibroblasts. (Modified from Travers et al. 2016)

The specific characteristics of myofibroblasts include increased expression of contractile proteins (including α -smooth muscle actin [α SMA] and the embryonic isoform of smooth muscle myosin), adhesion proteins (such as tensin and α v β ₃ integrin), cell surface receptors (such as TGF- β type II receptor and angiotensin AT1 receptor), structural ECM proteins (collagen I, collagen III and fibronectin)

and matricellular proteins (Turner et al. 2013, Prabhu et al. 2016, van den Borne et al. 2010).

In addition to the surviving local fibroblasts and circulating bone marrow progenitors (Prabhu et al. 2016), cells from proximal viable areas also seem to be recruited to undergo myofibroblast transdifferentiation. These cell types include endothelial cells (Zeisberg et al. 2007), as well as epicardial epithelial cells and pericytes (Hinz et al. 2007). The exact origin of myofibroblasts and the differentiating paths remain debated (Prabhu et al. 2016). There is also evidence of different functional roles of myofibroblast subsets that are determined by cellular origin and external regulation (Turner et al. 2013). A recent study showed Tcf21-expressing resident fibroblasts to be the primary source of myofibroblasts in mice and suggested the expression of periostin to be a general marker for myofibroblast subpopulations (Kanisicak et al. 2016). The exact type of cardiac injury may also induce different populations of cells to become myofibroblasts (Braitsch et al. 2013). Overall, myofibroblasts remain a poorly defined cell type regarding their origins and exact functions *in vivo* (Kanisicak et al. 2016)

The highly plastic ECM network serves as a scaffold for cellular proliferation and facilitates the dynamic action of signal molecules. Damaged ECM is enriched through the deposition of several members of the matricellular protein family that are significantly upregulated in the infarcted heart. Matricellular proteins are irrelevant in the mechanical support, but may bind to matrix proteins and cell receptors that direct the signaling cascades (Prabhu et al. 2016).

Other prompt mediators involved in myofibroblast activation are the TGF- β family (particularly TGF- β 1) and renin-angiotensin-aldosterone system (RAAS); particularly angiotensin II (Ang II) seems to be the predominant effector of cardiac fibrosis development (Travers et al. 2016). Important mediators of myofibroblast function also include endothelin, RhoA-MRTF-SRF signaling pathway, transient receptor potential channels (TRPCs), connective tissue growth factor (CTGF), platelet-derived growth factor (PDGF), integrins, interferones, adrenergic signaling (Travers et al. 2016), fibronectin extra domain A splice variant (FN-ED-A), myocardin-related transcription factor A (MRTF-A), as well as a wide range of microRNAs (Turner et al. 2013).

Hemodynamic overload and cardiac remodeling increase the synthesis and secretion of natriuretic peptides A and B (ANP and BNP) in the myocardium. These peptides regulate a number of key elements associated with cardiac fibrosis, such as TGF- β 1 and ET-1, transcription factor GATA4, and local RAAS (Kerkelä 2015). In addition to reducing blood pressure, cardiac hypertrophy, and fibrosis, NP signaling may also contribute to angiogenesis (Kerkelä 2015). Recombinant

BNP treatment has been shown to induce a dose-related decrease in pulmonary-capillary wedge pressure in patients with HF (Szabo et al. 2014).

Maturation phase

The final stage of the infarct healing process is characterized by the clearance of matricellular proteins and cross-linking of ECM, resulting in the formation of a dense collagenous scar. Reparative cells are inactivated and/or undergo apoptosis, and the fibrogenic growth factor (including TGF- β and AngII) signaling is terminated. Myofibroblast density in the scar and in the infarct border is significantly decreased. Exact proapoptotic molecules, as well as the inhibitory signaling for the termination of fibrogenic activity remain unknown (Prabhu et al. 2016).

2.1.7 Adverse remodeling and heart failure

Heart failure (HF) is a clinical syndrome (Dick et al. 2016) defined as heart dysfunction leading to insufficient blood supply for the metabolic needs of an organism that causes symptoms (Urmaliya et al. 2016). HF can be associated with a wide variety of left ventricle (LV) functional abnormalities resulting in the inability of the heart to fill with or eject blood (Urmaliya et al. 2016).

Patients surviving an initial MI remain at risk of developing progressive HF due to adverse post-infarct remodeling. Inadequate remodeling is dependent not only on the initial size of infarct, but also on specific characteristics of the reparative response. The pathogenesis of adverse cardiac remodeling leading to HF involves a combination of geometric, cellular and molecular alterations in both the infarcted and the remote, non-infarcted myocardium (Chen et al. 2016). These changes occur due to either insufficient compensatory mechanisms, or their inability to compensate for the loss of myocardial tissue, thereby leading to changes, such as excess hypertrophy of surviving cardiomyocytes and excess reactive fibrosis.

Adverse inflammation

Inflammatory response to MI injury is extraordinarily complex. Adequate inflammatory response is essential for infarct healing, yet there are numerous steps at which genetic, epigenetic, or environmentally modulated changes of molecular expression and/or activities can occur, augmenting the intensity or prolonging the duration of inflammatory responses, thus predisposing to adverse LV remodeling (Westman et al. 2016).

Inadequately elevated levels of inflammatory mediators, including TNF- α and other pro-inflammatory cytokines (Mann 2015) and alarmins, persistence of pro-inflammatory monocytes, dendritic cells (DCs), T cells and M1 macrophage populations, as well as insufficient transition toward M2 polarization are among the factors that predispose to LV remodeling and adverse outcome (Anzai et al. 2013, Prabhu et al. 2016). In addition to acting as an inflammatory marker, C-reactive protein (CRP) may also be directly involved in the worsening of pathological condition by amplifying the inflammation and promoting the renin-angiotensin system (RAS) and oxidative stress (Anzai 2013).

The proinflammatory monocyte (CD14⁺/CD16⁻) increase in blood during the early phase of ST segment elevation myocardial infarction (STEMI) has a negative correlation with the degree of cardiac functional recovery (Anzai 2013). Moreover, activated mononuclear splenocytes recruited to the failing heart in order to promote apoptosis and fibrosis, contribute to LV dysfunction (Prabhu et al. 2016).

Adverse myofibroblast activity

Myofibroblasts have a dual role depending on their prevalence and spatial location in the remodeling process. They play key roles in post-MI recovery, but also in adverse cardiac remodeling, fibrosis and progression to HF. While myofibroblasts do not have similar contractile capabilities as cardiomyocytes have, their function is essential for a robust scar formation, and the prevention of further contractile dysfunction of viable myocardium. Low myofibroblast density in the infarct area results in a poorly structured, expansive and vulnerable scar, which is prone to rupture. This leads to systolic dysfunction and subsequent adverse myocardial remodeling (Turner et al. 2013).

Activation of matrix-producing myofibroblasts is a key event in tissue fibrosis (Gabbiani 2003, Frangogiannis 2016). Neurohumoral mediators, cytokines, and growth factors directly stimulate a fibrogenic program, triggering myofibroblast conversion and stimulating the synthesis of large amounts of structural matrix proteins in injured and remodeling tissues (Frangogiannis 2017). Fibronectin deposition in the pressure-overloaded heart may be involved in myofibroblast transdifferentiation and has been implicated as an important mediator in pathological cardiomyocyte hypertrophy (Konstandin et al. 2013). Overall, excessive myofibroblast activity, particularly in the remote, non-infarcted myocardium, drives fibrosis and myocardial stiffness, resulting in contractile dysfunction, arrhythmias and HF progression (Turner et al. 2013). The effects of myofibroblast density on post-MI remodeling are visualized in Figure 3.

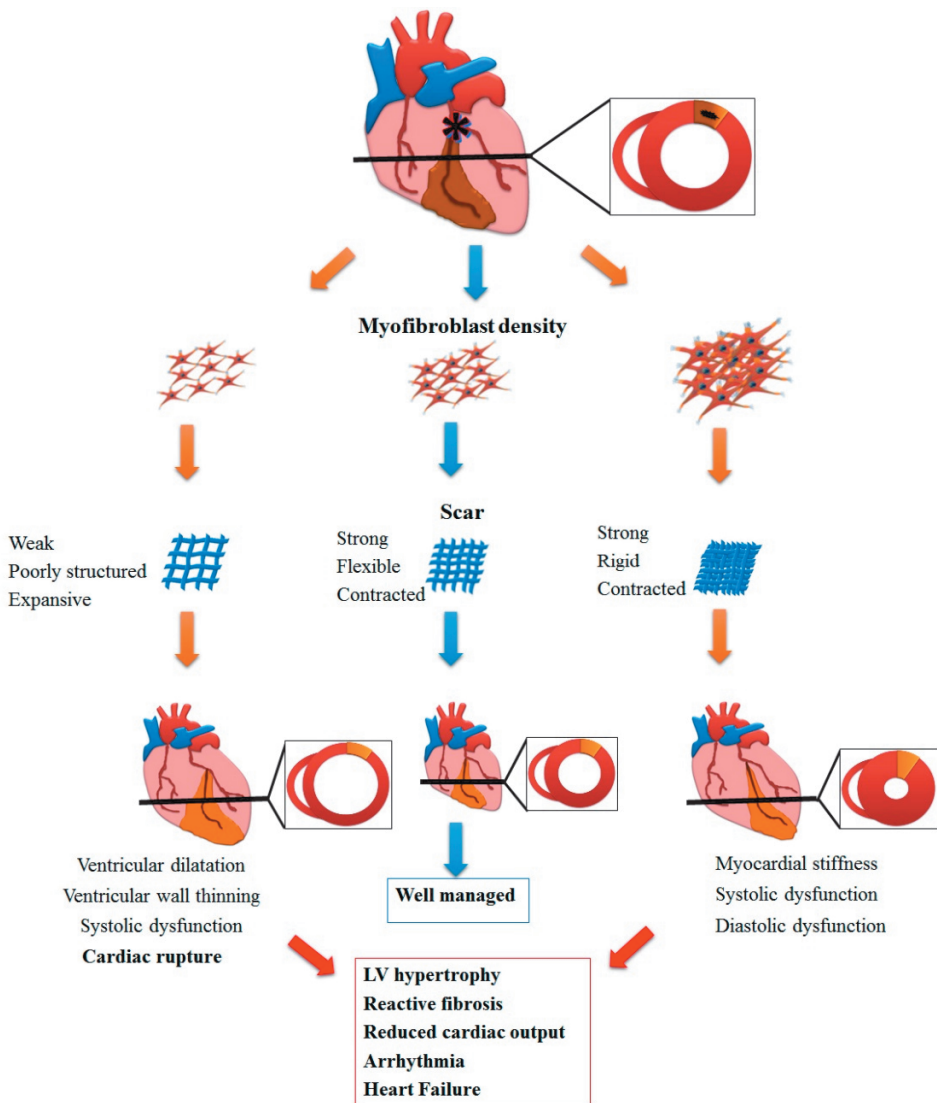


Figure 3. Effects of myofibroblast density on post-MI remodeling. (Modified from Turner et al. 2013)

Neurohormonal activation

Activation of the sympathetic nervous system (SNS) is a hallmark of heart failure and counteracting therapies are associated with improved survival. The parasympathetic and sympathetic cardiovascular regulation balance shifts in response to increased end-diastolic pressure or decreased stroke volume during the onset of LV systolic dysfunction. Decreased cardiac output in patients with HF results in the discharge of high-pressure baroreceptors in the LV, carotid sinus, and aortic arch. This generates signals to the central nervous system (CNS), leading, in turn, to the activation of efferent SNS pathways that innervate the heart, kidney, peripheral vasculature, and skeletal muscles. Afferent signals to the CNS also

stimulate the cardioregulatory centers in the brain that stimulate the release of arginine vasopressin from the posterior pituitary (Nohria et al. 2004, Hartupee et al. 2017). Balance may be re-established initially, but as HF progresses, central neural networks transform and ordinarily dormant autonomic reflexes are activated. Regardless of the etiology of HF, the net result is vagal attenuation and, over time, progressively pathological augmentation of sympathetic outflow and catecholamine release (Floras et al. 2015).

Ang-II has been described as the most important effector peptide of the RAS (Achard et al. 2001), with an essential physiological role in vasoconstriction, regulation of salt homeostasis, kidney function, and blood pressure, as well as pathological hypertension. Expression of Ang-II is not restricted to circulation, and it is locally generated in multiple tissues (Achard et al. 2001). The RAAS components; renin, angiotensin converting enzyme (ACE), angiotensin-I (Ang-I), angiotensin II (Ang-II), as well as angiotensin II receptors, have been found in various tissues including kidney, lungs, adrenal glands, blood vessels and in discrete brain regions (Chai et al. 1993). Cardiomyocyte stretch triggers the production of ACE and Ang-I, hence Ang-II (van Wamel et al. 2001, de Haas et al. 2014). Ang-II is both expressed and activated by macrophages and myofibroblasts (Sun et al. 1994). Studies show that Ang-II drives cardiac fibrosis via inducing collagen growth. This is driven by the way of activating TGF- β through angiotensin 1 receptor (AT1R), and extracellular signal-regulated kinase through an interleukin 6 (IL-6) dependent mechanism (Leask et al. 2015). Interestingly, IL-6 knockout mice are also resistant to adverse cardiac inflammation (González 2015). Ang-II also induces endothelin 1 (ET-1) through extracellular signal-regulated kinase, ROS, and transcription factors (Weng et al. 2014). The physiologically active ET-1 isoform is a powerful mitosis-driving factor and vasoconstrictor (Leask et al. 2015). Through the endothelin A (ETA) receptor, it also increases collagen production in cardiac fibroblasts (Hafizi et al. 2004). ET-1 is predominantly produced by endothelial cells, but also by macrophages, cardiomyocytes, and fibroblasts (Chen et al. 2000).

Calcium overload

Calcium overload in HF is a crucial mediator of cell death and the development of malignant arrhythmias. Due to the dysregulation of cardiac sarcoplasmic reticulum (SR) proteins, calcium ATPase activity becomes insufficient, resulting in impaired containment of Ca^{2+} in SR and Ca^{2+} overload in cytoplasm during diastole. Other abnormalities also develop in SR calcium channels that cause continuous Ca^{2+} leak and further increase cytoplasmic calcium overload (Braunvald 2013, Terentyev et al. 2016, Kramer et al. 2017).

Mitochondrial abnormalities

Strong evidence exists for mitochondrial hyperplasia in the failing heart, reduced organelle size, and structural failures along the inner membranes. Excessive production of ROS leads to inefficiency in electron transfer, and thus, in oxidative phosphorylation. This makes mitochondria in the failing heart unable to respond with sufficient ATP production during the periods of increased energy demand. Dysfunctional mitochondria also release cytochrome c into the cytosolic compartment of the cell, an event that will activate the apoptosis program (Kramer et al. 2017).

Table 1. Factors contributing to myocardial recovery after MI

Phase	Inflammatory	Proliferative	Scar maturation	Progressive HF
<i>Time frame*</i>	0-4 days	4-14 days	>14 days	Weeks – months
<i>Signaling pathways</i>	ROS, IL-1 β , IL-6, IL18, IFN- γ , TNF- α , NOS2, IL-12 α , CD206 ^{low} , HSP60, LOX, COX, MMPs, other DAMPs, ...	IL-10, TGF- β , LXA4, Ang-II, RvE, VEGF, fibronectin, tryptase, arginase-1, eicosanoids, ...		<i>Persistent inflammatory and fibrogenic pathways</i>
<i>Active cells</i>	-Injured cardiomyocytes and epicardial cells -Neutrophils -Ly6C ^{hi} monocytes -M1 macrophages -Mast cells -Lymphocytes	-Myofibroblasts -Apoptotic neutrophils -Ly6C ^{lo} monocytes -M2 macrophages -Dendritic cells -Regulatory T-cells -Stem cells	-Pericytes -M2 macrophages	-Ly6C ^{hi} monocytes -M1 macrophages -Dendritic cells -T-cells
<i>Tissue level effects</i>	-Acute inflammation -Immune cell recruitment -Tissue digestion ROS, etc.	-Inflammatory regulation and resolution -ECM degradation -Angiogenesis -Collagen formation	-Matrix crosslinking -Myo- /fibroblast apoptosis -Scar maturation -Microvessel coating -Homeostasis resurgence	-Cardiomyocyte hypertrophy -Reactive fibrosis

*Time frames according to murine models (Prabhu et al. 2016).

Table 1 presents a summary of the signaling pathways, active cells, and tissue level effects in the inflammatory, proliferative, scar maturation, and progressive HF phases as discussed above.

2.1.8 Role of CD44, integrins and gelatinases

Integrins

Integrins are transmembrane receptors forming connections between cells and ECM and, in some cases, also cell-to-cell interactions. Their prime function is to couple the ECM to the cytoskeleton inside the cell. Integrin receptors are obligate heterodimers, composed of two different chains, termed α and β subunits. Each subunit has several variations, which form 24 different heterodimer combinations (Chen et al. 2015).

Integrin expression can be distinct on specific cell types and can vary depending on the developmental or pathological state. In addition, specific integrin receptors can bind to one or several ligands, and a single receptor ligand can be bound by several integrin heterodimers. Cardiac myocytes, fibroblasts and endothelial cells significantly increase integrin expression after MI. Integrins are involved in the TGF β activation, epithelial to mesenchymal transition (EMT) regulation, AngII synthesis, and the regulation of MMP activity. Thus, they are essential in the cellular conversion into myofibroblasts (Chen et al. 2015).

In particular, $\alpha_v\beta_3$ integrin is highly expressed on endothelial cells during angiogenesis in the infarcted and border zone regions as part of the early infarct healing process. Its expression in the early phases also correlates strongly to later cardiac fibrosis and predicts long-term LV remodeling (Sherif et al. 2012).

CD44

CD44, a cell-surface glycoprotein, is involved in various cellular functions, including cell proliferation, adhesion, migration, hematopoiesis, and lymphocyte activation (Jordan et al. 2015). Adhesive interactions between CD44 and hyaluronan (HA) have been implicated in the regulation of leukocyte trafficking within various tissues (McDonald et al. 2015). Upregulation of CD44 expression can lead to augmented recruitment of various leukocyte subsets to sites of inflammation, and impaired CD44 surface expression can result in attenuation of leukocyte trafficking kinetics (McDonald 2015).

The degrading ECM plays an important role both in triggering inflammatory cascades and the regulation of reparative responses (Rienks et al. 2014). Hyaluronan is a large polysaccharide molecule present in the ECM of healthy myocardial tissue and acting as a shock absorbent and providing mechanical support. During ischemic myocardial injury, HA is fragmented into water binding low molecular weight (LMW) particles that contribute to interstitial edema (Arslan et al. 2011) and activate inflammatory pathways. LMW HA clearance through

interaction with transmembrane adhesion molecule CD44 restrains inflammatory response (Frangogiannis 2012).

Gelatinases (MMP-2 and MMP-9)

Matrix metalloproteinases (MMPs) are potent proteolytic enzymes. In addition to their function in ECM remodeling, more recent research has highlighted new MMP functions, such as the proteolysis of substrates other than ECM proteins, including signaling molecules. MMP localization to subcellular organelles, and the proteolysis of susceptible intracellular proteins in those subcellular compartments have also indicated a much more complex role of MMPs in tissue function and remodeling (Chen et al. 2016). Ineffective infarct healing, resulting in lethal cardiac rupture, has also been linked with higher MMP activity in the infarct area (van den Borne et al. 2010).

MMP-9 coordinates multiple aspects of LV remodeling, such as direct molecular effects on ECM and inflammatory protein turnover, as well as indirect effects on major cell types that coordinate the cardiac wound healing (Iyer et al. 2016). MMP-9 is secreted by endogenous cardiomyocytes, endothelial cells, and fibroblasts. MMP-9 expression and activity is robustly elevated by non-resident leukocytes that infiltrate the infarct in response to ischemic injury. MMP-9 levels increase dramatically after MI and remain elevated during the first week, mirroring leukocyte activity (DeLeon-Pennell et al. 2015). Deletion of MMP-9 has been reported to protect the myocardial tissue against no-flow ischemia-reperfusion-induced injury in mice (Romanic et al. 2002).

MMP-9 proteolytically processes a wide variety of ECM proteins and other molecules, such as growth factors and inflammatory mediators. ECM degradation further enhances leukocyte infiltration by increasing the permeability of the cardiac microvasculature and releasing ECM-bound chemoattractants (Stefanidakis et al. 2004). MMP-9 contributes to post-MI wound granulation, wound contraction, and collagen deposition, thus determining the scar formation efficacy and quality, which, in turn, directly contributes to LV function (DeLeon-Pennell et al. 2015). On the other hand, MMP-9 is essential for sufficient angiogenesis and capillary branching in ischemic tissues (Johnson et al. 2004)

Neutrophils are the dominant initial (detectable at 15 minutes after MI) source of MMP-9, exerting early effects in the damaged tissue by degrading ECM and facilitating macrophage infiltration (Zamilpa et al. 2012). However, ischemic cardiac myocytes are also an important MMP-9 source (Iyer et al. 2017).

ECM provides the structural integrity surrounding the myocytes, and limiting MMP activity to the site of necrotic debris removal and keeping it at sufficient amounts.

An imbalance between MMPs and TIMPs provides a major mechanism for the extension of infarction into the remote area (Phatharagee et al. 2007, Iyer et al. 2017).

M1 phenotype macrophages express MMP-9 and stimulate ECM degradation. However, MMP-9 also polarizes macrophages toward the M2 phenotype by processing inflammatory molecules, including chemokine ligand 4 (CXCL-4), IL-8, CXCL-12 and TGF- β_1 (Van Lint et al. 2007). The MMP-9 mediated proteolysis of cytokines and chemokines influences leukocyte trafficking and creates positive and negative feedback loops (Van Lint et al. 2007). MMP-9 secreted by M1 macrophages stimulates myofibroblast proliferation (Lambert et al. 2008) and migration (Iyer et al. 2017), whereas the increase of MMP-9 expression in myofibroblasts associates with a decrease in the collagen synthesis rate.

Other cellular sources of MMP-9 are endothelial cells and lymphocytes. The cell source of MMP-9 is relevant, because MMP-9 function is dictated by the presence of substrates available for proteolytic processing. MMP, cell, and substrate presence are all managed in time and location (Iyer et al. 2017). MMP-9 has both negative and positive effects on LV after MI. Thus, there are several areas where additional studies are required to provide a more complete understanding of MMP-9 functions (Iyer et al. 2017).

Similar to MMP-9, the cellular sources of MMP-2 in post-infarct myocardium include leukocytes, myocytes and endothelial cells. In comparison to MMP-9, MMP-2 has a wide spectrum of substrates including signaling and ECM-structure proteins. Cardiac fibroblasts express MMP-2 intracellularly. The intracellular actions of MMP-2 are still poorly understood and despite the biochemical and imaging evidence for intracellular MMP-2, a great deal of skepticism towards intracellular MMP-2 biology still exists (DeCoux et al. 2014).

MMP-2 is rapidly activated by oxidative stress and the peak expression of MMP-2 is recorded during the first 3 days of post-infarct regeneration (Nepomnyashchikh et al. 2015). Ang II stimulation significantly increases MMP-2 expression in surviving cardiomyocytes (Coker et al. 2001), which may partly explain the adverse effects of neurohormonal signaling in ischemia/reperfusion (I/R) injury and possible cardiac rupture. Significant improvement in the survival after MI was observed in MMP-2 knock-out mice, which was attributable both to the inhibition of early cardiac rupture, and the development of later-stage LV dysfunction (Hayashidani 2003).

2.1.9 Overview of HF therapy

The previously described neurohormonal model for HF forms the cornerstone for current HF therapy. The deleterious effects of sustained SNS and RAAS activation on the heart are counteracted by β -adrenergic blocking agents (β -blockers), ACE inhibitors, Ang II type I receptor blockers (ARBs), and mineralocorticoid-receptor antagonists (MRAs) (Hartupee et al. 2017). ACE inhibitors or ARBs in combination with β -blockers are recommended for all symptomatic HF patients with reduced ejection fraction (EF) to inhibit neurohormonal activation. Mineralocorticoid/ aldosterone receptor antagonists MRAs may also be used in selected patients.

Dual angiotensin receptor neprilysin inhibitors (ARNIs), acting on the RAAS and the neutral endopeptidase system, have been developed as a new therapeutic class of agents. ACE inhibitors and β -blockers are also recommended preventively for patients with asymptomatic LV systolic dysfunction to reduce the risk of HF development (Poninkowski et al. 2016).

Diuretics can improve signs and symptoms of congestion, although their effects on morbidity and mortality have not been confirmed in randomized controlled trials (Poninkowski et al. 2016).

Cardiac resynchronization therapy (CRT) improves cardiac performance, symptoms and well-being in adequately selected patients, also reducing morbidity and mortality (Sohaib et al. 2015). Not all patients respond favorably to CRT, and the detailed guidelines by the European Society of Cardiology (Poninkowsky et al. 2016) for patient selection include various characteristics, such as QRS duration, EF percentage, and New York Heart Association (NYHA) class.

Implantable cardioverter-defibrillators (ICDs) are effective in preventing cardiac arrests by correcting ventricular arrhythmias, thus reducing the risk of sudden death in high-risk patients with HF (Theuns et al. 2010).

Catheter-based interventions for the treatment of valvular dysfunctions have also advanced significantly (Higgins et al. 2017). It is important to detect severe CAD or valvular heart disease in patients with HF, because their surgical treatment can correct the underlying cause of HF.

Mechanical circulatory support (MCS) using left ventricular assist devices (LVAD) has also developed in an effective method for circulatory support and end-organ perfusion (Higgins et al. 2017).

Heart transplantation is the gold standard of biological replacement for end-stage congestive HF. However, its long-term success is limited by donor availability, perioperative infections, and complications related to chronic immunosuppression, such as cellular rejection, development of malignancies, and transplant allograft vasculopathy (Higgins et al. 2017).

2.2 Advances in noninvasive assessment of cardiac function

Cardiac imaging is very useful for diagnosing HF, both in the demonstration of dysfunction and underlying structural disease, as well as its etiology and molecular mechanisms (Saraste et al. 2017). Understanding the molecular pathophysiological mechanisms is essential for the successful development and application of new molecular-targeted therapies (Bax et al. 2015, Thackeray et al. 2016(1), Saraste et al. 2017).

Molecular level radionuclide imaging of the myocardium has undergone significant evolution in recent years in terms of both hardware and software technologies, and the development of target-specific tracers. This progress has been driven by the success of other imaging techniques (MRI, echocardiography, CT) (Acampa et al. 2016), and increased demand for diagnostic tools to assist in tailoring therapy and selecting candidates for expensive therapies (such as left-ventricular assist devices, valvular prostheses and cardioverter-defibrillators) and managing complications, such as implant infections (Juneau et al. 2017).

2.2.1 Blood biomarkers

Brain natriuretic peptides (BNP and N-terminal pro B-type natriuretic peptide (NT-proBNP)) are the most commonly measured biomarkers of HF (Ponikowski et al. 2016). Natriuretic peptides are successful tools not only for diagnosing/excluding HF but also for predicting outcome in the diagnosis (van Kimmerdale et al. 2012) and, thus far, the most studied candidates for use in therapy guidance (Ibrahim et al. 2017).

The clinical utility of high sensitivity troponin (hsTnT) in the diagnosis of myocardial infarction is unquestioned (Kramer et al. 2017). Regardless of their cause, hsTnT concentrations are prognostic for adverse outcomes and predict LV remodeling (Ibrahim et al. 2017).

Various other circulating molecular biomarkers, such as growth differentiation factor 15 (GDF-15) (van Kimmerdale et al. 2012), or ST2 (a protein member of

the interleukin 1 [IL-1] receptor family) (Dieplinger et al. 2015, Ibrahim et al. 2017), have also been indicated for detecting of neurohormonal activity, myocyte stretch and/or necrosis, systemic inflammation, oxidative stress, extracellular matrix turnover, and extracardiac processes, such as renal function. However, the production of these potential biomarkers is not cardiac specific (van Kimmerdale et al. 2012, Ibrahim et al. 2017) and thus it may be more feasible for HF prognosis assessment rather than initial diagnostics.

2.2.2 Cardiac ultrasound

Cardiac ultrasound, or echocardiography, is the primary cardiac imaging modality in HF because of its low cost, harmless nature, quick acquisition (Awan et al. 2015) and good availability. Cardiac ultrasound is an effective tool for anatomical and functional imaging, allowing the measurement of EF, assessment of diastolic function, and detection of valvular heart disease. In some patients, cardiac ultrasound suffers from poor image quality (Awan et al. 2015, Rajpoot et al. 2009), which is significantly dependent on the skills of the performing physician. Training of the clinicians in image acquisition, analysis, and interpretation, is equally important to the technical performance of this modality. Excessive guidelines have been established for the knowledge base, practical experience, and continued maintenance of competency. Still, for example, full-featured equipment and selected stable subjects, do not prepare for critically ill patients and small bedside devices (Spencer et al. 2013). A recent review found that data quality in cardiac ultrasound research is infrequent, and methods vary substantially (Crowley et al. 2016). The lack of well-defined prognostic cutoff points for novel parameters in relation to specific endpoints, and the insufficient information on optimal timing for performing cardiac ultrasound, is also a challenge (Prastaro et al. 2017).

2.2.3 Cardiac magnetic resonance

In recent years, cardiac MRI (CMR) has become the most reliable non-invasive method for the estimation of ventricular volumes, wall motion and cardiac function (Lota et al. 2017) with the spatial resolution reaching $1.4 \times 1.9 \times 6.0$ mm (Wagner et al. 2003). A large evidence base has also emerged, supporting the prognostic impact of impaired systolic function based on reduced LVEF as visualized by CMR (Khan et al. 2017). More specific prognostic CMR markers of myocardial damage in STEMI include the initial infarct size (Orn et al. 2007), microvascular obstruction (MVO) (Husser et al. 2010), intramyocardial hemorrhage (IMH) (Ganame et al. 2009) and the proportion of non-infarcted ischaemic area at risk

(AAR) (Ganali et al. 2012). Late gadolinium enhancement (LGE) cardiac MRI can be used to accurately detect focal myocardial fibrosis not only in the postinfarct scar formation, but also in various other conditions, such as cardiomyopathies (Ambale-Venkatesh et al. 2017).

MRI signal appears as high or low (bright or dark), depending on the pulse sequence used and the type of tissue in the image region of interest (ROI). Various CMR sequence approaches (T1, T2 and T2* mapped, contrast enhanced, LGE) offer robust and validated surrogate markers, providing an accurate visualization of pathophysiology, assessment of myocardial injury and remaining function, as well as predictive values for medium to long-term outcome of LV function, remodeling and HF prognosis (Khan et al. 2017).

2.2.4 Computed tomography

Cardiac CT angiography (CTA) has evolved from the early 4-slice acquisition systems to the modern, high temporal and spatial resolution multislice cardiac CT with up to 320 simultaneous slices and faster gantry rotational systems. Today, entire examinations can be completed in less than 5 seconds, and the volume of contrast material required continues to decrease (Levine et al. 2015). CTA has proved clinically useful for the purpose of excluding obstructive CAD because of its high sensitivity and negative predictive value, but the ability of CTA to identify functionally significant CAD has remained challenging (Gonzalez et al. 2015).

A strong correlation between CTA and CMR for EF assessment has been shown in multiple studies (Levine et al. 2015). CTA is also useful for the detection of regional wall motion abnormalities, approaching the resolution achievable by CMR (Yamamuro et al. 2005). Thus, CTA may be feasible for use in patients with limitations regarding other imaging modalities, such as confined echocardiographic windows or implants that prevent MR imaging. However, CTA has inferior temporal resolution as compared to CMR, resulting in slight overestimations of end-systolic volume and EF, especially in patients with a reduced EF (Sharma et al. 2014).

2.2.5 Molecular imaging of cardiac tissue

Single-photon emission computed tomography (SPECT) myocardial perfusion imaging has been available since 1970s and an extensive amount of evidence has been published substantiating its diagnostic and prognostic value (Mc Ardle et al. 2012). SPECT radiotracers can be injected during some form of cardiovascular

stress, either dynamic exercise or pharmacological stress (e.g. adenosine). Myocardial ischemia is suspected when there is reduced tracer uptake on stress images which is reversible on the rest acquisition (reversible defects), whereas irreversible perfusion defects on stress and rest images generally correspond to areas of myocardial necrosis (Angelidis et al. 2017).

Evidence of left ventricular (LV) cavity dilatation may be either permanent or transient. Transient LV cavity dilatation during stress has been associated with the presence of significant CAD and is considered an independent predictor of cardiac events (uz Zaman et al. 2011, Xu et al. 2012, Angelidis et al. 2017).

Positron emission tomography (PET) has become increasingly available largely due to its wide utilization in clinical oncology (Bengel et al. 2009). In addition, nuclear cardiology has benefited significantly from modern hybrid devices combining PET imaging with CT or MRI. Improvement in imaging technologies has led to evolution beyond isolated visualization of myocardial perfusion, toward characterization of detailed molecular processes (Saraste et al. 2017). Detection of underlying molecular processes, instead of visualizing current cardiac function, may present an opportunity to predict the development of HF in the very early stages, thus facilitating tailored therapy with significant effects on the outcome. Recent advancements in the development of PET tracers for cardiac repair imaging are assembled in Table 2.

Advantages of SPECT imaging include wide availability of the diagnostic modality, well-established and worldwide familiarity with the technique, lower cost of equipment, less expensive radiotracers and combination with dynamic stress testing. However, compared to PET, SPECT requires longer duration of the acquisition, which results in lower resolution images prone to artefacts, and causes higher radiation burden. Advantages of PET include superior diagnostic capability, especially for obese and multi-vessel disease patients, quantifiable blood flow evaluation, integration of functional and anatomical information with combined PET/CT cameras, which are more widespread than SPECT/CT. PET imaging also has better spatial and contrast resolution, as well as lower frequency of artefacts. Still, PET equipment is of higher cost and mostly requires on-site cyclotrons. Also, short physical half-life of most commonly used radiotracers do not permit stress testing. (Angelidis et al. 2017)

Hardware and software developments

Cardiac PET combined with multi-slice CT allows for attenuation correction and quantification of PET studies. In addition, stepwise algorithms developed to combine contrast-enhanced coronary CT angiography with PET imaging have enabled a comprehensive detection of both the morphologic and functional aspects

of coronary artery disease (Acampa et al. 2015). This has led to advanced software developments capable of a combined analysis of vascular integrity and myocardial tissue perfusion in specific areas of ailing vessels (Javadi et al. 2010). The multi-modality information has been shown to influence and refine targeted interventional therapy (Bengel 2017). More recently, PET has also been integrated with MRI scanners (Rischpler et al. 2013) thus offering broader options for the characterization of myocardial tissue.

Table 2. PET tracers for post-infarct cardiac imaging

Target	Tracer	Tracer type	Experimental setting	References
<i>Cardiac perfusion</i>				
Myocardial blood flow (MBF)	^{82}Rb H_2^{15}O $^{13}\text{NH}_3$	Small molecules	Clinical	(Maddahi et al. 2014)
Mitochondrial complex 1	^{18}F -flurpiridaz	Small molecule	Clinical	(Packard et al. 2014)
<i>Cardiomyocyte viability</i>				
Glucose metabolism	^{18}F -FDG	Small molecule	Clinical	(Schinkel et al. 2007)
Oxygen consumption	^{11}C -acetate	Small molecule	Clinical	(Knaapen et al. 2007)
Fatty acid metabolism	^{18}F -FTHA ^{11}C -palmitate ^{68}Ga fatty acids ^{18}F -FCPHA	Fatty acids	Clinical Clinical Swiss mice Rhesus monkey	(Tuunanen et al. 2011) (de Jong et al. 2009) (Jindal et al. 2014) (Shoup et al. 2005)
<i>Inflammation</i>				
Glucose metabolism	^{18}F -FDG	Small molecule	Clinical Pig MI model Mice MI model	(Lawal et al. 2016) (Lautamäki et al. 2009) (Lee et al. 2012)
Amino acid metabolism	^{11}C -methionine	Amino acid	Clinical	(Thackeray et al. 2016(2))
CXCR4 receptor	^{68}Ga -pentixafor	Peptide	Clinical	(Gourni et al. 2011, Lapa et al. 2015)
<i>Angiogenesis</i>				
$\alpha_v\beta_3$ integrin	^{18}F -galacto-RGD, ^{68}Ga -NODAGA-RGD, ^{68}Ga -TRAP(RGD) ₃ ^{18}F -fluciclatide	Peptides Peptide	Clinical Preclinical MI models Clinical	(Makowski et al. 2008) (Sherif et al. 2012; Laitinen et al. 2013...) (Jenkins et al. 2017)
<i>ECM remodeling and fibrosis</i>				
Angiotensin converter enzyme (ACE)	^{18}F -fluorobenzoyl-lisinopril	Peptide	Excised human cardiac tissue	(Dilsizian et al. 2007)
Angiotensin 1 receptor (AT1R)	^{11}C - KR31173	Small molecule	Pig MI model	(Fukushima et al. 2012)
Matrix crosslinking	^{18}F -XIII factor	Protein	ApoE ^{-/-} mice MI model	(Majmudar et al. 2013)
<i>Sympathetic innervations</i>				
Norepinephrine transporters (NETs)	^{11}C -HED ^{18}F -LMI1195	Small molecule Small molecule	Clinical Clinical	(Fallavollita et al. 2014) (Sinusas et al. 2011)
Adrenergic receptors	^{11}C -epinephrine ^{11}C -phenylephrine	Small molecules	Pig MI model	(Lautamäki et al. 2015)

SPECT is a widely used conventional technology for radionuclide-based myocardial perfusion imaging that has also benefited from the introduction of hybrid SPECT/CT devices (Goetze et al. 2007). The new cadmium-zinc-telluride semiconductor crystal (CZT) technology has also resulted in a significant progress of cardiac SPECT imaging. The sensitivity of CZT systems is 4–10 fold higher than that of regular SPECT, and detectors can also be positioned closer to the region of interest, resulting in increased spatial resolution (Herzog et al. 2010, Imbert et al. 2012).

Software advancements have significantly improved image data handling (Bengel 2017). Novel iterative reconstruction algorithms of tomographic data generate less noisy images while also reducing acquisition time (Piccinelli et al. 2015). Other advanced algorithms include co-registration of separately acquired nuclear and tomographic images (Schepis et al. 2007), algorithms for respiratory and cardiac motion correction (Slomka et al. 2015), and blood flow quantification (Tahari et al. 2015). With the currently available PET scanners and post-processing algorithms, images can be reconstructed with a spatial resolution of 4–7 mm (Saraste et al. 2017).

Myocardial perfusion

Myocardial perfusion imaging with SPECT and PET modalities under rest and stress is a primary application in nuclear cardiology focusing on the assessment of CAD severity and providing information about individual risk for subsequent cardiac events. This, in turn, is useful in identifying patients suitable for intervention therapies regarding long-term outcome (Bengel 2017, Saraste et al. 2017). PET imaging combined with kinetic modeling can be used to quantify myocardial blood flow (MBF) during rest and stress, thus allowing the quantification of coronary flow reserve (CFR) (Saraste et al. 2012). Quantification of regional MBF and CFR may characterize the severity of multi-vessel CAD disease, and detect aberrations of blood supply in all major coronary artery vascular territories (Johnson et al. 2016). Myocardial perfusion imaging has been standardized for clinical cardiology guidelines (Montalescot et al. 2013) and technical performance methodology (Verberne et al. 2015). It is still unclear, however, whether the quantitative measurements of CFR can successfully direct HF therapy.

^{99m}Tc -labeled perfusion tracers are commonly used for clinical SPECT imaging (Ben Bouallègue et al. 2015). Clinically used PET tracers include ^{82}Rb , H_2^{15}O and $^{13}\text{NH}_3$. Due to their short half-lives, ^{15}O and ^{13}N require an on-site cyclotron (Maddahi et al. 2014). ^{82}Rb has a short half-life as well, but can be produced more conveniently with a generator. Perfusion studies performed with ^{18}F -flurpiridaz

have also shown encouraging results, generating data in line with (that of) commonly accepted methods (Packard et al. 2014).

SPECT is less accurate than PET for absolute quantification (MBF) (Agostini et al. 2018). However, recently, higher sensitivity, fast sampling and ROI-focused imaging capabilities of CZT-SPECT, as well as improvements in iterative reconstruction algorithms, have enabled dynamic cardiac SPECT studies, which can provide absolute quantitation of myocardial flow reserve (Klein et al. 2014, Wells et al. 2014, Agostini et al. 2018). In a recently published study, CFR was shown as a stronger predictor of cardiovascular mortality than maximal MBF. Integrated physiological assessment of coronary circulatory function based on the concordant or discordant impairment of CFR and maximal MBF identified unique prognostic phenotypes of patients with known or suspected CAD (Gupta et al. 2017).

Cardiomyocyte metabolism and viability

While having a role as an adjunct decision-making tool in the comprehensive evaluation of CAD/HF patients, helping to predict the response to revascularization and acting as a marker of prognosis, the usefulness of myocardial viability imaging remains controversial (Bax et al. 2015, Saraste et al. 2017). ^{18}F -FDG PET can be used to visualize dysfunctional ischemic myocardium that is still potentially recoverable after revascularization (Bax et al. 2015). Flow-metabolism mismatch, i.e., the preserved or increased ^{18}F -FDG uptake in combination with decreased perfusion, is the most commonly used marker of damaged myocardium capable of functional recovery after revascularization (Schinkel et al. 2007). Other myocyte metabolism tracers include ^{11}C -labeled acetate for measuring oxygen consumption in both ventricles (Knaapen et al. 2007), various compounds reflecting fatty acid utilization, such as ^{18}F -fluoro-6-thia-heptadecanoic acid (^{18}F -FTHA) (Tuunanen et al. 2011) and ^{11}C -palmitate (de Jong et al. 2009), as well as several ^{68}Ga -labeled fatty acids currently in development (Jindal et al. 2014).

Adverse inflammation

Techniques aiming at detection of plaque inflammation apply the most commonly used PET tracer, 2-deoxy-2- ^{18}F -fluoro-*D*-glucose (^{18}F -FDG) as the metabolic marker of plaque activity (Strauss et al. 2017). Another clinically available tracer is ^{18}F , which, being a marker of micro-calcification, and thus, of plaque activity, has also been studied for the imaging of atherosclerosis (Joshi et al. 2014). More specific tracers are used to target inflammatory cell recruitment, differentiation, and activation, as well as specific inflammatory pathways, such as chemokine receptors, protease activity, apoptosis, integrins, and other adhesion proteins (Tavakoli et al. 2014). Some of these tracers, including choline analogs (Bucerius

et al. 2008, Kato et al. 2009), translocator protein (TSPO) targeted tracers (Gaemperli et al. 2012), and somatostatin targeting tracers (Malmberg et al. 2015, Pedersen et al. 2015), have also been clinically tested for imaging of inflammatory processes in atherosclerotic lesions. In combination with PET, CT-derived angiographic morphology information is an important component of vessel wall imaging, permitting the precise visualization of a small target (Bengel 2017). Infarcted myocardium shares many pathobiology pathways with damaged vessel wall, and many of the inflammation imaging approaches employed in atherosclerosis have also been utilized for the characterization of infarct healing. As described previously, excessive or prolonged inflammation during post-infarct healing may impair the infarct scar homeostasis. Thus, the imaging of the inflammatory response triggered by severe ischemia or other forms of myocardial damage facilitates the prediction of the healing process (Bengel et al. 2013).

In a recent clinical study (Rischpler et al. 2016) performed with hybrid PET/MRI, the intensity of ^{18}F -FDG uptake in the myocardium after AMI showed a clear inverse correlation with the functional outcome at 6 months. Still, ^{18}F -FDG imaging for inflammation in myocardium has significant limitations. ^{18}F -FDG PET may not be able to distinguish the different leukocyte subpopulations that have different or even opposing roles in the complex process of infarct healing. As a glucose analog, ^{18}F -FDG is also taken up by a variety of cells with high energy consumption, such as surviving cardiomyocytes. This unspecific uptake can, to some extent, be suppressed with a high-fat diet, prolonged fasting, and heparin injections. (Rischpler et al. 2016)

In addition to ^{18}F -FDG (Lautamäki et al. 2009, Lee et al. 2012), ^{11}C -methionine is another metabolic marker aimed to detect the extent of myocardial inflammation and predicting recovery after myocardial infarction (Thackeray et al. 2016(2)). A new CXCR4 chemokine receptor targeting PET tracer, pentixafor, labeled with ^{68}Ga , has also been evaluated for imaging of cardiac inflammation (Gourni et al. 2011). Its uptake showed high variability between patients (Lapa et al. 2015), which may have implications in terms of adverse outcome prediction.

Angiogenesis

An integrin subtype, $\alpha_v\beta_3$, has been confirmed as an essential mediator of angiogenesis (Meoli et al. 2004), and its expression is significantly increased in the endothelial during the post-infarct healing process (Sun et al. 2003). Arginine-glycine-aspartate motif (RGD) binds to $\alpha_v\beta_3$ integrin, and several RGD motif containing peptides (including oligomers and cyclic peptides) have been evaluated for angiogenesis imaging, some tracers also in clinical settings (Makowski et al. 2008, Jenkins et al. 2017). The multimerization of RGD domains increases the affinity and uptake of tracers (Dijkgraaf et al. 2007). A disarranging factor remains

as $\alpha_v\beta_3$ integrin is also expressed by macrophages and myofibroblasts after MI (Sun et al. 2003, van den Borne 2008), which may impair the specific detection of angiogenesis.

Extracellular matrix remodeling and fibrosis

A quantitative assessment of myocardial fibrosis can be achieved with CMR, whereas more specific molecular mechanisms of fibrosis formation, such as MMP activity and neurohormonal actions (RAA system in particular), can be visualized with specific nuclear imaging probes (de Haas et al. 2014).

In an initial preclinical study to evaluate MMP imaging potential, MMPs activation was visualized in the infarct area within the first few weeks after MI (Su et al. 2005). Changes in LV end-diastolic volumes correlate with the uptake of the broad-spectrum MMP targeting probe, ^{99m}Tc -RP805. The MMP imaging signal has also been linked with the development of regional myocardial strain and, thus, it may predict LV remodeling and deformation (Sahul et al. 2011).

Extensive studies have been performed on probes targeting RAS, which is an important factor driving collagen formation and fibrosis (de Haas et al. 2014). An ACE inhibitor, ^{18}F -labeled lisinopril has showed uptake adjacent to regions with increased collagen deposition in excised human hearts (Dilsizian et al. 2007). Lisinopril has also been labeled with ^{99m}Tc and evaluated for *in vivo* myocardial ACE-1 targeting in preclinical settings (Femia et al. 2008, Dilsizian et al. 2012).

AT1R receptor has also been targeted with a selective antagonist referred to as KR31173 and labeled with ^{11}C , which showed increased myocardial retention in both infarct and remote areas in a pig model (Fukushima et al. 2012). Initial clinical experiments also confirmed the safety of the probe (Fukushima et al. 2012).

Autonomic nerve damage

Sympathetic nerve terminals are more sensitive to ischemia as compared to myocytes, and the denervated areas of viable myocardium contribute to the risk of ventricular arrhythmias (Kramer et al. 2010) and HF progression after MI (Jacobson et al. 2010). Catecholamine analogs targeting norepinephrine transporters (NETs) have been studied, with successful results, in order to visualize this sympathetic nerve damage. These tracers include ^{123}I -metaiodobenzylguanidine (^{123}I -MIBG) (Jacobson et al. 2010), ^{11}C -metahydroxyephedrine (^{11}C -HED) (Fallavollita et al. 2014), and N-[3-bromo-4-(3- ^{18}F -fluoro-propoxy)-benzyl]-guanidine (LMI1195) (Sinusas et al. 2011).

3 AIMS OF THE STUDY

The purpose of this study was to evaluate novel tracers for imaging of myocardial repair after myocardial infarction (MI) in a surgical rat model. One of the tracers was also evaluated for imaging of atherosclerotic lesions in a hypercholesterolemic mouse model.

The specific aims of this study were:

1. To evaluate an $\alpha_v\beta_3$ integrin targeting ^{68}Ga -labeled dimeric RGD-peptide for PET imaging of angiogenesis after MI in rat.
2. To evaluate CD44 targeting ^{68}Ga -labeled hyaluronan conjugates for the assessment of inflammation rate after MI in rat.
3. To evaluate an MMP-2/9 targeting ^{68}Ga -peptide for the assessment of gelatinase expression related to ECM remodeling and inflammation after MI in rat.
4. To explore the feasibility of a novel ^{68}Ga -peptide probe in the assessment of MMP-2/9 expression related to inflammation in atherosclerotic plaques in mouse.

4 MATERIALS AND METHODS

4.1 Animal Models

Genetically modified mice were used as an animal model for atherosclerosis, and rats with surgical coronary artery ligation were used as a model for MI. The study protocols were approved by the National Animal Experiment Board in Finland and the Regional State Administrative Agency for Southern Finland. All experiments were carried out in compliance with the relevant European Union directives.

4.1.1 Atherosclerosis model (IV)

Genetic strains

Low-density lipoprotein receptor deficient mice expressing only apolipoprotein B (LDLR^{-/-}ApoB^{100/100}, strain #003000, Jackson Laboratory, Bar Harbor, ME, USA) were used. The mice were kept on a Western-type diet to accelerate the development of atherosclerosis. In the diet, 42% of calories consisted of fat and 0.2% of cholesterol (TD 88137 Adjusted Calories Diet, Harlan Teklad, Canada). Nine C57BL/6N mice on regular chow diet (CRM [E], product code 801730, 9.1% calories from fat, Special Diet Services, Essex, United Kingdom) were used as controls. Control strain was chosen because of the C57BL/6N background of LDLR^{-/-}ApoB^{100/100} model.

Study design

Nine (5 males, 4 females) atherosclerotic mice, kept on a Western-type diet for 4.4 months, starting at the age of 3.5 months, were used in the study, and nine C57BL/6N mice were used as controls. The age and weight of the mice at the time of tracer injection were 8.2 ± 0.70 months and 38 ± 8.0 g for LDLR^{-/-}ApoB^{100/100} mice and 3.9 ± 0.86 months and 31 ± 5.8 g for controls. During the study, the mice were housed under standard conditions (lighting and humidity) with *ad libitum* access to water and feed.

4.1.2 Surgical myocardial infarction model (I-III)

MI was induced by ligation of the left coronary artery (LCA) as previously described, with some modifications (Pfeffer et al. 1979). A Sprague Dawley rat

strain (Strain Code 400, Charles River Laboratories, Wilmington, MA, USA) was used in the studies. Prior to operation, 0.2 mg/kg of buprenorphine (Temgesic; Schering-Plough, Espoo, Finland) was administered intramuscularly for analgesia. Analgesia was continued for 72 hours after the operation (0.2 mg/kg of buprenorphine every 12 hours). Rats were anesthetized with a combination of inhaled isoflurane (Vet Medic Animal Health, Parola, Finland) (induction only) and subcutaneous injection of 10 mg/kg of xylazine (Rompun; Orion Pharma, Espoo, Finland) and 90 mg/kg of ketamine (Ketaminol; Orion Pharma, Espoo, Finland). Body temperature was maintained using a heating pad. The rats were connected to a rodent ventilator (TOPO dual mode ventilator; Kent Scientific, Torrington, CT, USA), and the heart was exposed by a left lateral thoracotomy through the fourth intercostal space, the pericardium was opened and LCA was ligated near its origin. Ligation was confirmed visually by the pale appearance of the myocardium at risk. The ribs, muscle layer and skin were sewed tightly with a dissolving string. The anesthesia was reversed after the operation with intramuscular injection of 1 mg/kg atipamezole (1 mg/kg Antisedan; Orion Pharma, Espoo, Finland). The sham operation consisted of the same protocol except for the closure of LCA. Operative mortality was approximately 25% in both the coronary ligation and sham-operated groups and occurred during the first 2 days after the surgery. Animals that did not develop MI (scar <4% of the LV circumference) were excluded from the stud. The rats were studied 7 days (I-III) and 4 weeks (I, III) after MI.

4.2 ⁶⁸Ga-labeled tracers

⁶⁸Ga-DOTA-E-[c(RGDfK)]₂ (I)

Targeted radiolabeled peptides containing arginine-glycine-aspartic acid (RGD) can detect the upregulation of integrins after ischemic myocardial injury. Multimerization of the RGD domains increases the affinity and uptake of tracers (Dijkgraaf et al. 2007), which may be important for detecting changes in integrin expression in tissues with relatively low baseline expression levels, such as the myocardium. The binding affinity of dimeric ⁶⁸Ga-labeled 1,4,7,10-tetraazacyclododecane-1,4,7,10-tetraacetic acid (DOTA)-conjugated RGD peptide, ⁶⁸Ga-DOTA-E-[c(RGDfK)]₂, as determined in a solid-phase competitive binding assay, was about 5-fold higher as compared with ⁶⁸Ga-DOTA-RGD monomer, and the competitive binding assays indicated that the tracer is specific for $\alpha_v\beta_3$ integrin (Dijkgraaf et al. 2011). From oligomeric RGD peptides, the dimer was considered the best compromise between high target uptake and low

accumulation in non-target organs, such as kidney, liver and intestines. (Dijkgraaf et al. 2007 and 2011).

⁶⁸Ga-NOTA-hyaluronan conjugates (II)

Hyaluronan (HA) is a linear polysaccharide composed of a repeating disaccharide unit of D-glucuronic acid and N-acetyl-D-glucosamine. Interaction between HA (length of 6–8 monosaccharides) and its cell-surface adhesion receptor CD44 has been found to play an important role in cell migration, tumorigenesis, metastasis, and the regulation of immune responses (Gee et al. 2004). HA is also recognized as a pharmacologically active signaling molecule, and a variety of cell types respond to HA of different sizes (Gaffney et al. 2010). The influence of the conjugated HA-clusters on the cellular uptake of the phosphorothioate oligonucleotides was previously tested in a CD44-expressing cell line (Karskela et al. 2008). Enrichment of the HA conjugate of potential therapeutic oligonucleotides could lead to enhanced internalization by endocytosis, and eventually, also to increased concentration in the cytoplasm. Conjugation to HA may meet these challenges via the CD44/HA-binding mechanism related to inflammatory conditions. In the present study, of various ⁶⁸Ga-labeled 1,4,7-triazacyclononane-1,4,7-triacetic acid (NOTA)-chelated oligonucleotide HA-conjugates, ⁶⁸Ga-NOTA-HA-hexasaccharide-T6 and ⁶⁸Ga-NOTA-HA-hexasaccharide-anti-miR-15b were evaluated for *in vivo* imaging of post-MI inflammation.

⁶⁸Ga-DOTA-conjugated gelatinase (MMP-2/9) ligand (III-IV)

The peptide was identified from phage display library and selected on the basis of its ability to bind chemically activated MMP-9 and to inhibit both MMP-9 and MMP-2 (Koivunen et al. 1999). The ⁶⁸Ga-labeled peptide tracer has been shown to provide good target-to-background ratio for PET imaging of tumor xenografts expressing MMP-9 in rats (Ujula et al. 2010). The purpose of this study was to evaluate the feasibility of the peptide for studying the distribution and extent of gelatinase expression during the MI healing process and post-MI LV remodeling.

4.3 *In vivo* tracer stability measurements

Animals were intravenously injected with tracers, and blood and urine samples were obtained at several time-points (for details, see the original publications). Plasma was separated by centrifugation and the proteins of plasma and urine were precipitated with acetonitrile (1:1, v/v). The supernatant obtained after centrifugation was analyzed by radio-high-performance liquid chromatography

(HPLC) (Jupiter C18, 10 × 250-mm, 300 Å, 5- μ m; Phenomenex, Torrance, CA, USA). The HPLC conditions were as follows: flow rate = 5 mL/min; λ = 215 nm; A = 0.1% trifluoroacetic acid (TFA)/water; B = 0.1% TFA/acetonitrile. A/B gradient: 0–5 min, 97/3; 5–15 min, from 97/3 to 0/100.

4.4 *In vivo* PET/CT

PET imaging (I-IV)

In vivo PET/CT imaging was performed for a subset of animals before *ex vivo* measurements in each study. Animals were imaged using a small-animal PET/CT (Inveon Multimodality; Siemens Medical Solutions, Knoxville, TN, USA). The animals were anesthetized using 1.5% isoflurane, their body temperature was maintained using a heating pad throughout the imaging, and tracers were injected through a catheter placed in the tail vein. PET data were acquired for 20 (III), 60 (I-IV) or 120 (II) min, starting at the time of injection, and sorted into 30×3 s, 9×10 s, 4×30 s, 5×60 s, and 2-22×300 s frames. The images were reconstructed using an ordered-subset expectation maximization algorithm (OSEM2D) with 4 iterations.

Contrast-enhanced CT (I-IV)

Immediately after PET, the intravascular iodinated contrast agent eXIATM160XL (Binitio Biomedical Inc, Ottawa, ON, Canada) was injected (200 μ l for rats and 100 μ l for mice) and high resolution CT was acquired. CT acquisition consisted of up to 160 projections (for rats) with the exposure time of 1250 ms, X-ray voltage of 80 kV, and anode current of 500 μ A for a 220° rotation. CT images were reconstructed using a filtered back-projection algorithm.

Myocardial perfusion imaging (¹¹C-acetate) (I)

Myocardial perfusion was studied in a subset of rats after injection of 50±8.4 MBq of ¹¹C-acetate in 0.4–1.0 mL over 10 seconds via the tail vein. PET acquisition started prior to tracer injection and continued in three dimensions for 10 minutes in the list-mode format. Attenuation CT was performed without moving the animal. The ¹¹C-acetate PET data were sorted into 30×3 s, 9×10 s, 4×30 s, and 5×60 s frames. The images were iteratively reconstructed using an ordered-subset expectation maximization in 2 dimensions (OSEM2D) algorithm with a ramp filter and cut-off at the Nyquist frequency (0.5 cycles/voxel), and CT-based attenuation correction.

Data analysis (I-IV)

The alignment of PET and CT images was automatic and confirmed visually by anatomical landmarks (Figure 4). Image analysis was done using Carimas software v.2.5-2.9 (Turku PET Centre, Turku, Finland). Data were normalized and corrected for the injected radioactivity dose and radionuclide decay. Several regions of interest (ROIs) were defined according to high-resolution CT images: infarcted zone (I-III) or aortic arch (IV), remote myocardium, blood pool, chest wall scar (I-II), as well as a number of relevant organs, depending on the studied tracer and imaging target. Myocardial ROIs in the sham-operated rats were defined in the septum for comparison with remote myocardium and in the anterior wall for comparison with the infarcted area in order to compensate for potential spill-over activity from the chest wall wound (I-IV). The results were reported as mean radioactivity concentrations (Bq/ml), converted to standardized uptake values (SUVs) (I-III) or percentages of injected radioactivity dose per gram (%ID/g) as a function of time after injection, i.e., as time-activity curves (TACs).

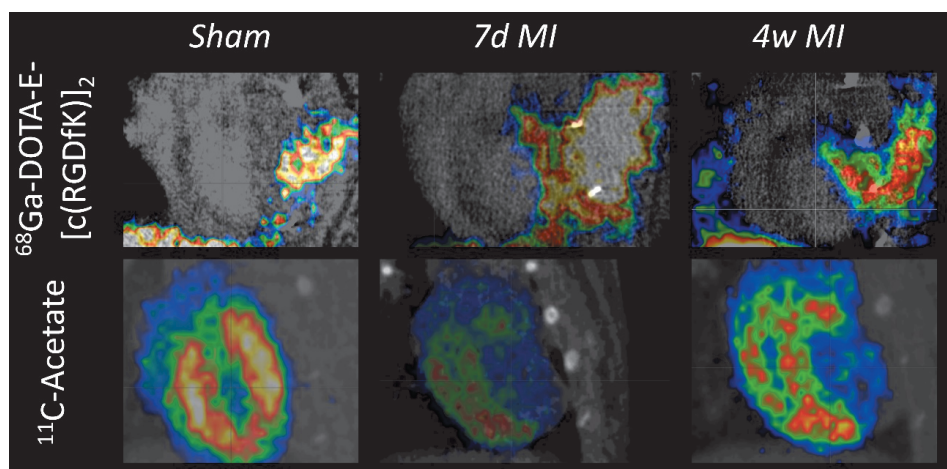


Figure 4. Example of *in vivo* imaging of rat myocardium. Fused ^{68}Ga -DOTA-E-[c(RGDfK)]₂ PET/CT images demonstrate tracer uptake in sham-operated rats, and at 7 days and 4 weeks post-MI. In addition to the infarct scar, the tracer also accumulates into the operation scar in thoracic wall. Tracer uptake is also present in the thoracotomy scar in the chest wall. Correspondingly, examples of myocardial perfusion imaging with ^{11}C -acetate are also shown.

PET data modeling (I)

The dynamic ^{68}Ga -DOTA-E-[c(RGDfK)]₂ PET data were analyzed by means of graphical Logan method and compartmental modeling (Zhang et al. 2006, Kim et al. 2013). Blood TACs were converted to plasma TACs using the mean plasma/blood ratio of radioactivity measured from the blood samples that were taken immediately after PET imaging. The image-derived input function was further corrected with parent fractions, measured from separate animals, two to three per time point. Logan plots were calculated using either the metabolite-

corrected plasma or total plasma as input to compare if metabolite correction is necessary for up to 60-min imaging. Two-tissue compartmental models were fitted to data, weighting data by sample frequency only. The fitting limits were modified from the default because it was expected that blood volume may be very high in these tissue types, and some tissues may also include high spillover from heart cavities. Parametric images of distribution volumes were obtained by using Logan plots. The modeling images and data were then compared with the SUV results.

4.5 *Ex vivo* studies

Ex vivo biodistribution (I-IV)

The isoflurane anesthetized animals were intravenously (i.v.) injected with ^{68}Ga -labeled tracers via tail vein. At 30 (III) / 60 (IV) / 70 (II) / 75 (I) minutes after tracer injection, depending on the tracer and animal model, a blood sample was obtained by cardiac puncture and then the animals were killed by cervical dislocation. Various tissues were excised, weighed and measured for radioactivity using a gamma counter (Triathler 3", Hidex, Turku, Finland). Radioactivity values were normalized by injected radioactivity dose, decay with a delta time between injection and measurement, animal weight, and the weight of tissue. The biodistribution results of the tracers' accumulation were expressed as SUV (I-III) or %ID/g (IV).

Specificity of tracer binding (III-IV)

In order to assess the specificity of ^{68}Ga -DOTA-peptide accumulation in atherosclerotic lesions (IV) or the heart 7 days after coronary ligation (III), a subset of the studied animals were i.v. injected with 1.4 $\mu\text{mol}/\text{kg}$ (approximately ≥ 20 $\mu\text{mol}/\text{L}$ of blood volume, $\text{IC}_{50} = 10$ $\mu\text{mol}/\text{L}$) of a specific MMP-2/9 inhibitor [H-Cys¹-Thr-Thr-His-Trp-Gly-Phe-Thr-Leu-Cys¹⁰-OH (cyclic:1 \rightarrow 10)] (product number 444251, Merck KGaA, Darmstadt, Germany) 5 minutes prior to the administration of ^{68}Ga -DOTA-peptide. In addition, 3 rats (III) were injected with an approximately 500-fold amount (in comparison to the administered ^{68}Ga -DOTA-peptide) of unlabeled peptide.

4.5.1 *Zymography (IV)*

To visualize the enzymatic activity of MMPs, fresh aorta and plasma samples of 5 $\text{LDLR}^{-/-}\text{ApoB}^{100/100}$ mice were homogenized (aortas), diluted into zymogram sample buffer (BioRad, Hercules, CA, USA) and an equal volume was added to

each lane of the zymogram gels (10% gelatin; BioRad). The gels were run, renaturated and developed using BioRad zymogram buffers, according to the manufacturer's instructions. The gels were stained using Coomassie Brilliant blue, and destained using a solution containing methanol and acetic acid.

4.6 Autoradiography

Data acquisition (I-IV)

The excised aorta (IV) or LV (I-III) were frozen in isopentane and sliced into serial 8- μm and 20- μm longitudinal (IV) or transverse (LV) cryosections for the analysis of tracer uptake by means of digital autoradiography. Air-dried sections were opposed to an imaging plate (Fuji Imaging Plate BAS-TR2025, Fuji Photo Film Co., Tokyo, Japan). After >2 radionuclide half-lives, the plates were scanned with Fuji BAS-5000 analyzer (Fuji, Tokyo, Japan; internal resolution of 25 μm).

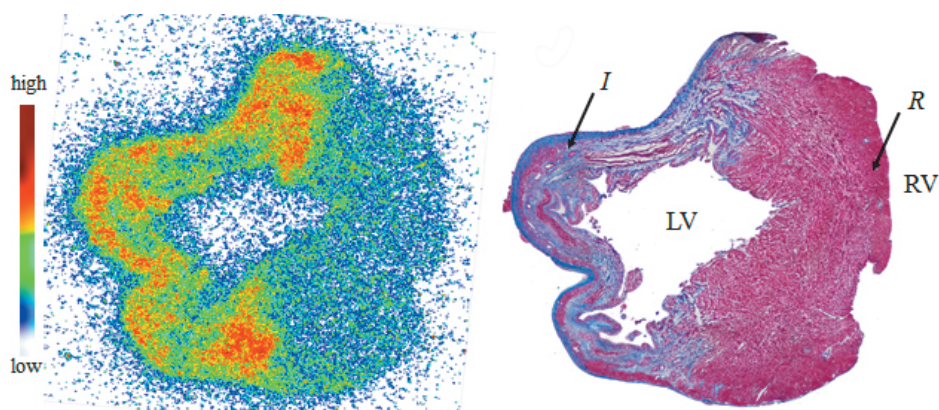


Figure 5. An example of autoradiography. ^{68}Ga -DOTA-E-[c(RGDfK)]₂ autoradiograph of a transverse section of LV and adjacent section stained with Masson's trichrome. Right ventricle (RV) has been removed. Regions of interest were defined as the infarct scar (*I*) and remote area (*R*). The figure shows clear uptake of the tracer in the infarcted area, whereas the uptake in the remote area of the damaged myocardium remains relatively low.

Autoradiography analysis (I-IV)

Radioactivity accumulation was measured in the 20- μm sections, which provided better count statistics. Autoradiographs were co-registered with the images of the same tissue sections stained with hematoxylin and eosin (HE). Tracer accumulation was measured as counts per area (photostimulated luminescence per square millimeter, PSL/ mm^2) with TINA software v. 2.1 (Raytest Isotopenmessgeräte, GmbH, Straubenhardt, Germany). After careful co-

registration of autoradiographs and histological images, ROIs were defined as plaque lesions, vessel wall, and adventitia (IV) or the whole infarcted area and an area in the remote non-infarcted portion of the damaged LV (I-III) (Figure 5). The background area count densities were subtracted from the image data. Uptake in the autoradiographs was normalized using a mathematical algorithm that takes into account the radionuclide decay, injected radioactivity dose, time from injection to imaging plate exposure, and the exposure time.

4.7 Histology and immunohistochemistry

General histology (I-IV)

In addition to HE staining of 20- μ m sections, 8- μ m sections were used for more specific analysis. Masson's trichrome (Sigma-Aldrich, St. Louis, MO, USA) staining was used to distinguish fibrosis and collagen from cardiomyocytes and to confirm the location and size of the infarcted area (I-III). Vascular histology and the location of atherosclerotic lesions was visualized with Movat pentachrome staining (IV). Adjacent 8- μ m sections were also stained with various antibodies to visualize the imaging targets, as well as relevant inflammatory and cardiac repair processes.

Macrophage activity: CD68 (I-III) and Mac-3 (IV)

CD68 is a glycoprotein binding to LDL. It is well established as a marker for the various cells of the macrophage lineage and was used as a marker of macrophage activity within the infarcted rat myocardium. Staining was performed using the mouse monoclonal anti-rat CD68 antibody at 1:10,000 dilution (product number MCA341GA, AbD Serotec, Munich, Germany).

Macrophages within the mouse atherosclerotic plaques were visualized with Mac-3 (also known as CD107b or lysosome-associated membrane protein 2) staining. Aortic cryosections were incubated with rat anti-mouse Mac-3 antibody at 1:5,000 dilution (product number 550292, Clone M3/84, BD Pharmingen, Franklin Lakes, NJ, USA).

Angiogenesis: CD31 (I, III)

CD31, a platelet endothelial cell adhesion molecule-1 (PECAM-1), is an integral membrane glycoprotein, which is robustly expressed in early and mature endothelial cells, as well as platelets and leukocyte subpopulations. It is a sensor of endothelial cell response to stress, and is involved in the regulation of leukocyte migration. It is known to have various roles in vascular biology, particularly in

angiogenesis, which was visualized with monoclonal anti-rat CD31 antibody at dilution 1:10,000 (product number MCA1334GA, AbD Serotec).

Target molecules: CD61 (I), CD44 (II), MMP-2 and MMP-9 (III-IV)

β_3 integrin subunit, which is also known as CD61 antigen, was visualized with mouse anti-rat CD61 antibody at dilution 1:5,000 (product number MCA1773, AbD Serotec). (I)

CD44 is a major cell-surface receptor for HA and their interaction has been found to play an important role in cell migration, tumorigenesis, metastasis, and the regulation of immune responses. CD44 is composed of many transmembrane glycoproteins with extensive molecular heterogeneity, and not all CD44 expressing cell types bind HA. Mouse monoclonal 1F1 antibody provided by Sirpa Jalkanen's group (Ristamäki et al. 1997) was used to visualize CD44 positive cells in the infarcted area of the damaged myocardium. (II)

Polyclonal anti-MMP-2 (dilution 1:100, product number ab19167, Merck, Darmstadt, Germany), and polyclonal anti-MMP-9 (dilution 1:1,000, product number ab38898, Abcam, Cambridge, UK) antibodies were used to detect gelatinase producing cells both in the atherosclerotic aorta and the damaged myocardium. (III-IV)

Double staining (III)

Double stainings with anti-MMP-9 (1:1,000) and either CD68 (1:15,000) or monoclonal antibody for α -smooth muscle actin (1:10,000, Product number A5228, Sigma-Aldrich) were performed in several sections to identify cell types expressing MMP-9.

Immunohistochemistry analysis (I-IV)

Digital images of the stained sections were captured with 3D Histech Panoramic 250 Flash digital slide scanner (3D Histech, Budapest, Hungary). The size of the MI was measured in Masson's trichrome stained sections as circumferential percentage of the infarct scar of the whole endocardial length of the LV. Each staining was analyzed with Image-J software v. 1.46 (National Institutes of Health, Bethesda, MD, USA) using specific colorthreshold values. Mean percentages of positive areas in scar tissue from each animal (I-III) or each atherosclerotic lesion (IV) were plotted against normalized tracer accumulation in adjacent tissue sections as measured with digital autoradiography.

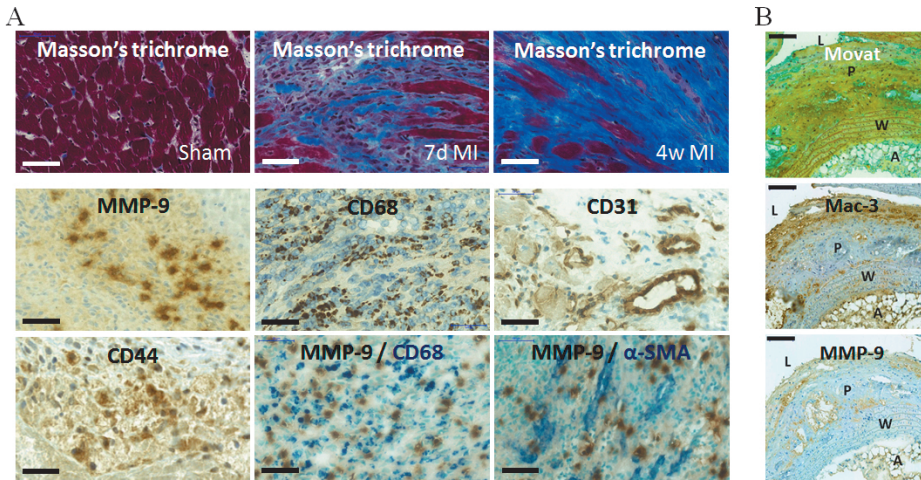


Figure 6. Examples of histology and immunohistochemistry. **A:** Micrographs show Masson's trichrome stained left ventricular myocardium of a sham-operated animal and of the infarcted area at 7 days and 4 weeks after coronary ligation. Myocytes appear red and collagen fibers blue. Other micrographs show examples of various immunostainings as well as double stainings 7 days after coronary ligation. **B:** Longitudinal sections of the mouse atherosclerotic aorta show general histology visualized with Movat pentachrome, as well as Mac-3 and MMP-9 stainings. L: lumen, P: plaque, W: wall, A: adventitia. Scale bars are 50 μm (**A**) and 100 μm (**B**).

4.8 Statistical analysis

All data are expressed as means \pm SDs. Statistical analysis was performed with SPSS Statistics software v. 21-24 (IBM, NY, USA). For the comparison of different tissues from the same subject, Student's t-test for paired data was applied. An unpaired Student's t test or Independent-Samples Mann-Whitney U test was used for comparison between two study groups. Comparisons of three groups were done with either Independent-Samples Kruskal-Wallis test or ANOVA with Dunnett's correction. Spearman's rank test or Pearson 2-tailed product-moment correlation coefficient was used to analyze correlations between two continuous variables. P values less than 0.05 were considered statistically significant.

5 RESULTS

5.1 Gelatinase (MMP-2/9) imaging in atherosclerosis (IV)

5.1.1 Plaque size, inflammation, and gelatinase (MMP-2/9) activity

All LDLR^{-/-}ApoB^{100/100} mice developed atherosclerotic plaques, whereas no lesions were detected in the control (C57BL/6N) group. Plaques were mostly of the fibroatheroma type, with a well-defined fibrous cap and macrophage infiltration visualized by Mac-3 staining. Disposition of MMP-9 within the lesions was more diffuse, with only a few clearly positive cells co-localizing with Mac-3 positive macrophages (Figure 6B). Zymography revealed a high concentration of activated MMP-9 in the plasma of atherosclerotic mice, whereas the active enzyme was not detectable in the aorta. Activated MMP-2, on the other hand, was present in the aorta, whereas MMP-2 activity in plasma appeared (to be) lower than that of MMP-9.

5.1.2 Tracer biodistribution, autoradiography, immunohistochemistry and *in vivo* PET/CT

Tracer uptake in the whole aorta did not differ between the atherosclerotic (0.43 ± 0.19 %ID/g) and control (0.52 ± 0.25 %ID/g, $p = 0.61$) groups. Blood radioactivity concentration in atherosclerotic mice was 1.8-fold higher (1.3 ± 0.40 %ID/g, $p = 0.017$) as compared with healthy controls (0.69 ± 0.21 %ID/g). The pre-treatment of mice with MMP-2/9 inhibitor decreased tracer uptake in atherosclerotic aorta by 55% ($p = 0.030$) and in blood by 52% ($p = 0.030$). (IV)

Quantitative autoradiography showed higher uptake of MMP-2/9 targeted tracer in atherosclerotic plaques (11 ± 3.0 PSL/mm²) as compared with normal vessel wall (6.4 ± 2.8 PSL/mm²; plaque-to-wall ratio 1.8 ± 0.34 , $p = 0.0029$). The areal percentage of Mac-3 positive macrophages in plaque lesions correlated closely with the uptake of the MMP-2/9 targeted tracer ($R = 0.91$, $p < 0.001$), but MMP-9 staining did not show any statistically significant correlation ($R = 0.40$, $p = 0.099$) with the tracer uptake.

In vivo PET/CT imaging was unsuccessful in showing focally increased uptake associated with the atherosclerotic lesions.

5.2 Imaging of myocardial healing after MI

5.2.1 Histology and immunohistochemistry (I-III)

Measured as the percentage of the LV circumference, the size of MI ranged between 12–67% at 7 days and 12–62% at 4 weeks after coronary ligation. None of the sham-operated rats had MI. Histology demonstrated a necrotic core surrounded by granulated tissue containing abundant myofibroblasts, neovessels, and macrophages at 7 days after coronary ligation. Masson's trichrome staining demonstrated that the scar tissue contained less dense collagen at 7 days than at 4 weeks after MI. There was also more interstitial collagen in the remote, non-infarcted myocardium at 4 weeks after MI as compared with the sham-operated rats. (I-III)

Immunohistochemistry showed the presence of numerous CD68-positive macrophages and CD31-positive endothelial cells in the infarcted area both at 7 days and 4 weeks after MI. CD61 (β_3 integrin subunit), CD44 (HA receptor), MMP-2 and MMP-9 positive cells were also present in the infarcted area at 7 days after MI. Only few positive cells were detected in the remote non-infarcted myocardium. Double staining showed that MMP-9 positivity co-localized often with CD68-positive macrophages, whereas there was no co-localization with α -smooth muscle actin staining in the infarcted area.

5.2.2 *In vivo* stability of the tracers (I, III)

The radiochemical purity of the tracers was >95% throughout the studies. ^{68}Ga -DOTA-E-[c(RGDfK)]₂ peptide showed feasible *in vivo* stability, with the proportion of total radioactivity in plasma originating from the intact tracer being $94 \pm 3.2\%$ at 45 min and $68 \pm 6.1\%$ at 60 min after injection. Only one radioactive metabolite was detected. Based on the retention time of 3.5 min, the metabolite most probably was a detached DOTA chelator. The radioactivity was rapidly excreted through kidneys and appeared 98% as intact tracer in urine at 75 min after injection. (I)

In contrast, the proportion of intact MMP-2/9 targeting tracer rapidly decreased after injection. At 30 minutes after i.v. injection, $17\% \pm 1.6\%$ of plasma total radioactivity was accounting from the intact tracer. (III)

5.2.3 PET/CT imaging (I, III)

In vivo ^{68}Ga -DOTA-E-[c(RGDfK)]₂ PET/CT images showed focally increased tracer uptake in the LV myocardium at 7 days and 4 weeks post-MI, which co-localized with the perfusion defect area in the ^{11}C -acetate images (Figure 7). There was increased tracer uptake in the infarcted area both at 7 days (MI/remote ratio 2.25 ± 0.24 , $p < 0.001$) and 4 weeks (MI/remote ratio 2.13 ± 0.37 , $p = 0.03$) after MI. Tracer uptake was also increased in the remote area (1.3-fold, $p < 0.04$) at 4 weeks after MI as compared to myocardium of the sham-operated controls.

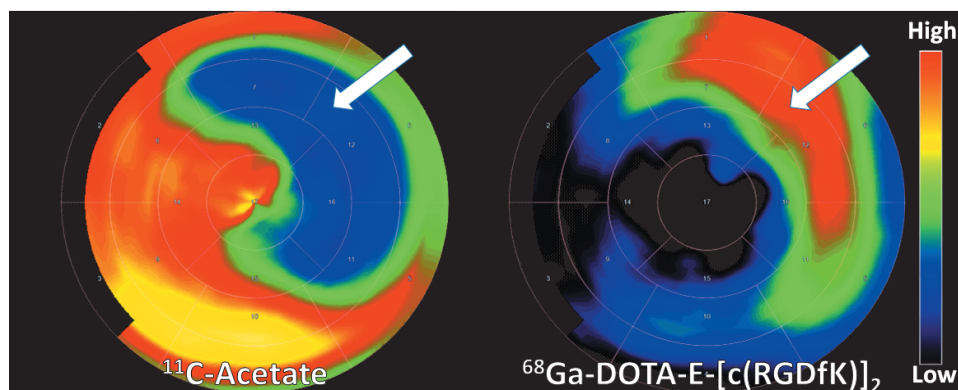


Figure 7. Examples of ^{11}C -acetate and ^{68}Ga -DOTA-E-[c(RGDfK)]₂ uptake in damaged myocardium at 7 days after MI. The polar map shows clear ^{68}Ga -DOTA-E-[c(RGDfK)]₂ uptake in the anterolateral LV wall co-localizing with a perfusion defect in the ^{11}C -acetate scan. Images are presented using standardized 17-segmental myocardial imaging as proposed by the American Heart Association (Cerqueira et al. 2002).

Based on PET/CT imaging, blood concentration of the gelatinase targeting ^{68}Ga -DOTA-peptide decreased slowly. Radioactivity concentration was higher in the blood than myocardium throughout the imaging period, up to 60 minutes. Thus, no specific signal from the infarcted area of myocardium was visible either at 7 days or 4 weeks after coronary ligation. Interestingly, blood radioactivity concentration was lower in healthy animals than in animals subjected to either coronary ligation or sham operation ($p < 0.001$).

5.2.4 Ex vivo studies (I-IV)

As compared with the sham-operated rats, ^{68}Ga -DOTA-E-[c(RGDfK)]₂ uptake in the LV myocardium (including both the infarcted and remote myocardium) of the rats with coronary ligation was 2.2-fold higher at 7 days post-MI (SUV 0.52 ± 0.13 vs. 0.24 ± 0.01 , $p < 0.001$) and 2.4-fold higher at 4 weeks post-MI (SUV 0.53 ± 0.09 vs. 0.23 ± 0.03 , $p < 0.001$). Average myocardium-to-blood ratio was 3.6 ± 1.7

($p = 0.01$) at 7 days and 2.9 ± 1.8 ($p < 0.001$) at 4 weeks post-MI. In other organs, the differences between the groups did not reach statistical significance. Radioactivity accumulated strongly into liver and excreted rapidly through kidneys to the urine. (I)

^{68}Ga -NOTA-HA-hexasaccharide-T6 uptake in the LV was 1.8-fold higher at 7 days post-MI as compared to the sham-operated rats and 4.5-fold higher as compared to healthy controls (SUV 0.18 ± 0.0031 , 0.10 ± 0.0088 and 0.040 ± 0.0068 , respectively). Average myocardium-to-blood ratio was 0.78 at 7 days post-MI, which prevented *in vivo* imaging of damaged myocardium with this tracer. See the original publication (II) for tracer uptake in other organs. (II)

The uptake of MMP-2/9 targeting ^{68}Ga -DOTA-peptide in the LV myocardium was significantly higher in rats with coronary ligation than rats with sham operation at 7 days (SUV 0.40 ± 0.13 vs. 0.59 ± 0.072 , $p = 0.030$) and at 4 weeks (0.39 ± 0.067 vs. 0.58 ± 0.14 , $p = 0.019$) after surgery. Blood radioactivity concentration was comparable between the rats with coronary ligation or sham operation (1.2 ± 0.34 vs. 1.26 ± 0.31). (III. Tracer uptake in the whole aorta was at the same level both in the atherosclerotic (0.43 ± 0.19 %ID/g) and control (0.52 ± 0.25 %ID/g, $p = 0.61$) mice. The highest radioactivity uptake was observed in kidneys and urine in both mice strains. The blood radioactivity concentration in the atherosclerotic mice was 1.8-fold higher (1.3 ± 0.40 %ID/g, $p = 0.017$) as compared with the healthy controls (0.69 ± 0.21 %ID/g). Radioactivity was rapidly excreted through kidneys (8.0 ± 2.9 %ID/g in atherosclerotic mice) to urine (440 ± 160 %ID/g). (IV)

MMP-2/9 binding specificity (III)

The pre-treatment of rats with MMP-2/9 inhibitor reduced tracer binding in the LV myocardium by 24% (from 0.59 ± 0.07 SUV to 0.45 ± 0.033 SUV, $p = 0.002$). The excessive amount of unlabeled peptide, in turn, reduced the tracer uptake in the LV myocardium by 48% (to 0.30 ± 0.024 , $p < 0.001$). There were also reductions in other tissues, including plasma, blood, liver, spleen, lungs, and skeletal muscle. (III)

5.2.5 Autoradiography (I-IV)

Average ^{68}Ga -DOTA-E-[c(RGDfK)]₂ uptake in the infarcted area was 5.1 ± 1.6 -fold higher than in the remote myocardium at 7 days post-MI. At 4 weeks post-MI, the uptake was still 4.1 ± 1.0 -fold higher. Tracer uptake was also increased in the remote, non-infarcted myocardium both at 7 days and at 4 weeks post-MI as compared with the corresponding myocardial wall of the sham-operated rats (7.5

± 1.4 vs. 5.5 ± 0.7 PSL/mm², $p = 0.006$ and 8.5 ± 0.8 vs. 5.4 ± 0.1 PSL/mm², $p < 0.001$, respectively). (I)

MMP-2/9 binding ⁶⁸Ga-DOTA-peptide uptake showed clear focal increase in the infarcted area both at 7 days and 4 weeks after MI. The average MI-to-remote ratio was 2.5 ± 0.46 at 7 days and 3.1 ± 0.98 at 4 weeks. There were no differences in ⁶⁸Ga-DOTA peptide uptake between the remote, non-infarcted areas of the rats with MI and the myocardium of the sham-operated rats either 7 days or 4 weeks after coronary ligation. There was also a strong correlation between the size of MI and the amount of ⁶⁸Ga-DOTA-peptide uptake in autoradiography images both in the remote ($r_s = 0.86$, $p = 0.007$) and infarcted ($r_s = 0.96$, $p < 0.001$) areas at 7 days after MI. Correlations observed at 4 weeks were $r_s = 0.93$, $p < 0.001$ and $r_s = 0.79$, $p = 0.010$. (III)

The MI-to-remote ratios of the studied tracers are visualized in Figure 8.

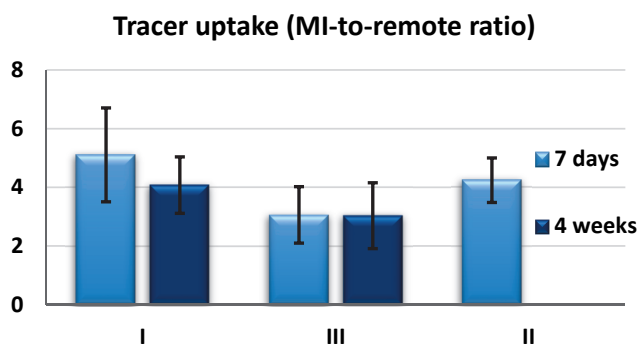


Figure 8. MI-to-remote ratio of tracer uptake in damaged rat myocardium as quantified by *ex vivo* autoradiography at 7 days and 4 weeks after coronary ligation. I: ⁶⁸Ga-DOTA-E-[c(RGDfK)]₂, III: ⁶⁸Ga-DOTA conjugated MMP-2/9 ligand, II: ⁶⁸Ga-NOTA-HA-hexasaccharide-T₆.

Tracer uptake in atherosclerotic plaques (11 ± 3.0 PSL/mm²) of LDLR^{-/-} ApoB^{100/100} mice was higher than in normal vessel wall (6.4 ± 2.8 PSL/mm²; plaques-to-wall ratio 1.8 ± 0.34 , $p = 0.0029$). (IV)

Tracer uptake vs. immunohistochemistry (I, III, IV)

In the infarcted area, ⁶⁸Ga-DOTA-E-[c(RGDfK)]₂ uptake correlated closely ($r_s = 1.000$, $p < 0.001$) with integrin β_3 chains (CD61 positive area). Correlation to endothelial cells (CD31 antibodies) was visible at 4 weeks ($r_s = 0.83$, $p = 0.021$), but not at 7 days after MI, and no correlation with the area of macrophage staining was observed either at 7 days or 4 weeks. The correlation of tracer uptake with the amount of collagen visualized with Masson's trichrome was inverse ($r_s = -0.915$, $p < 0.001$). (I)

There was a correlation between the uptake of ^{68}Ga -DOTA-peptide and CD68-positive macrophages in the infarcted area at 7 days after MI ($r_s = 0.94$, $p = 0.002$). Tracer uptake also correlated with CD31-positive endothelial cells both at 7 days ($r_s = 1.0$, $p < 0.001$) and at 4 weeks ($r_s = 1.0$, $p < 0.001$) after MI. No correlations with the areal percentage of collagen were detected. (III)

Tracer uptake in mouse atherosclerotic plaques correlated strongly with the amount of Mac-3 positive macrophages ($R = 0.91$, $p < 0.001$), but weakly with MMP-9 staining ($R = 0.40$, $p = 0.099$). (IV)

6 DISCUSSION

6.1 Animal models

6.1.1 *LDLR^{-/-}ApoB^{100/100} atherosclerotic mice*

The lipid profile of the atherosclerosis model used in the study resembles human familial hypercholesterolemia (Heinonen et al. 2007). MMP, and specifically gelatinase, activity is present both in human and mouse atherosclerotic plaques. Still, significant differences in the overall atherosclerosis pathobiology remain. Clinically relevant human plaques develop in coronary and carotid arteries, whereas in mice, the disease focuses on the aorta (Zhang et al. 1992). Contrary to human disease, plaque ruptures are extremely rare in mouse models and the presence of both intima smooth muscle cells and neoangiogenesis is almost non-existent. Mouse atherosclerosis also exhibits certain differences in inflammatory processes, which, contrary to human disease, tend to diminish with age. In addition, experimental animals live in sterile conditions and do not commonly confront infections during their lifespan, which may affect disease development (Hellberg 2017). The small size of the animals creates significant limitations for the *in vivo* imaging, which are even more apparent with small imaging targets, such as atherosclerotic plaques, due to the limitations in PET resolution. *In vivo* imaging proved unsuccessful in this study, although the analysis of the gelatinase targeting tracer uptake showed some promising results *ex vivo*.

6.1.2 *Rat model of myocardial infarction*

Surgical murine MI models have been in use for decades (Pfeffer et al. 1979) in both biology and therapy studies, as well as for the development of diagnostic imaging. Despite the similar molecular patterns of MI pathobiology, significant differences, such as the lack of collateral arteries in rat heart, are apparent between murine MI/HF models and human MI, or large (porcine) models of HF. In the present studies, the size of myocardial infarction in rats ranged up to 67% of LV circumference, which would undoubtedly be fatal for humans. The rats were followed up for 4 weeks after coronary ligation, and none of them died later than 48 h after coronary ligation, which suggests that rats are less prone to cardiac arrhythmias. Also, no apparent effect on animal wellbeing was observed after the termination of analgesia at 72 hours after the operation.

The present studies confirmed the feasibility of a surgical rat model for the initial assessment of PET tracers for myocardial imaging targeting specific molecules. LGE MRI remains the gold standard for imaging of cardiac fibrosis, which is a complex process with vast numbers of ECM components involved. Molecular imaging targeting specific molecules, including integrins, MMPs, collagen, etc. may assist in the diagnosis, staging, and treatment of cardiac fibrosis in the near or distant future (Baues et al. 2017). Target molecules were present in rat myocardium, as confirmed with immunohistochemistry. Moreover, interstitial fibrosis was observed in the remote, non-infarcted areas of damaged myocardium, which may be relevant for the purpose of assessing potential HF imaging targets. Rat heart is also of sufficient size for cardiac imaging in terms of the resolution of small-animal PET/CT modalities, thus enabling sufficiently potent tracer uptake to be visualized *in vivo*.

6.2 The evaluated PET tracers

6.2.1 $^{68}\text{Ga-DOTA-E-[c(RGDfK)]}_2$

The present study confirmed the feasibility of *in vivo* $^{68}\text{Ga-DOTA-E-[c(RGDfK)]}_2$ PET for detecting increased β_3 integrin expression in rat heart after MI. *In vivo* imaging also showed increased uptake both in the infarcted area and remote myocardium, consistently with *ex vivo* analyses.

The 5.1-fold (range 3.7 – 8.3) higher uptake of $^{68}\text{Ga-DOTA-E-[c(RGDfK)]}_2$ is sufficiently high and comparable to previous studies, in which the RGD uptake in the infarcted area has ranged between 3.9 and 5.2 (van den Borne et al. 2008, Sherif et al. 2012, Gao et al. 2012, Laitinen et al. 2013). A considerable limitation of the study was the lack of a direct comparison with other RGD-based tracers.

This study also showed feasible tracer kinetics. The tracer remained very stable ($94 \pm 3.2\%$) up to 45 min after injection and the metabolite correction of the *in vivo* data had only a minor effect on the results, thus suggesting the metabolite correction to be unnecessary. The results also showed that SUV measurements from static images are comparable with the kinetic modeling of distribution volume, thereby simplifying *in vivo* analyses.

The extracellular space augmentation in the MI scar may have influenced the high distribution volume. This effect, however, is most probably insignificant due to the long dynamic imaging, comparable SUV values and the fact that no difference in K1 values was found between the infarcted and sham-operated groups. Altogether,

this indicates that the ^{68}Ga -DOTA-E-[c(RGDfK)]₂ accumulation is independent of perfusion.

Tracer uptake showed strong correlation to β_3 integrin expression in the infarcted area, but not to the amount of macrophages. The areal percentage of β_3 integrin subunit (CD61) in the infarcted area was significantly lower as compared with CD31 positive endothelial cells. CD61 expression did not confine to vascular structures either. Although neovascularization peaks at 1 week after the ischemic injury (Meoli et al. 2004), a direct correlation between the area of positive CD31 staining and tracer uptake was detected at 4 weeks after the injury, indicating a dominating role of angiogenesis as an RGD target in the later stages of scar formation. Additionally, an inverse correlation between positive collagen staining and tracer uptake was detected in the infarcted area, which most probably indicates a decrease of β_3 integrin expression in the final stages of the collagenous scar formation (van den Borne et al. 2008 and 2010). The lack of correlation with the amount of mature, dense collagen does not rule out the feasibility of RGD uptake measurement, which reflects the formation of myocardial fibrosis by detecting processes preceding actual collagen deposition.

While β_3 integrin subunit has mainly been detected on endothelial and smooth muscle cells (Manso et al. 2009), the activated fibroblasts expressing both $\alpha_v\beta_3$ and $\alpha_v\beta_5$ integrins may also, in part, be responsible for the RGD binding (van den Borne et al. 2008). This is in line with the fact that integrins are involved in many parallel processes and expressed by various types, both during the initial infarct healing and subsequent myocardial remodeling (Manso et al. 2009, Kuppuswamy et al. 1997, Higuchi et al. 2007). In addition to the infarcted area, ^{68}Ga -DOTA-E-[c(RGDfK)]₂ uptake was also increased in the remote, non-infarcted myocardium, both 7 days and 4 weeks after MI. Detection of these ECM alterations, which lead to the formation of interstitial fibrosis outside the scar area, may have important implications for detection of diffuse myocardial pathologies in ischemic and non-ischemic myocardial diseases (Higuchi et al. 2007).

6.2.2 ^{68}Ga -NOTA-HA-hexasaccharide-*T*₆

Sufficient myocardial uptake of the tracer indicated the initial potential of CD44 targeting for imaging the post-MI healing processes. Further analysis is required to establish *in vivo* stability of the tracer, as well as the binding specificity. Correct dosage and better specific radioactivity could also increase blood clearance and thus facilitate reliable *in vivo* imaging. More potent and smaller probes targeting CD44 receptors or HA turnover should also be considered for development. However, HA also has a great amount of functions in various tissues, acting both

as a mechanical structure and a signaling molecule. This may prove to be challenging in terms of the imaging of specific molecular actions.

6.2.3 ⁶⁸Ga-DOTA conjugated gelatinase (MMP-2/9) ligand

Myocardial infarction

Autoradiography showed increased tracer uptake in the infarcted area as compared to remote myocardium as well as the myocardium of the sham-operated rats both at 7 days and 4 weeks after MI, which is in line with the findings concerning the time course and localization of gelatinase activity after MI in previous studies (Sahul et al. 2011). The peptide used in the present study has previously shown high selectivity to gelatinases as compared with other MMP types (Koivunen et al. 1999). Pre-treatment with MMP-2/9 inhibitor lowered tracer uptake significantly, indicating specific uptake in the myocardium. Still, the autoradiography signal could also be partly attributed to the non-specific tissue uptake due to residual tracer molecules and radiometabolites in the blood pool.

Tracer uptake correlated with macrophages and endothelial cells in the infarcted area. Double staining showed co-localization of MMP-9 with CD68-positive macrophages, but not with α -smooth muscle actin, even if both MMP-9 and MMP-2 have previously been shown to play a role in post-ischemic neovascularization (Chen et al. 2009).

The tracer was rapidly metabolized, and radioactivity in blood pool remained high up to 60 minutes. Accordingly, tracer uptake in damaged myocardium was not detectable by *in vivo* PET. Thus, although *ex vivo* analyses demonstrated clear tracer uptake in the infarcted myocardium, *in vivo* imaging was not feasible due to the low myocardium-to-blood ratio.

Atherosclerosis

Increased uptake of the tracer was also clear in inflamed atherosclerotic plaques as compared to normal vessel wall. Tracer uptake correlated closely with the areal percentage of macrophages, reflecting a portion of inflammatory activity in these lesions. The pre-treatment of mice with MMP-2/9 inhibitor also decreased tracer uptake in the aorta, indicating the specificity of tracer binding, and zymography confirmed the presence of activated MMP-2 in atherosclerotic aorta.

However, the blood radioactivity concentration remained higher as compared to the aorta. Thus, tracer uptake in atherosclerotic lesions was not detectable by *in vivo* PET/CT.

Previously, broad-spectrum MMP targeting tracers have yielded promising results in terms of their correlation to inflammation markers, as well as sufficient spatial resolution and target-to-background ratio to enable *in vivo* imaging in small-animal models of atherosclerosis (Fujimoto et al. 2008, Hermann et al. 2012). Still, further understanding of the pathophysiological roles of each MMP subtype in each different form and exact time course in correlation with plaque size and vulnerability development is warranted in order to ensure adequately focused tracer evolution and development of an imaging-based plaque vulnerability screening protocol.

6.3 Future aspects

Nuclear cardiology continues to be a dynamic, rapidly evolving field of diagnostic nuclear medicine with a strong trend towards integrating nuclear techniques with CT or MR-derived datasets (Bengel et al. 2017). Although the clinical applications of novel tracers for imaging myocardial infarction are yet to be determined, the molecular imaging of new targets can also clarify the pathogenesis of heart failure and be potentially useful in order to study the effects of the used therapies (Saraste et al. 2017).

In vivo imaging of vulnerable atherosclerotic plaques has also advanced significantly since the first observation of ^{18}F -FDG accumulation in atherosclerotic arteries (Rudd et al. 2002). Multimodal imaging devices allow for the visualization of ever smaller targets and numerous new tracers for atherosclerosis are being developed and evaluated (Hellberg 2017). In addition to detecting vulnerable plaques, the focus of imaging has also shifted towards the study of disease pathobiology and therapy response.

RGD-motif based PET tracers targeting $\alpha_v\beta_3$ integrin have been evaluated extensively in experimental models of myocardial infarction. Initial clinical studies have also been performed (Jenkins et al. 2017) and are continuing. Both in experimental and clinical studies of AMI, the RGD-based radiotracers accumulate in the infarcted area of myocardium at 3 days and peaked at 1–3 weeks after MI, thus correlating with both angiogenesis and scar formation rates, as well as adverse remodeling.

Due to the wide spectrum of both the physiological and pathophysiological roles of MMPs, the question remains whether further development of MMP imaging probes should focus on broad-spectrum MMP screening or on detecting more specific subpopulations and forms of various MMP enzymes. To date, the development of gelatinase-selective probes has been challenging due to the

similarities in MMP-2 and MMP-9 enzyme structure, although the affinity of auspicious probes can potentially be steered towards either one (Selivanova et al. 2013).

Another potential challenge in gelatinase imaging are the soluble gelatinases detected in patients with unstable atherosclerotic lesions (Nenster et al. 2013, Servello et al. 2014, Tan et al. 2014) and after myocardial infarction (Giannikos et al. 2016), which may impair imaging of target tissues. New tracers for imaging the activation of MMP subtypes, such as a dual isotope, activatable, cell penetrating peptide probe (van Duijnhoven et al. 2014), are being actively developed in pursuit to amplify signal intensity.

The higher β^+ energy of ^{68}Ga as compared with other radionuclides, such as the commonly used ^{18}F , results in an undeniably lower *in vivo* PET resolution. Still, ^{68}Ga tracers have the advantage of easy and fast radiolabeling with a generator-produced radionuclide, excluding the necessity of an on-site cyclotron and, in this way, enabling wider availability of PET imaging. The development of multimodality imaging devices that combine molecular and anatomical imaging (PET/CT and PET/MRI) has greatly advanced the field of nuclear cardiology.

Soft tissue imaging has benefited significantly from the introduction and development of PET/MRI. MRI has substantially better soft-tissue contrast as compared to/with CT, and the variety of MRI sequences allow for even more versatile tailoring of dual imaging sequences (Rischpler et al. 2013). The high spatial resolution of MRI is also an advantage for imaging small targets, such as atherosclerotic plaques or specific regions of myocardium. However, the longer imaging durations of MRI as compared to CT may limit the wider use of PET/MRI. Further developments are also needed regarding MRI attenuation correction methods and motion corrections, as well as the correction of partial volume effects (Rischpler et al. 2013, Bailey et al. 2016). Thus, despite its increasing utilization it is unlikely for PET/MRI to completely replace PET/CT in nuclear cardiology.

Many of the known molecular mechanisms involved in myocardial healing after MI have been shown to have both beneficial and adverse impacts depending on the extent and time-frame of their expression or activity. Thus, in addition to the development of imaging techniques, including the validation of molecular imaging probes, further understanding of molecular pathophysiology is essential in order to establish screening protocols that are useful for detecting and monitoring the development of HF.

7 SUMMARY AND CONCLUSIONS

Three novel ^{68}Ga -labeled PET tracers for imaging of myocardial repair (after MI), and one for imaging of atherosclerosis were evaluated in the studies. The main conclusions were as follows:

1. ^{68}Ga -DOTA-E-[c(RGDfK)]₂ peptide is a potential new tracer for PET imaging of increased $\alpha_v\beta_3$ integrin expression that is associated with ECM alterations in the infarcted and remote areas of myocardium following MI.
2. ^{68}Ga -NOTA-HA-hexasaccharide-T₆ showed promising MI-to-remote ratio. Further analysis would be required in order to establish the *in vivo* stability of the tracer as well as the specificity of its binding. Correct dosage and better specific radioactivity could also increase blood clearance and thus enable reliable *in vivo* imaging.
3. MMP-2/9 targeting ^{68}Ga -DOTA-peptide accumulates in the damaged rat myocardium after an ischemic injury. However, tracer instability and slow *in vivo* clearance make it unsuitable for further evaluation in MI imaging.
4. MMP-2/9 targeting ^{68}Ga -DOTA-peptide showed tracer uptake in inflamed mouse atherosclerotic lesions, but due to low target-to-background ratio, the tracer did not allow for *in vivo* imaging of MMP-2/9 activation in the vessel wall.

^{68}Ga -DOTA-E-[c(RGDfK)]₂ showed the most optimal characteristics for imaging of myocardial healing processes, whereas ^{68}Ga -NOTA-HA-hexasaccharide-T₆ indicated promising potential, thus warranting further tracer development. MMP-2/9 targeting showed significant limitations.

ACKNOWLEDGMENTS

This study was conducted during the years 2011–2017 in Turku PET Centre and the Institute of Clinical Medicine, Department of Clinical Physiology and Nuclear Medicine at the Turku University Hospital and the University of Turku in Turku, Finland. I wish to express my gratitude to Professor Jaakko Hartiala (Head of the Department of Clinical Physiology and Nuclear Medicine during the first years of the study), Adjunct Professor Jukka Kemppainen (Head of the Department of Clinical Physiology and Nuclear Medicine since May 2016) and Professor Juhani Knuuti (Director of Turku PET Centre) for providing excellent facilities and cutting-edge technology for the research.

I would like to express my deepest gratitude to my supervisors, Professor Anne Roivainen and Associate Professor Antti Saraste, for all the valuable help, guidance and support I have received from both of you during these years. Your input in editing the manuscripts has been essential. Anne, thank you for giving me the opportunity to work in your research group and introducing me to the world of PET imaging. It has always been easy to come by your office with my endless worries and questions. Thank you for the supportive atmosphere of encouragement you create for us. Your expertise in preclinical imaging has been crucial to my work. Antti, it has been highly inspirational watching your effectiveness and skill in managing a remarkable number of ongoing research projects along with clinical work. Your ample knowledge of cardiology and clinical imaging has been most useful for me with this thesis, both in executing the research and understanding its relevance to clinical practice. Your genuinely positive attitude has also helped me through many difficult phases of the research. I have also been able to rely on my supervisors for ensuring continued financing for the studies. In addition to Anne and Antti, I wish to thank Juhani for acquiring research funds and taking a keen interest in my research and making useful and helpful points during our group meetings.

I wish to thank the official reviewers of my thesis: Professor Risto Kerkelä and Professor Olivier Gheysens. I appreciate your prompt work, positive review, and valuable, constructive comments and suggestions. Your input has significantly improved this thesis. I also warmly thank my follow-up committee members, Professor Mikko Savontaus and Professor Juhani Knuuti for giving the necessary guidance and support enabling me to focus, define and perform the study projects.

I would like to thank Professor Mika Scheinin, Director of the FinPharma Doctoral Program, and Professor Markku Koulu, Director of Drug Research Doctoral Programme, University of Turku. I would also like to acknowledge DRDP

coordinator Eeva Valve, who has been an excellent organizer and a great support in guiding me through the doctoral studies bureaucracy.

Ville Kytö is warmly acknowledged for performing excellent surgery on the study subjects. The long days operating in the basement went by flying and we managed to solve numerous challenges thanks to your confident approach and unwavering positive mindset.

I also wish to thank Pekka Saukko for providing pathology expertise. Seppo Ylä-Herttua from the University of Eastern Finland is acknowledged for essential collaboration within the CoE plaque imaging projects. Pirjo Nuutila at Turku Pet Centre is warmly thanked for significant intellectual contribution and providing financial support.

I wish to acknowledge the staff of the Central Animal Laboratory of the University of Turku. Director Ulla-Marjut Jaakkola, staff members Aila Saari and Nina Kulmala as well as veterinarian Rafael Frias are also sincerely thanked. The animal technicians, especially Anitta Niittymäki (in memoriam), Riina Valtonen, Nea Konttinen, and Terhi Hiltula-Maisala deserve great thanks for taking good care of the animals.

Erica Nyman has been an essential and highly qualified assistance with histotechnology, as well as in performing tissue sectioning along with Marja-Riitta Kajaala and, more often than not, working way past office hours. Liisa Lempiäinen is sincerely thanked for performing immunohistochemistry. Your professional skill and inventive resourcefulness are amazing! Timo Kattelus is acknowledged for skilled help with image processing, Ville Aalto and Eliisa Löyttyniemi are thanked for helping with statistics.

I would like to thank all the co-authors and project collaborators, especially Ingrid Dijkgraaf and Cheng-Bin Yim for providing in-depth knowledge of RGD chemistry, and Vesa Oikonen for performing proficient PET modeling. Pasi Virta, Harri Lönnberg, Sirpa Jalkanen, Tiina Laitiala-Leinonen, Päivi Poijärvi-Virta, Jussi Mäkilä and Satish Jadhav are thanked for your time, work, and intellectual input. Päivi Marjamäki is warmly thanked for the kind support and skillful assistance including, but not limited to, the in vitro studies. Johanna Tuomela is acknowledged for helpfulness and skillful zymography analyses.

Great thanks go to Xiang-Guo Li, Tiina Saanijoki, Olli Metsälä and Meeri Käkelä, for optimizing and performing the ^{68}Ga -labeling of the tracers as well as putting up with a 'lively' schedule. Without your input, this work would not have been possible! Semi Helin is acknowledged for the ^{11}C -acetate synthesis.

Turku PET Centre personnel, both past and present, are thanked for all the help and creation of a positive work atmosphere. Laura Jaakkola, Mirja Jyrkinen and Lenita Saloranta are kindly thanked for help with secretarial matters. I would also like to acknowledge Marko Tähtäläinen and Rami Mikkola for their efficient assistance in the IT issues. Carimas team is thanked for creating and improving the PET analysis software used in this work. I also wish to thank Sanna Suominen, Eija Salo and Heidi Partanen, as well as all the other laboratory technicians, for their help in the PET Centre laboratory, especially with the Wizard measurements. Also, Marita, Virva, Mia and others, thank you for the inspiring conversations in the coffee room!

Aake Honkaniemi and Leena Tokoi-Eklund have been essential in the animal imaging and all the related practical issues. Thank you for the work you've done! Minna Aatsinki is warmly acknowledged for scheduling PET imaging and Tarja Keskitalo for taking care of the dosimeters. Physicists Mika Teräs, Marko Tirri and Tuula Tolvanen are acknowledged for all the help with technical issues and radiation safety management.

Special thanks to Lea Heinonen-Eerola at Integra OY for exceptionally minded and thorough language check of this manuscript, which has improved quality and readability of this text significantly!

Johanna Silvola and Anu Autio are thanked for sharing experience and expertise. All past and present members of the cardiac and gallium groups are also thanked for their astute interest in the ongoing projects and fruitful discussions. Anni and other undergraduate students are thanked for their input.

Thanks to Heidi Liljenbäck for essential help with animal studies, as well as for the proficient skill in keeping the lab, and me, organized. Jenni Virta is also acknowledged for the help with animal imaging and related lab work. Mia Ståhle is warmly thanked for skilled help in various tasks, as well as the exceptionally positive work attitude and reliability!

Special thanks to Sanna Hellberg for guidance into everything PET related and all the years of studying and working together and side by side! Miikka Tarkia is greatly thanked for the friendship and peer support, as well as for providing scientific inspiration and setting the bar, not to mention the contribution to keeping up the testosterone levels in the analysis bunker.

Throughout these years, our group members have been a colossal mental support! Thank you Helena, Riikka, Maria, Juho, Sauli, Petteri, Petri, Reija, Olli, Ariana and all of you mentioned above, as well as all the colleagues, co-workers and coffee-break buddies I may have forgotten to add to this list, for your support,

practical ideas (the importance of coffee-table talks!), examples of success, hilarious laughs, ‘sparkling’ (Virtanen 2017) Fridays, spare time activities and unforgettable congress trips!

Besides the people directly or indirectly involved in this thesis work, I would like to thank all my medical school buddies, especially those in our study group. With your help and peer support I might actually get through the school.

Finally, I would like to extend my deepest gratitude to my family members for tolerating me, especially during these stressful years. My limitless gratitude and love to my grandmother and our medical matriarch Tamara. Your unconditional support has been one of the few things I have always been able to rely on, since 1985. Special thanks to my grandmother Olga (in memoriam) for her endless amount of love and care. Sincere thanks to my sister Vera, a wonderful friend and the brightest person I know. Best times are associated with our briefly overlapped childhood! I wish you success in all your endeavors! Great thanks to my mother Elena for the absolutely tremendous amount of support during these years. Also thanks to my father Alexander for the motivation. I also wish to extend my sincere gratitude to my mother-in-law Lyudmila. Your help with childcare has been paramount to us! Love to my son Andreas, who has had to put up with an absent father too many times during these years. Keep up your toughness and smile! Most of all, great thanks to my beloved wife Inga, for your love, support, and gargantuan patience in putting up with me! There is Life after PhD, let’s make it a great one!

The studies were conducted within the Finnish Centre of Excellence in Molecular Imaging in Cardiovascular and Metabolic Diseases supported by the Academy of Finland, the University of Turku, the Turku University Hospital, and Åbo Akademi University. This study was also funded by the Hospital District of Southwest Finland/Turku University Hospital (EVO/ERVA grant), the Finnish Cultural Foundation (Finland Proper Regional Fund), Academy of Finland, Sigrid Jusélius Foundation, the Finnish Foundation for Cardiovascular Research, the Maud Kuistila Memorial Foundation, Ida Montin’s foundation, and Emil Aaltonen foundation. I would also like to thank the Scandinavian and Finnish Isotope Societies, as well as the Drug Research Doctoral Programme for awarding travel grants.

Turku, May 2018



Max Kiugel

REFERENCES

- Abilleira S, Bevan S, Markus HS. (2006) The role of genetic variants of matrix metalloproteinases in coronary and carotid atherosclerosis. *J Med Genet.* 43:897–901
- Acampa W, Gaemperli O, Gimelli A, et al. (2015) Role of risk stratification by SPECT, PET, and hybrid imaging in guiding management of stable patients with ischaemic heart disease: expert panel of the EANM cardiovascular committee and EACVI, *Eur Heart J Cardiovasc Imaging.* 16:1289–1298
- Acampa W, Buechel RR, Gimelli A. (2016) Low dose in nuclear cardiology: state of the art in the era of new cadmium-zinc-telluride cameras, *Eur Heart J Cardiovasc Imaging.* 17:591–595
- Achard J, Fournier A, Mazouz H, Caride VJ, Penar PL, Fernandez LA. (2001) Protection against ischemia: a physiological function of the renin-angiotensin system. *Biochem Pharmacol.* 62(3):261-71
- Agostini D, Roule V, Nganoa C. et al. (2018) First validation of myocardial flow reserve assessed by dynamic 99mTc-sestamibi CZT-SPECT camera: head to head comparison with 15O-water PET and fractional flow reserve in patients with suspected coronary artery disease. *The WATERDAY study.* *Eur J Nucl Med Mol Imaging.* doi: 10.1007/s00259-018-3958-7. [Epub ahead of print]
- Angelidis G, Giamouzis G, Karagiannis G. et al. (2017) SPECT and PET in ischemic heart failure. *Heart Fail Rev.* 22(2):243-261
- Anzai A, Anzai T, Nagai S, et al. (2012) Regulatory role of dendritic cells in postinfarction healing and leftventricular remodeling. *Circulation* 125:1234–45
- Aono J, Suzuki J, Iwai M, et al. (2012) Deletion of the Angiotensin II Type 1a Receptor Prevents Atherosclerotic Plaque Rupture in Apolipoprotein E^{-/-} Mice. *Arterioscler Thromb Vasc Biol.* 32:1453-1459
- Mc Ardle B, Ziadi MC, Ruddy TD, Beanlands RS (2012) Nuclear perfusion imaging for functional evaluation of patients with known or suspected coronary artery disease: the future is now. *Futur Cardiol* 8(4):603–622
- Arslan F, de Kleijn DP, Pasterkamp G. (2011a) Innate immune signaling in cardiac ischemia. *Nat Rev Cardiol.* 8(5):292-300
- Arslan F, Smeets MB, Riem Vis PW, et al. (2011b) Lack of fibronectin-EDA promotes survival and prevents adverse remodeling and heart function deterioration after myocardial infarction. *Circ Res.* 108:582–592
- Awan R, Rajpoot K. (2015) Spatial and spatio-temporal feature extraction from 4D echocardiography images. *Comput Biol Med.* 64:138–147
- Bailey DL, Pichler BJ, Gückel B, et al. (2016) Combined PET/MRI: from status quo to status go. Summary report of the fifth international workshop on PET/MR imaging; February 15- 19, 2016; Tübingen, Germany. *Mol Imaging Biol* 18:637–650
- Bardy GH, Lee KL, Mark DB, et al. (2005) Amiodarone or an implantable cardioverter-defibrillator for congestive heart failure. *N Engl J Med.* 352:225–237
- Baues M, Dasgupta A, Ehling J, et al. (2017) Fibrosis imaging: Current concepts and future directions. *Adv Drug Deliv Rev.* 121:9-26
- Bax JJ, Delgado V. (2015) Myocardial viability as integral part of the diagnostic and therapeutic approach to ischemic heart failure. *J Nucl Cardiol.* 22:229–245
- Ben Bouallègue F, Roubille F, Lattuca B, et al. (2015) SPECT myocardial perfusion reserve in patients with multivessel coronary disease: correlation with angiographic findings and invasive fractional flow reserve measurements. *J Nucl Med.* 56:1712–1717
- Bench TJ, Jeremias A, Brown DL. (2011) Matrix metalloproteinase inhibition with tetracyclines for the treatment of coronary artery disease. *Pharmacological Research* 64: 561– 566
- Bengel FM, Higuchi T, Javadi MS, Lautamaki R. (2009) Cardiac positron emission tomography. *J Am Coll Cardiol* 54:1–15

- Bengel FM, George RT, Schuleri KH, Lardo AC, Wollert KC. (2013) Image-guided therapies for myocardial repair: concepts and practical implementation. *Eur Heart J Cardiovasc Imaging* 14:741–751
- Bengel FM. (2017) Issue “noninvasive molecular imaging and theranostic probes”: New concepts in myocardial imaging. *Methods*. [Epub ahead of print]
- Bergmann SR, Fox KA, Rand AL, et al. (1984) Quantification of regional myocardial blood flow in vivo with H215O. *Circulation*. 70(4):724-33
- Boag SE, Das R, Shmeleva EV, et al. (2015) T lymphocytes and fractalkine contribute to myocardial ischemia/reperfusion injury in patients. *J Clin Invest*. 125:3063–3076
- Bolli R, Marbán E. (1999) Molecular and cellular mechanisms of myocardial stunning. *Physiol Rev* 79:609-34
- van den Borne SW, Isobe S, Verjans JW, et al. (2008) Molecular imaging of interstitial alterations in remodeling myocardium after myocardial infarction. *J Am Coll Cardiol* 52:2017–2028
- van den Borne SW, Diez J. et al. (2010) Myocardial remodeling after infarction: the role of myofibroblasts. *Nat Rev Cardiol* 7:30–37
- Braitsch, C. M., Kanisicak, O., van Berlo, J. H., Molkenkin, J. D. & Yutzey, K. E. Braunwald E (2013) Heart failure. *JACC Heart Fail*. 1(1):1–20 Differential expression of embryonic epicardial progenitor markers and localization of cardiac fibrosis in adult ischemic injury and hypertensive heart disease. *J. Mol. Cell. Cardiol*. 65, 108–119
- Braunwald E (2013) Heart failure. *JACC Heart Fail*. 1(1):1–20
- Bucerius J, Mani V, Moncrieff C, et al. (2014) Optimizing 18F-FDG PET/CT imaging of vessel wall inflammation: the impact of 18FFDG circulation time, injected dose, uptake parameters, and fasting blood glucose levels. *Eur J Nucl Med Mol Imaging* 41:369–383
- Buja LM, Vander Heide RS (2016) Pathobiology of Ischemic Heart Disease: Past, Present and Future. *Cardiovascular Pathology* 25:214-220
- Bäck M, Ketelhuth DFJ, Agewall S. (2010) Matrix Metalloproteinases in Atherothrombosis. *Progress in Cardiovascular Diseases* 52:410-428
- Bonafè F, Govoni M, Giordano E, Caldarrera CM, Guarnieri C, Muscari C. (2014) Hyaluronan and cardiac regeneration. *Journal of Biomedical Science* 21:100
- van den Borne SW, Isobe S, Verjans JW, et al. (2008) Molecular imaging of interstitial alterations in remodeling myocardium after myocardial infarction. *J Am Coll Cardiol*. 52:2017–2028
- van den Borne SW, Cleutjens JP, Hanemaaijer R, et al. (2009) Increased matrix metalloproteinase-8 and -9 activity in patients with infarct rupture after myocardial infarction. *Cardiovasc Pathol*. 18:37–43
- van den Borne SW, Diez J, Blankesteyn WM, et al. (2010) Myocardial remodeling after infarction: the role of myofibroblasts. *Nat Rev Cardiol*. 7(1):30-7
- Caiani EG, Corsi C, Sugeng L, et al. (2006) Improved quantification of left ventricular mass based on endocardial and epicardial surface detection with real time three dimensional echocardiography. *Heart*. 92:213–219
- Canali E, Masci P, Bogaert J, et al. (2012) Impact of gender differences on myocardial salvage and post-ischaemic left ventricular remodelling after primary coronary angioplasty: new insights from cardiovascular magnetic resonance. *Eur Heart J Cardiovasc Imaging* 13: 948-953
- Cerqueira, M.D., Weissman, N.J., Dilsizian, V, et al. (2002) “Standardized Myocardial Segmentation and Nomenclature for Tomographic Imaging of the Heart. A Statement for Healthcare Professional from the Cardiac Imaging Committee of the Council on Clinical Cardiology of the American Heart Association.” *Circulation* 105: 539–42
- Chai SY, Zhuo J, Mendelsohn FA. (1993) Localization of components of the renin-angiotensin system and site of action of inhibitors. *Arzneimittelforschung*. 43(2A):214-21

- Chatterjee S, Ghosh J, Lichstein E, Aikat S, Mukherjee D. (2012) Meta-analysis of cardiovascular outcomes with dronedarone in patients with atrial fibrillation or heart failure. *Am J Cardiol* 110:607–613
- Chen B, Frangogiannis NG. (2017) Immune cells in repair of the infarcted myocardium. *Microcirculation*. 24(1). doi: 10.1111
- Chen C, Feng Y, Zou L, et al. (2014) Role of extracellular RNA and TLR3-Trif signaling in myocardial ischemia-reperfusion injury. *J Am Heart Assoc*. 3(1):e000683
- Chen F, Eriksson P, Hansson GK, et al. (2005) Expression of matrix metalloproteinase 9 and its regulators in the unstable coronary atherosclerotic plaque. *Int J Mol Med*. 15(1):57–65
- Chen R, Zhu M, Ashraf M. (2016) Non-invasive evaluation of heart function with four-dimensional echocardiography. *PLoS One*. 2016;11:e0154996
- Chen S, Evans T, Mukherjee K, Karmazyn M, Chakrabarti S. (2000) Diabetes induced myocardial structural changes: role of endothelin-1 and its receptors. *J Mol Cell Cardiol*. 32:1621–1629
- Cochain C, Zerneck A. (2017) Macrophages in vascular inflammation and atherosclerosis. *Pflugers Arch - Eur J Physiol* [Epub ahead of print]
- Cohen MV and Downey JM (2011) Ischemic Postconditioning: From Receptor to End-Effector. *Antioxid Redox Signal* 14(5):821–31
- Coker ML, Jolly JR, Joffs C, Etoh T, Holder JR, Bond BR, Spinale FG. (2001) Matrix metalloproteinase expression and activity in isolated myocytes after neurohormonal stimulation. *Am J Physiol Heart Circ Physiol* 281: 543–551
- DeCoux A, Lindsey ML, Villarreal F, Garcia RA, Schulz R. (2014) Myocardial matrix metalloproteinase-2: inside out and upside down. *J Mol Cell Cardiol*. 77:64–72.
- Crowley AL, Yow E, Barnhart HX. et al. (2016) Critical Review of Current Approaches for Echocardiographic Reproducibility and Reliability Assessment in Clinical Research. *J Am Soc Echocardiogr*. 29(12):1144–1154
- Dae MW, Herre JM, O'Connell JW, Botvinick EH, Newman D, Munoz L. (1991) Scintigraphic assessment of sympathetic innervation after transmural versus nontransmural myocardial infarction. *J Am Coll Cardiol*. 17:1416–1423.
- Detmers PA, Lo SK, Olsen-Egbert E, Walz A, Baggiolini M, Cohn ZA. (1990) Neutrophil-activating protein 1/interleukin 8 stimulates the binding activity of the leukocyte adhesion receptor CD11b/CD18 on human neutrophils. *J Exp Med*. 171:1155–1162
- Dick SA, Epelman S. (2016) Chronic Heart Failure and Inflammation: What Do We Really Know? *Circ Res* 119(1):159–76
- Dieplinger B, Mueller T. (2015) Soluble ST2 in heart failure. *Clin Chim Acta*. 443:57–70
- Dijkgraaf I, Kruijtz JA, Frielink C et al (2006) Synthesis and biological evaluation of potent alphavbeta3-integrin receptor antagonists. *Nucl Med Biol*. 33:953–961
- Dijkgraaf I, Kruijtz JA, Liu S, et al. (2007) Improved targeting of the alphavbeta3 integrin by multimerisation of RGD peptides. *Eur J Nucl Med Mol Imaging* 34:267–273
- Dijkgraaf I, Yim CB, Franssen GM, et al. (2011) PET imaging of alphavbeta3 integrin expression in tumours with 68Ga-labelled mono-, di- and tetrameric RGD peptides. *Eur J Nucl Med Mol Imaging* 38:128–137
- Dilsizian V, Eckelman WC, Loreda ML, Jagoda EM, Shirani J. (2007) Evidence for tissue angiotensin-converting enzyme in explanted hearts of ischemic cardiomyopathy using targeted radiotracer technique. *J Nucl Med*. 48:182–187.
- Dilsizian V, Zynda TK, Petrov A, et al. (2012) Molecular imaging of human ACE-1 expression in transgenic rats. *J Am Coll Cardiol Cardiovasc Imaging*. 2012;5:409–418
- McDonald B, Kubes P. (2015) Interactions between CD44 and Hyaluronan in Leukocyte Trafficking. *Front Immunol*. 17;6:68
- van Duijnhoven SM, Robillard MS, Hermann S, et al. (2014) Imaging of MMP activity in postischemic cardiac remodeling using radiolabeled MMP-2/9 activatable peptide probes. *Mol Pharm*. 11:1415–23

- Dutta P, Courties G, Wei Y, Leuschner F, Gorbатов R, Robbins C, Iwamoto Y. (2012) Myocardial infarction accelerates atherosclerosis. *Nature* 487(7407): 325–329
- Dutta P, Nahrendorf M. (2015) Monocytes in myocardial infarction. *Arterioscler Thromb Vasc Biol.* 35(5):1066-70
- Entman ML, Youker K, Shoji T, et al. (1992). Neutrophil induced oxidative injury of cardiac myocytes. A compartmented system requiring CD11b/CD18-ICAM-1 adherence. *J Clin Invest.* 90:1335–1345
- Fallavollita JA, Heavey BM, Luisi AJ Jr, et al. (2014) Regional myocardial sympathetic denervation predicts the risk of sudden cardiac arrest in ischemic cardiomyopathy. *J Am Coll Cardiol.* 63:141–149
- Faris RF, Flather M, Purcell H, Poole-Wilson PA, Coats AJ. (2012) Diuretics for heart failure. *Cochrane Database Syst Rev* 2:CD003838.
- Femia FJ, Maresca KP, Hillier SM, et al. (2008) Synthesis and evaluation of a series of $^{99m}\text{Tc}(\text{CO})_3^+$ lisinopril complexes for in vivo imaging of angiotensin-converting enzyme expression. *J Nucl Med.* 49:970–977
- Floras JS, Ponikowski P (2015) The sympathetic/parasympathetic imbalance in heart failure with reduced ejection fraction. *Eur Heart J* 36(30):1974–182b
- Frangiannis NG (2012) Regulation of the inflammatory response in cardiac repair. *Circ Res.* 110(1):159-73.
- Frangiannis NG (2016) Fibroblast - Extracellular Matrix Interactions in Tissue Fibrosis. *Curr Pathobiol Rep.* 4(1): 1-18
- Frangiannis NG (2017) The extracellular matrix in myocardial injury, repair, and remodeling. *J Clin Invest.* 127(5): 1600-1612
- Fujimoto S, Hartung D, Ohshima S, et al. (2008) Molecular imaging of matrix metalloproteinase in atherosclerotic lesions: resolution with dietary modification and statin therapy. *J Am Coll Cardiol.* 52(23):1847-57
- Fukushima K, Bravo PE, Higuchi T, et al. (2012) Molecular hybrid positron emission tomography/ computed tomography imaging of cardiac angiotensin II type 1 receptors. *J Am Coll Cardiol.* 60:2527–2534
- Gabbiani G. (2003) The myofibroblast in wound healing and fibrocontractive diseases. *J Pathol.* 200:500–503
- Gaffney, J., Matou-Nasri, S., Grau-Olivares, M., and Slevin, M. (2010) Therapeutic applications of hyaluronan. *Mol. BioSyst.* 6, 437–443
- Gaemperli O, Shalhoub J, Owen DRJ, et al. (2012) Imaging intraplaque inflammation in carotid atherosclerosis with ^{11}C -PK11195 positron emission tomography/computed tomography. *Eur Heart J* 33:1902–1910
- Ganame J, Messalli G, Dymarkowski S, et al. (2009) Impact of myocardial haemorrhage on left ventricular function and remodelling in patients with reperfused acute myocardial infarction. *Eur Heart J* 30: 1440-1449
- Gao H, Lang L, Guo N, et al. (2012) PET imaging of angiogenesis after myocardial infarction/reperfusion using a one-step labeled integrin-targeted tracer ^{18}F -AIF-NOTA-PRGD2. *Eur J Nucl Med Mol Imaging.* 39:683–692
- Gee, K., Kryworuchko, M., and Kumar, A. (2004) Recent advances in the regulation of CD44 expression and its role in inflammation and autoimmune diseases. *Arch. Immunol. Ther. Exp.* 52, 13–26
- Gonzalez JA, Lipinski MJ, Flors L, Shaw PW, Kramer CM, Salerno M. (2015). Meta-Analysis of Diagnostic Performance of Coronary Computed Tomography Angiography, Computed Tomography Perfusion, and Computed Tomography-Fractional Flow Reserve in Functional Myocardial Ischemia Assessment Versus Invasive Fractional Flow Reserve. *Am J Cardiol.* 116(9):1469-78
- McGhie AI, Corbett JR, Akers MS, et al. (1991) Regional cardiac adrenergic function using ^{123}I -metaiodobenzylguanidine tomographic imaging after acute myocardial infarction. *Am J Cardiol.* 67:236–242
- Giannakos E, Vardali E, Bartekova M, Fogarassyova M, Barancik M, Radosinska J. (2016) Changes in activities of circulating MMP-2 and MMP-9 in patients suffering from heart failure in relation to gender, hypertension and treatment: a cross-sectional study. *Physiol Res.* 65(1)149-52

- Gimbrone MA Jr, García-Cardeña G. (2016) Endothelial Cell Dysfunction and the Pathobiology of Atherosclerosis. *Circ Res.* 118(4): 620–636.
- Gisterå A, Hansson GK. (2017) The immunology of atherosclerosis. *Nat Rev Nephrol.* 13(6):368-380. doi: 10.1038/nrneph.2017.51. Epub 2017 Apr 10
- Goetze S, Brown TL, Lavelly WC, Zhang Z, Bengel FM. (2007) Attenuation correction in myocardial perfusion SPECT/CT: effects of misregistration and value of reregistration. *J Nucl Med.* 48 (2007) 1090–1095
- González GE, Rhaleb NE, D'Ambrosio MA, et al. (2015) Deletion of interleukin-6 prevents cardiac inflammation, fibrosis and dysfunction without affecting blood pressure in angiotensin II-high salt-induced hypertension. *J Hypertens.* 33:144–152
- Gourni E, Demmer O, Schottelius M, et al. (2011) PET of CXCR4 expression by a (68)Ga-labeled highly specific targeted contrast agent. *J Nucl Med.* 52:1803-1810
- Gupta A, Taqueti VR, van de Hoef TP. et al. (2017). Integrated Noninvasive Physiological Assessment of Coronary Circulatory Function and Impact on Cardiovascular Mortality in Patients With Stable Coronary Artery Disease. *Circulation.* 136(24):2325-2336
- Haas HJ, Arbustini E, Fuster V, Kramer CM, Narula J. (2014) Molecular imaging of the cardiac extracellular matrix. *Circ Res.* 114(5):903-15
- Hafizi S, Wharton J, Chester AH, Yacoub MH. (2004) Profibrotic effects of endothelin-1 via the ETA receptor in cultured human cardiac fibroblasts. *Cell Physiol Biochem.* 14:285–292
- Hansson GK, Libby P, Tabas I. (2015) Inflammation and plaque vulnerability. *J Intern Med* 278(5): 483-493
- Hartupee J, Mann DL. (2017) Neurohormonal activation in heart failure with reduced ejection fraction. *Nat Rev Cardiol.* 14(1):30-38
- Hayashidani S, Tsutsui H, Ikeuchi M, et al. (2003) Targeted deletion of MMP-2 attenuates early LV rupture and late remodeling after experimental myocardial infarction. *Am J Physiol Heart Circ Physiol.* 285(3):1229-35
- Heinonen SE, Leppänen P, Kholová I, et al (2007) Increased atherosclerotic lesion calcification in a novel mouse model combining insulin resistance, hyperglycemia, and hypercholesterolemia. *Circ Res* 101:1058–1067
- Hellermann JP, Jacobsen SJ, Redfield MM, Reeder GS, Weston SA, Roger VL. (2005) Heart failure after myocardial infarction: clinical presentation and survival. *Eur J Heart Fail.* 7(1):119-25
- Hendriks G, Vöö S, Bauwens M, Post MJ, Mottaghy FM. (2016) SPECT and PET imaging of angiogenesis and arteriogenesis in pre-clinical models of myocardial ischemia and peripheral vascular disease. *Eur J Nucl Med Mol Imaging* 43:2433-2447
- Hellberg S. (2017) Evaluation of macrophage – targeting PET tracers for imaging of inflammation in atherosclerosis. *Annales Universitatis Turkuensis.* ISSN 2343-3213
- Herter J, Zarbock A. (2013) Integrin Regulation during Leukocyte Recruitment. *J Immunol.* 190:4451–4457
- Herzog BA, Buechel RR, Katz R, et al. (2010) Nuclear myocardial perfusion imaging with a cadmium-zinc-telluride detector technique: optimized protocol for scan time reduction, *J Nucl Med.* 51:46–51
- Herzog C, Lorenz A, Gillmann HJ, et al. (2014) Thrombomodulin's lectin-like domain reduces myocardial damage by interfering with HMGB1-mediated TLR2 signalling. *Cardiovasc Res.* 101:400–410
- Heusch G. (2015) Treatment of Myocardial Ischemia/Reperfusion Injury by Ischemic and Pharmacological Postconditioning. *Compr Physiol.* 5(3):1123-45
- Higgins RSD, Kilic A, Tang DG. (2017) Surgical Treatment of Heart Failure. *Surg Clin North Am.* 97(4):923-946
- Higuchi T, Wester HJ, Schwaiger M. (2007) Imaging of angiogenesis in cardiology. *Eur J Nucl Med Mol Imaging* 34:S9–S19
- Higuchi T, Bengel FM, Seidl S, et al. (2008) Assessment of $\alpha\beta 3$ integrin expression after myocardial infarction by positron emission tomography. *Cardiovasc Res.* 78:395–403
- Hinz B, Phan SH, Thannickal VJ, Galli A, Bochaton-Piallat ML, Gabbiani G. (2007) The myofibroblast: one function, multiple origins. *Am J Pathol.* 170:1807–1816

- Hopps E, Caimi G. (2012) Matrix metalloproteinases in metabolic syndrome. *European Journal of Internal Medicine* 23:99–104
- Hou J, Wang L, Jiang J, et al. (2013) Cardiac stem cells and their roles in myocardial infarction. *Stem Cell Rev.* 9(3): 326-38
- Huebener P, Abou-Khamis T, Zymek P, et al. (2008) CD44 Is Critically Involved in Infarct Healing by Regulating the Inflammatory and Fibrotic Response. *J Immunol.* 180:2625–2633
- Husser O, Bodí V, Sanchis J, et al. (2010) The sum of ST-segment elevation is the best predictor of microvascular obstruction in patients treated successfully by primary percutaneous coronary intervention. *Cardiovascular magnetic resonance study. Rev Esp Cardiol.* 63: 1145-1154
- Ibrahim NE, Januzzi JL Jr (2017) Beyond Natriuretic Peptides for Diagnosis and Management of Heart Failure. *Clin Chem.* 63(1):211-222
- Ibrahim el-SH. (2011) Myocardial tagging by cardiovascular magnetic resonance: evolution of techniques-pulse sequences, analysis algorithms, and applications. *J Cardiovasc Magn Reson.* 13: 36. doi: 10.1186/1532-429X-13-36
- Imbert L, Poussier S, Franken PR, et al. (2012) Compared performance of high-sensitivity cameras dedicated to myocardial perfusion SPECT: a comprehensive analysis of phantom and human images. *J Nucl Med.* 53:1897–1903
- Ito H. (2006) No-reflow phenomenon and prognosis in patients with acute myocardial infarction. *Nat Clin Pract Cardiovasc Med.* 3:499-506
- Iyer RP, Jung M, Lindsey ML. (2016) MMP-9 signaling in the left ventricle following myocardial infarction. *Am J Physiol Heart Circ Physiol.* 311(1):H190-8
- Jacobson AF, Senior R, Cerqueira MD, et al. (2010) Myocardial iodine-123 metaiodobenzylguanidine imaging and cardiac events in heart failure. Results of the prospective ADMIRE-HF (AdreView Myocardial Imaging for Risk Evaluation in Heart Failure) study. *J Am Coll Cardiol* 55:2212–2221
- Javadi MS, Lautamaki R, Merrill J, et al. (2010) Definition of vascular territories on myocardial perfusion images by integration with true coronary anatomy: a hybrid PET/CT analysis. *J Nucl Med* 51:198–203
- Jenkins WS, Vesey AT, Stirrat C, et al. (2017) Cardiac $\alpha V\beta 3$ integrin expression following acute myocardial infarction in humans. *Heart.* 103(8):607-615
- Jennings RB, Sommers HM, Smyth GA, Flack HA, Linn H. (1960) Myocardial necrosis induced by temporary occlusion of a coronary artery in the dog. *Arch Pathol* 70:68-78
- Jindal A, Mathur A, Pandey U, Sarma HD, Chaudhari P, Dash A. (2014) Development of ^{68}Ga -labeled fatty acids for their potential use in cardiac metabolic imaging. *J Labelled Comp Radiopharm.* 57(7):463-9
- Johnson C, Sung HJ, Lessner SM, Fini ME, Galis ZS. (2004) Matrix metalloproteinase-9 is required for adequate angiogenic revascularization of ischemic tissues: potential role in capillary branching. *Circ Res* 94: 262–268
- Johnson JL, Baker AH, Oka K, Chan L, Newby AC, Jackson CL, George SJ. (2006) Suppression of atherosclerotic plaque progression and instability by tissue inhibitor of metalloproteinase-2: involvement of macrophage migration and apoptosis. *Circulation* 113(20):2435-44
- Johnson NP, Gould KL, Di Carli MF, Taqueti VR (2016) Invasive FFR and noninvasive CFR in the evaluation of ischemia: what is the future? *J Am Coll Cardiol.* 67:2772–2788
- de Jong HW, Rijzewijk LJ, Lubberink M et al. (2009) Kinetic models for analysing myocardial $[(11)\text{C}]$ palmitate data. *Eur J Nucl Med Mol Imaging.* 36(6):966-78
- Jordan AR, Racine RR, Hennig MJ, Lokeshwar VB. (2015) The Role of CD44 in Disease Pathophysiology and Targeted Treatment. *Front Immunol.* 6:182
- Joshi NV, Vesey AT, Williams MC, et al. (2014) ^{18}F -fluoride positron emission tomography for identification of ruptured and high-risk coronary atherosclerotic plaques: a prospective clinical trial. *Lancet.* 383:705–713

- Juneau D, Golfam M, Hazra S, et al. (2017) Positron emission tomography and single-photon emission computed tomography imaging in the diagnosis of cardiac implantable electronic device infection: a systematic review and meta-analysis. *Circ Cardiovasc Imaging* 10(4)
- Kain V, Prabhu SD, Halade GV. (2014) Inflammation revisited: inflammation versus resolution of inflammation following myocardial infarction. *Basic Res Cardiol*. 109:444
- Kalogeris T, Baines CP, Krenz M, Korthuis RJ. (2012) Cell biology of ischemia/reperfusion injury. *Int Rev Cell Mol Biol* 298:229-317
- Kalogeris T, Baines CP, Krenz M, Korthuis RJ (2016) Ischemia/Reperfusion. *Compr Physiol*. 7(1): 113–170
- Kanisicak O, Khalil H, Ivey MJ, et al. (2016) Genetic lineage tracing defines myofibroblast origin and function in the injured heart. *Nat Commun*. 7:12260
- Karskela, M., Virta, P., Malinen, M., Urtti, A., and Lönnberg, H. (2008) Synthesis and cellular uptake of fluorescently labelled multivalent hyaluronan disaccharide conjugates of oligonucleotide phosphorothioates. *Bioconjugate Chem*. 19, 2549–2558
- Kato K, Schober O, Ikeda M, et al. (2009) Evaluation and comparison of ¹¹C-choline uptake and calcification in aortic and common carotid arterial walls with combined PET/CT. *Eur J Nucl Med Mol Imaging* 36:1622–1628
- Kerkelä R, Ulvila J, Magga J. (2015) Natriuretic Peptides in the Regulation of Cardiovascular Physiology and Metabolic Events. *J Am Heart Assoc*. 4(10):e002423
- Ketelhuth D, Bäck M. (2011) The Role of Matrix Metalloproteinases in Atherothrombosis. *Curr Atheroscler Rep* 13:162–169
- Khan JN, McCann GP. (2017) Cardiovascular magnetic resonance imaging assessment of outcomes in acute myocardial infarction. *World J Cardiol* 9(2): 109-133
- Kieffer P, Giummelly P, Schjoth B, Carteaux JP, Villemot JP, Hornebeck W, Atkinson J. (2001) Activation of metalloproteinase-2, loss of matrix scleroprotein content and coronary artery calcification. *Atherosclerosis* 157(1):251-4.
- Kim JH, Kim YH, Kim YJ et al (2013) Quantitative positron emission tomography imaging of angiogenesis in rats with forelimb ischemia using ⁶⁸Ga-NOTA-c(RGDyK). *Angiogenesis*. 16:837–846
- van Kimmenade RRJ, Januzzi JL. (2012) Emerging biomarkers in heart failure. *Clin Chem* 58:127–38
- Klein R, Hung G-U, Wu T-C. et al. (2014) Feasibility and operator variability of myocardial blood flow and reserve measurements with ^{99m}Tc-sestamibi quantitative dynamic SPECT/CT imaging. *J Nucl Cardiol*. 21:1075–88
- Kleinbongard P, Skyschally A, Heusch G. (2017) Cardioprotection by remote ischemic conditioning and its signal transduction. *Pflugers Arch*. 469(2):159-181
- Knaapen P, Germans T, Knuuti J, et al. (2007) Myocardial energetics and efficiency: current status of the noninvasive approach. *Circulation*. 115:918–927
- Koivunen E, Arap W, Valtanen H, et al. (1999) Tumor targeting with a selective gelatinase inhibitor. *Nat Biotechnol*. 17:768–74
- Kolwicz SC Jr, Purohit S, Tian R. (2013) Cardiac metabolism and its interactions with contraction, growth, and survival of cardiomyocytes. *Circ Res*. 113(5):603-16
- Kukielka GL, Smith CW, LaRosa GJ, et al. (1995) Interleukin-8 gene induction in the myocardium after ischemia and reperfusion in vivo. *J Clin Invest*. 95:89–103
- Kuppuswamy D, Kerr C, Narishige T, et al. (1997) Association of tyrosine-phosphorylated c-Src with the cytoskeleton of hypertrophying myocardium. *J Biol Chem* 272:4500–4508
- Laitinen I, Notni J, Pohle K, et al. (2013) Comparison of cyclic RGD peptides for $\alpha v \beta 3$ integrin detection in a rat model of myocardial infarction. *EJNMMI Res* 3:38
- Lambert JM, Lopez EF, Lindsey ML. (2008) Macrophage roles following myocardial infarction. *Int J Cardiol*. 130: 147–158
- Lapa C, Reiter T, Werner RA, et al. (2015) [⁶⁸Ga]Pentixafor-PET/CT for imaging of chemokine receptor 4 expression after myocardial infarction. *JACC Cardiovasc Imaging* 8:1466–1468

- Laskey WK. (2005) Brief repetitive balloon occlusions enhance reperfusion during percutaneous coronary intervention for acute myocardial infarction: a pilot study. *Catheter Cardiovasc Interv* 65:361-7
- Lautamaki R, Schuleri KH, Sasano T, et al. (2009) Integration of infarct size, tissue perfusion, and metabolism by hybrid cardiac positron emission tomography/computed tomography: evaluation in a porcine model of myocardial infarction. *Circ Cardiovasc Imaging*. 2:299-305
- Lautamaki R, Sasano T, Higuchi T. et al. (2015) Multiparametric molecular imaging provides mechanistic insights into sympathetic innervation impairment in the viable infarct border zone. *J Nucl Med*. 56(3):457-63
- Lawal I, Sathekge M. (2016) F-18 FDG PET/CT imaging of cardiac and vascular inflammation and infection. *Br Med Bull*. 2016 Dec;120(1):55-74
- Lee WW, Marinelli B, van der Laan AM, et al. (2012) PET/MRI of inflammation in myocardial infarction. *J Am Coll Cardiol*. 59:153-63
- Levine A, Hecht HS. (2015) Cardiac CT Angiography in Congestive Heart Failure. *J Nucl Med*. 56 Suppl 4:46S-51S
- Li Y, Si R, Feng Y, et al. (2011) Myocardial Ischemia activates an injurious innate immune signaling via cardiac heat shock protein 60 and toll-like receptor 4. *J Biol Chem*. 286:31308-31319
- Libby P. (2002) Inflammation in atherosclerosis. *Nature* 420(6917):868-74
- Libby P. (2012) Mechanisms of Acute Coronary Syndromes and Their Implications for Therapy. *N Engl J Med*. 368:2004-2013
- Libby P. (2012) Inflammation in atherosclerosis. *Arterioscler Thromb Vasc Biol*. 32(9):2045-51
- Van Lint P, Libert C. (2007) Chemokine and cytokine processing by matrix metalloproteinases and its effect on leukocyte migration and inflammation. *J Leukoc Biol*. 82:1375-1381
- Lota AS, Gatehouse PD, Mohiaddin RH. T2 mapping and T2* imaging in heart failure. (2017) *Heart Fail Rev*. 22(4):431-440
- Lu Y, Qin W, Shen T, Dou L, Man Y, Wang S, Xiao C, Li J. (2011) The antioxidant N-acetylcysteine promotes atherosclerotic plaque stabilization through suppression of RAGE, MMPs and NF- κ B in ApoE-deficient mice. *J Atheroscler Thromb*. 18(11):998-1008
- Lugrin J, Parapanov R, Rosenblatt-Velin N, et al. (2015) Cutting Edge: IL-1 α is a crucial danger signal triggering acute myocardial inflammation during myocardial infarction. *J Immunol*. 194: 499-503
- Ma X, Zhang X, Li C, Luo M. (2006) Effect of postconditioning on coronary blood flow velocity and endothelial function and LV recovery after myocardial infarction. *J Interv Cardiol*. 19:367-75
- Maddahi J, Packard RR. (2014) Cardiac PET perfusion tracers: current status and future directions. *Semin Nucl Med*. 44:333-343
- Majmudar MD1, Keliher EJ, Heidt T, et al. (2013) Monocyte-directed RNAi targeting CCR2 improves infarct healing in atherosclerosis-prone mice. *Circulation*. 127(20):2038-46
- Makowski MR, Ebersberger U, Nekolla S, Schwaiger M. (2008) In vivo molecular imaging of angiogenesis, targeting α v β 3 integrin expression, in a patient after acute myocardial infarction. *Eur Heart J* 2008;29:2201
- Malmberg C, Ripa RS, Johnbeck CB, et al. (2015) Atherosclerosis in large arteries and its correlation with risk factors: head-to-head comparison with ^{68}Ga -DOTATOC in 60 Patients. *J Nucl Med* 56:1895-1900
- Mann DL. (2011) The emerging role of innate immunity in the heart and vascular system: for whom the cell tolls. *Circ Res*. 108(9):1133-45
- Mann DL. (2015) Innate immunity and the failing heart: the cytokine hypothesis revisited. *Circ Res*. 116(7):1254-68
- Manning AS, Hearse DJ. (1984) Reperfusion induced arrhythmias: mechanisms and prevention. *J Mol Cell Cardiol* 16:497-518
- Manso AM, Kang SM, Ross RS. (2009) Integrins, focal adhesions, and cardiac fibroblasts. *J Investig Med*. 57:856-860

- Mehrotra R, Alagesan R, Srivastava S. (2013) Quantitative assessment of left ventricular systolic function using 3-dimensional echocardiography. *Indian Heart J.* 65:620–628
- Meoli DF, Sadeghi MM, Krassilnikova S, et al. (2004) Noninvasive imaging of myocardial angiogenesis following experimental myocardial infarction. *J Clin Invest* 113:1684–1691
- Mercer-Rosa L, Seliem MA, Fedec A, et al. (2006) Illustration of the additional value of real-time 3-dimensional echocardiography to conventional transthoracic and transesophageal 2-dimensional echocardiography in imaging muscular ventricular septal defects: does this have any impact on individual patient treatment? *J Am Soc Echocardiogr.* 19:1511–1519
- Michel JB, Virmani R, Arbustini E, et al. (2011) Intraplaque haemorrhages as the trigger of plaque vulnerability. *Eur Heart J.* 32(16):1977-85
- Montalescot G, Sechtem U, Achenbach S, et al. (2013) ESC guidelines on the management of stable coronary artery disease: the Task Force on the management of stable coronary artery disease of the European Society of Cardiology. *Eur Heart J.* 34:2949–3003
- Moran, AE, Forouzanfar MH, Roth GA, Mensah, GA, Ezzati M, Murray CJL, Naghavi M. (2014) Temporal Trends in Ischemic Heart Disease Mortality in 21 World Regions, 1980 to 2010. The Global Burden of Disease 2010 Study. *Circulation* 129:1483-1492
- Murry CE, Jennings RB, Reimer KA. (1986) Preconditioning with ischemia: a delay of lethal cell injury in ischemic myocardium. *Circulation* 74:1124-1136
- Nagase H, Visse R, Murphy G. (2006) Structure and function of matrix metalloproteinases and TIMPs. *Microvasc Res* 71(2):85-90
- Nahrendorf M, Swirski FK, Aikawa E, et al. (2007) The healing myocardium sequentially mobilizes two monocyte subsets with divergent and complementary functions. *J Exp Med.* 204:3037–3047
- Nenseter MS, Narverud I, Græsdal A, et al. (2013) Elevated serum MMP-9/TIMP-1 ratio in patients with homozygous familial hypercholesterolemia: effects of LDL-apheresis. *Cytokine* 61(1):194-8
- Nepomnyashchikh LM, Lushnikova EL, Bakarev MA, et al. (2015) Immunohistochemical Analysis of MMP-2 Expression in the Myocardium During the Postinfarction Period. *Bull Exp Biol Med.* 159(4):505-10
- Newby AC. (2005) Dual role of matrix metalloproteinases (matrixins) in intimal thickening and atherosclerotic plaque rupture. *Physiol Rev.* 85(1):1-31
- Newby AC. (2006) Matrix metalloproteinases regulate migration, proliferation, and death of vascular smooth muscle cells by degrading matrix and non-matrix substrates. *Cardiovasc Res* 69(3):614-24
- Newby AC. (2008) Metalloproteinase Expression in Monocytes and Macrophages and its Relationship to Atherosclerotic Plaque Instability. *Arterioscler Thromb Vasc Biol* 28:2108-2114
- Newby AC. (2012) Matrix metalloproteinase inhibition therapy for vascular diseases. *Vascul Pharmacol.* 56(5-6):232-44
- Niu W, Qi Y. (2012) Matrix metalloproteinase family gene polymorphisms and risk for coronary artery disease: systematic review and meta-analysis. *Heart.* 98(20):1483-91
- Noble JA, Boukerroui D. (2006) Ultrasound image segmentation: a survey, *IEEE Trans. Med. Imaging* 25. 987–1010
- Nohria A, Cusco JA & Creager MA. (2004) Atlas of Heart Failure 4th edn (ed. Colucci, W. S.) Vol. 1 Ch. 6 101–126
- de Nooijer R, Verkleij CJ, von der Thüsen JH, et al. (2006) Lesional overexpression of matrix metalloproteinase-9 promotes intraplaque hemorrhage in advanced lesions but not at earlier stages of atherogenesis. *Arterioscler Thromb Vasc Biol.* 26(2):340-6
- Orn S, Manhenke C, Anand IS, et al. (2007) Effect of left ventricular scar size, location, and transmuralty on left ventricular remodeling with healed myocardial infarction. *Am J Cardiol* 99: 1109-1114
- Packard RR, Huang SC, Dahlbom M, Czernin J, Maddahi J. (2014) Absolute quantitation of myocardial blood flow in human subjects with or without myocardial ischemia using dynamic flurpiridaz F18 PET. *J Nucl Med.* 55:1438–1444

- Phatharajaree W, Phrommintikul A, Chattipakorn N. (2007) Matrix metalloproteinases and myocardial infarction. *Can J Cardiol* 23: 727–733
- Peterson DJ, Ju H, Hao J, et al. (1999) Expression of Gi-2 alpha and Gs alpha in myofibroblasts localized to the infarct scar in heart failure due to myocardial infarction. *Cardiovasc Res.* 41(3):575-85
- Pedersen SF, Sandholt BV, Keller SH, et al (2015) ⁶⁴Cu-DOTATATE PET/MRI for detection of activated macrophages in carotid atherosclerotic plaques: studies in patients undergoing endarterectomy. *Arterioscler Thromb Vasc Biol* 35:1696–1703
- Pfeffer MA, Pfeffer JM, Fishbein MC, et al. (1979) Myocardial infarct size and ventricular function in rats. *Circ Res.* 44:503–512
- Piccinelli M, Garcia EV. (2015) Advances in software for faster procedure and lower radiotracer dose myocardial perfusion imaging. *Prog Cardiovasc Dis.* 57:579–587
- Prabhu SD, Frangogiannis NG. (2016) The Biological Basis for Cardiac Repair After Myocardial Infarction. From Inflammation to Fibrosis. *Circulation Research.* 119:91-112
- Prastaro M, Pirozzi E, Gaibazzi N. et al. (2017) Expert Review on the Prognostic Role of Echocardiography after Acute Myocardial Infarction. *J Am Soc Echocardiogr.* 30(5):431-443
- Prescott MF1, Sawyer WK, Von Linden-Reed J, et al. (1999) Effect of matrix metalloproteinase inhibition on progression of atherosclerosis and aneurysm in LDL receptor-deficient mice overexpressing MMP-3, MMP-12, and MMP-13 and on restenosis in rats after balloon injury. *Ann N Y Acad Sci.* 878:179-90
- Rajpoot K, Grau V, Noble JA. (2009) Local-phase based 3D boundary detection using monogenic signal and its application to real-time 3-D echocardiography images, in: *IEEE International Symposium on Biomedical Imaging: From Nano to Macro.*
- Reimer KA, Lowe JE, Rasmussen MM, Jennings RB. (1977) The wavefront phenomenon of ischemic cell death. I. myocardial infarct size vs duration of coronary occlusion in dogs. *Circulation* 56(5):786–94
- Reimer KA, Jennings RB. (1979) The "wavefront phenomenon" of myocardial ischemic cell death. II. Transmural progression of necrosis within the framework of ischemic bed size (myocardium at risk) and collateral flow. *Lab Invest* 40(6):633–44
- Rienks M, Papageorgiou AP, Frangogiannis NG, Heymans S. (2014) Myocardial extracellular matrix: an ever-changing and diverse entity. *Circ Res.* 114:872–888
- Rischpler C, Nekolla SG, Dregely I, Schwaiger M. (2013) Hybrid PET/MR imaging of the heart: potential, initial experiences, and future prospects. *J Nucl Med.* 54:402–415
- Rischpler C, Dirschinger RJ, Nekolla SG, et al. (2016) Prospective Evaluation of ¹⁸F-Fluorodeoxyglucose Uptake in Postischemic Myocardium by Simultaneous Positron Emission Tomography/Magnetic Resonance Imaging as a Prognostic Marker of Functional Outcome. *Circ Cardiovasc Imaging.* 9(4):e004316
- Ristamäki R, Joensuu H, Lappalainen K, Teerenhovi L, Jalkanen S. (1997) Elevated serum CD44 level is associated with unfavorable outcome in non-Hodgkin's lymphoma. *Blood.* 90(10):4039-45.
- Rohde D, Schon C, Boerries M, et al. (2014) S100A1 is released from ischemic cardiomyocytes and signals myocardial damage via Toll-like receptor 4. *EMBO Mol Med.* 109:444
- Romanic AM, Harrison SM, Bao W, et al. (2002) Myocardial protection from ischemia/reperfusion injury by targeted deletion of matrix metalloproteinase-9. *Cardiovasc Res.* 54(3):549-58
- Sahul ZH, Mukherjee R, Song J, et al. (2011) Targeted imaging of the spatial and temporal variation of matrix metalloproteinase activity in a porcine model of postinfarct remodeling: relationship to myocardial dysfunction. *Circ Cardiovasc Imaging.* 4:381–91
- Saraste A, Kajander S, Han C, Nesterov SV, Knuuti J. (2012) PET: is myocardial flow quantification a clinical reality? *J Nucl Cardiol.* 19:1044–1059

- Schepis T, Gaemperli O, Koepfli P, et al. (2007) Use of coronary calcium score scans from stand-alone multislice computed tomography for attenuation correction of myocardial perfusion SPECT, *Eur J Nucl Med Mol Imaging* 34:11–19
- Schinkel AF, Bax JJ, Poldermans D, Elhendy A, Ferrari R, Rahimtoola SH. (2007) Hibernating myocardium: diagnosis and patient outcomes. *Curr Probl Cardiol.* 32:375–410
- Sharma A, Einstein AJ, Vallakati A, et al. (2014) Meta-analysis of global left ventricular function comparing multidetector computed tomography with cardiac magnetic resonance imaging. *Am J Cardiol.* 113:731–738
- Sherif HM, Saraste A, Nekolla SG, et al. (2012) Molecular imaging of early $\alpha\beta3$ integrin expression predicts long-term left-ventricle remodeling after myocardial infarction in rats. *J Nucl Med.* 53(2):318-23
- Shoup TM, Elmaleh DR, Bonab AA, Fischman AJ. (2005) Evaluation of trans-9-18F-fluoro-3,4-Methyleneheptadecanoic acid as a PET tracer for myocardial fatty acid imaging. *J Nucl Med.* 46(2):297-304
- Slomka PJ, Rubeaux M, Le Meunier L, et al. (2015) Dual-gated motion-frozen cardiac PET with flurpiridaz F 18. *J Nucl Med.* 56:1876–1881
- Staat P, Rioufol G, Piot C, et al. (2005) Postconditioning the human heart. *Circulation*;112:2143-8
- Stefanidakis M, Ruohtula T, Borregaard N, Gahmberg CG, Koivunen E. (2004) Intracellular and cell surface localization of a complex between $\alpha\text{M}\beta2$ integrin and promatrix metalloproteinase-9 progelatinase in neutrophils. *Journal of immunology.* 172:7060–7068
- Silvello DI, Narvaes LB, Albuquerque LC, et al. (2014) Serum levels and polymorphisms of matrix metalloproteinases (MMPs) in carotid artery atherosclerosis: higher MMP-9 levels are associated with plaque vulnerability. *Biomarkers.* 19(1):49-55
- Sinusas AJ, Lazewatsky J, Brunetti J, et al. (2014) Biodistribution and radiation dosimetry of LMI1195: first-in-human study of a novel 18F-labeled tracer for imaging myocardial innervation. *J Nucl Med.* 55:1445–1451
- Sohaib SMMA, Finegold JA, Nijjer SS, et al. (2015) Opportunity to increase life span in narrow QRS cardiac resynchronization therapy recipients by deactivating ventricular pacing: evidence from randomized controlled trials. *JACC Heart Fail.* 3:327–336
- Somasundaram P, Ren G, Nagar H, et al. (2005) Mast cell tryptase may modulate endothelial cell phenotype in healing myocardial infarcts. *J Pathol.* 205:102–111
- Spencer KT, Kimura BJ, Korcarz CE, Pellikka PA, Rahko PS, Siegel RJ. (2013) Focused cardiac ultrasound: recommendations from the American Society of Echocardiography. *J Am Soc Echocardiogr.* 26(6):567-81
- Stanley WC, Recchia FA, Lopaschuk GD. (2005) Myocardial Substrate Metabolism in the Normal and Failing Heart. *Physiological Reviews.* 85(3):1093-1129
- Stark C. (2017) Insight on thymosin beta 4 in animal models of myocardial injury. *ISSN* 2343-3213
- Strauss HW, Narula J. (2017) Imaging vulnerable plaque: a medical necessity or a scientific curiosity? *J Am Coll Cardiol.* 69:1792–1794
- Sugeng L, Weinert L, Lang RM. (2003) Left ventricular assessment using real-time three-dimensional echocardiography. *Heart.* 89 Suppl 3:iii29–iii36
- Sugeng L, Mor-Avi V, Weinert L, et al. (2006) Quantitative assessment of left ventricular size and function: side-by-side comparison of real-time three-dimensional echocardiography and computed tomography with magnetic resonance reference. *Circulation.* 114:654–661
- Su H, Spinale FG, Dobrucki LW, et al. (2005) Noninvasive targeted imaging of matrix metalloproteinase activation in a murine model of postinfarction remodeling. *Circulation.* 112(20):3157-67
- Sun Y, Cleutjens JP, Diaz-Arias AA, Weber KT. (1994) Cardiac angiotensin converting enzyme and myocardial fibrosis in the rat. *Cardiovasc Res.* 28:1423–1432
- Sun M, Opavsky MA, Stewart DJ, et al. (2003) Temporal response and localization of integrins $\beta1$ and $\beta3$ in the heart after myocardial infarction: regulation by cytokines. *Circulation.* 107(7):1046-52

- Szabo Z, Magga J, Alakoski T, et al. (2014) Connective tissue growth factor inhibition attenuates left ventricular remodeling and dysfunction in pressure overload-induced heart failure. *Hypertension*. 63:1235–1240
- Tahari AK, Lee A, Rajaram M, et al. (2014) Absolute myocardial flow quantification with (82)Rb PET/CT: comparison of different software packages and methods. *Eur J Nucl Med Mol Imaging*. 41:126–135
- Tan C, Liu Y, Li W, et al. (2014) Associations of matrix metalloproteinase-9 and monocyte chemoattractant protein-1 concentrations with carotid atherosclerosis, based on measurements of plaque and intima-media thickness. *Atherosclerosis*, 232(1):199–203
- Tarkia, M. (2015) Translational models of coronary artery disease, myocardial infarction and heart failure: development, validation and in vivo imaging studies using positron emission tomography. ISSN 0355-9483.
- Tavakoli S, Vashist A, Sadeghi MM. (2014) Molecular imaging of plaque vulnerability. *J Nucl Cardiol*. 21(6):1112–28
- Terentyev D, Hamilton S (2016) Regulation of sarcoplasmic reticulum Ca²⁺ release by serine-threonine phosphatases in the heart. *J Mol Cell Cardiol* 101:156–164
- Thackeray JT, Bengel FM. (2016(1)) Translational molecular nuclear cardiology. *Cardiol. Clin* 34:187–198
- Thackeray JT, Bankstahl JP, Wang Y, Wollert KC, Bengel FM (2016(2)) Targeting amino acid metabolism for molecular imaging of inflammation early after myocardial infarction. *Theranostics*. 6: 1768–1779
- Theuns DAMJ, Smith T, Hunink MGM, Bardy GH, Jordaens L. (2010) Effectiveness of prophylactic implantation of cardioverter-defibrillators without cardiac resynchronization therapy in patients with ischaemic or non-ischaemic heart disease: a systematic review and meta-analysis. *Europace*. 12:1564–1570
- Thygesen K, Alpert JS, White HD, Joint ESC/ACCF/AHA/WHF Task Force for the Redefinition of Myocardial Infarction. Universal definition of myocardial infarction. *Eur Heart J* 2007;28:2525–38; *Circulation* 2007;116:2634–53; *J Am Coll Cardiol* 2007;50:2173–95
- Thygesen K, Alpert JS, Jaffe AS, et al. (2012) Third universal definition of myocardial infarction. *J Am Coll Cardiol*. 60(16):1581–98
- Timmers L, Pasterkamp G, de Hoog VC, Arslan F, Appelman Y, de Kleijn DP. (2012) The innate immune response in reperfused myocardium. *Cardiovasc Res*. 94(2):276–83
- Travers JG, Kamal FA, Robbins J, Yutzey KE, Blaxall BC (2016) Cardiac Fibrosis: The Fibroblast Awakens. *Circ Res*. 118(6):1021–40
- Trial J, Baughn RE, Wygant JN (1999) Fibronectin fragments modulate monocyte VLA-5 expression and monocyte migration. *J Clin Invest*. 104:419–430
- Turner NA, Porter KE. (2013) Function and fate of myofibroblasts after myocardial infarction. *Fibrogenesis Tissue Repair*. 6(1):5
- Tuunanen H, Knuuti J. (2011) Metabolic remodelling in human heart failure. *Cardiovasc Res*. 90:251–257
- Ujula T, Huttunen M, Luoto P, et al. (2010) Matrix metalloproteinase 9 targeting peptides: syntheses, 68Ga-labeling, and preliminary evaluation in a rat melanoma xenograft model. *Bioconjug Chem*. 21(9):1612–21
- Urmaliya V, Franchelli G. (2017) A multidimensional sight on cardiac failure: uncovered from structural to molecular level. *Heart Fail Rev*. 22(3):357–370
- Varda-Bloom N, Leor J, Ohad DG, et al. (2000) Cytotoxic T lymphocytes are activated following myocardial infarction and can recognize and kill healthy myocytes in vitro. *J Mol Cell Cardiol*. 32:2141–2149
- Velagaleti RS, Pencina MJ, Murabito JM, et al. (2008) Long-term trends in the incidence of heart failure after myocardial infarction. *Circulation*. 118:2057–62
- Velasco O, Beckett MQ, James AW, et al. (2017) Real-Time Three-Dimensional Echocardiography: Characterization of Cardiac Anatomy and Function-Current Clinical Applications and Literature Review Update. *Biores Open Access*. 6(1):15–18

- Verberne HJ, Acampa W, Anagnostopoulos C, et al. (2015) EANM procedural guidelines for radionuclide myocardial perfusion imaging with SPECT and SPECT/CT: 2015 revision, *Eur J Nucl Med Mol Imaging*. 42:1929–1940
- Virag JI, Murry CE. (2003) Myofibroblast and endothelial cell proliferation during murine myocardial infarct repair. *Am J Pathol*. 163:2433–2440
- Virtanen H. (2017) Vascular adhesion protein-1 as in vivo target for imaging of leukocyte transendothelial migration in inflammation. ISSN 2343-3213
- de Vries MR, Niessen HWM, Löwik CWGM, Hamming JF, Jukema JW, Quax PHA (2012) Plaque Rupture Complications in Murine Atherosclerotic Vein Grafts Can Be Prevented by TIMP-1 Overexpression. *PLoS ONE* 7(10): e47134
- Wagner A1, Mahrholdt H, Holly TA, et al. (2003) Contrast-enhanced MRI and routine single photon emission computed tomography (SPECT) perfusion imaging for detection of subendocardial myocardial infarcts: an imaging study. *Lancet*. 361(9355):374-9
- van Wamel AJ, Ruwhof C, van der Valk-Kokshoom LE, Schrier PI, van der Laarse A. (2001) The role of angiotensin II, endothelin-1 and transforming growth factor-beta as autocrine/paracrine mediators of stretch-induced cardiomyocyte hypertrophy. *Mol Cell Biochem*. 218:113–124
- Weerasinghe P, Hallock S, Brown RE, Loose DS, Buja LM. (2013) A model for cardiomyocyte cell death: insights into mechanisms of oncosis. *Exp Mol Pathol* 94(1):289-300
- Welgus HG, Campbell EJ, Cury JD, Eisen AZ, Senior RM, Wilhelm SM, Goldberg GI. (1990) Neutral metalloproteinases produced by human mononuclear phagocytes. Enzyme profile, regulation, and expression during cellular development. *J Clin Invest* 86(5):1496-502
- Wells RG, Timmins R, Klein R. et al. (2014) Dynamic SPECT measurement of absolute myocardial blood flow in a porcine model. *J Nucl Med*. 55:1–7
- Weng X, Yu L, Liang P, et al. (2014) Endothelial MRTF-A mediates angiotensin II induced cardiac hypertrophy. *J Mol Cell Cardiol*. 80C:23–33
- Westman PC, Lipinski MJ, Luger D, Waksman R, Bonow RO, Wu E, Epstein SE. J (2016) Inflammation as a Driver of Adverse Left Ventricular Remodeling After Acute Myocardial Infarction. *Am Coll Cardiol*. 67(17):2050-60
- Yamamuro M, Tadamura E, Kubo S, et al. Cardiac functional analysis with multi-detector row CT and segmental reconstruction algorithm: comparison with echocardiography, SPECT, and MR imaging. *Radiology*. 2005;234:381–390.
- Xu Y, Arsanjani R, Clond M, Hyun M, Lemley M Jr, Fish M. et al. (2012) Transient ischemic dilation for coronary artery disease in quantitative analysis of same-day sestamibi myocardial perfusion SPECT. *J Nucl Cardiol* 19(3):465–473
- Yellon DM and Hausenloy DJ (2007) Myocardial Reperfusion Injury. *N Engl J Med* 357:1121-35
- Zamilpa R, Ibarra J, de Castro Bras LE. et al. (2012). Transgenic overexpression of matrix metalloproteinase-9 in macrophages attenuates the inflammatory response and improves left ventricular function post-myocardial infarction. *J Mol Cell Cardiol*. 53(5):599-608
- Dayah T, Chiao YA, Lowell W, Ahuja SS, D'Armiento J, Jin YF, Lindsey ML. (2012) Transgenic overexpression of matrix metalloproteinase-9 in macrophages attenuates the inflammatory response and improves left ventricular function post-myocardial infarction. *J Mol Cell Cardiol*. 53:599–608
- uz Zaman M, Fatima N, Samad A, Ishaq M, Wali A, Rehman K. et al. (2011) Predictive and prognostic values of transient ischemic dilatation of left ventricular cavity for coronary artery disease and impact of various managements on clinical outcome using technetium- 99 m sestamibi gated myocardial perfusion imaging. *Ann Nucl Med*. 25(8):566–570
- Zhang SH, Reddick R, Piedrahita JA, Maeda N (1992) Spontaneous hypercholesterolemia and arterial lesions in mice lacking apolipoprotein E. *Science* 258:468–471

- Zhang X, Xiong Z, Wu Y, et al. (2006) Quantitative PET imaging of tumor integrin $\alpha v\beta 3$ expression with 18 F-FRGD2. *J Nucl Med.* 47:113–121
- Zhao W, Meng R, Ma C, et al. (2017) Safety and Efficacy of Remote Ischemic Preconditioning in Patients with Severe Carotid Artery Stenosis Prior to Carotid Artery Stenting: A Proof-of-Concept, Randomized Controlled Trial. *Circulation.* [Epub ahead of print]
- Zhou D, Huang C, Lin Z, et al. (2014) Macrophage polarization and function with emphasis on the evolving roles of coordinated regulation of cellular signaling pathways. *Cell Signal.* 2014 Feb;26(2):192-7
- Zeisberg EM, Tarnavski O, Zeisberg M, et al. (2007) Endothelial-to-mesenchymal transition contributes to cardiac fibrosis. *Nat Med.* 13:952–961
- Zouggari Y, Ait-Oufella H, Bonnin P, et al. (2013) B lymphocytes trigger monocyte mobilization and impair heart function after acute myocardial infarction. *Nat Med.* 19:1273

Annales Universitatis Turkuensis



Turun yliopisto
University of Turku

ISBN 978-951-29-7266-1 (PRINT)
ISBN 978-951-29-7267-8 (PDF)
ISSN 0355-9483 (PRINT) | ISSN 2343-3213 (PDF)